NANO-DEVICES FOR MEASUREMENT OF THE BIO-EFFECTIVENESS OF IONIZING RADIATION

Jumaa Yousif Tamboul
(MSc.) Radiation Biophysics
School of Physics and Astronomy
University of St. Andrews, Scotland, UK

NANO-DEVICES FOR MEASUREMENT OF THE BIO-EFFECTIVENESS OF IONIZING RADIATION

BY:

JUMAA Y. TAMBOUL

Higher Diploma (Physics)
Surrey University (UK)
MSc. (Radiation Biophysics)
University of St. Andrews

A Thesis submitted for the Degree of Doctor of Philosophy
University of St. Andrews, St. Andrews, Fife, KY16 9SS,
Scotland, United Kingdom
- November 2001 -

CONTENTS OF THE THESIS

DECLARATION ii

CERTIFICATION iii

LIST OF PUBLICATIONS iv

ACKNOWLEDGEMENTS v

DEDICATIONS vi

ABSTRACT vii

TABLE OF CONTENTS ix

LIST OF TABLES xviii

LIST OF FIGURES xix

LIST OF ABBREVIATIONS AND NOTATIONS xxv

REFERENCES 205

DECLARATION

I, Jumaa Yousif TAMBOUL, hereby declare that this thesis has been written by me, that it is the record of my experimental and theoretical work carried out by me and it has not been submitted in any previous application for a higher degree .

This research has been carried out in the School of Physics and Astronomy in the University of St. Andrews under the supervision of Dr. D. P. Tunstall and Dr. D. E. Watt

Date .....

Signature of candidate.

.....

(Jumaa Y. Tamboul)

CERTIFICATION

I hereby certify that the candidate Jumaa Yousif Tamboul has fulfilled the conditions of the resolution and Regulations appropriate for the Degree of Doctor. of Philosophy in the University of St. Andrews and that the candidate is qualified to submit this thesis in application for that degree .

Signature of Supervisor

Date 6/3/2002

Dr. D. E. Watt

(Research Supervisor)

LIST OF PUBLICATIONS

Tamboul, J. Y.; . McDougall I. C. and Watt, D. E. (2000) . Nanometric gas counters, in Radiation Quality Assessment Based on Physical Radiation Interaction at the Nanometre Level. Ed. P. Colautti . LNL-I.N.F.N. (REP) 161/2000. I.N.F.N. Laboratori Nazionali di Legnaro, Via Romea, 4-I-35020, Padova, Italy.

Tamboul, J. Y. and Watt, D. E. (2001) . A proportional counter for measurement of the bio-effectiveness of ionizing radiation at DNA level; Nuclear Instruments and Methods in Physics Research B; Vol. 184, No. 4, pp 597 - 608 .

Grosswendt, B.; Baek, W. Y.; Alka, A.; Colauti, P.; Chechik, R.; Conte, V.; DeNardo, L.; Ségur, P.; Shchemelinin, S.; Tornielli, G.; Tamboul, J. Y.; McDougall, I. C.; Watt, D. E.; Pszona, S.; Kula, J.; and Marjanska, S. (2000) . Ionization-pattern investigation in nanometric gas volumes; In Radiation Quality Assessment Based on Physical Radiation Interaction at Nanometre Level, pp 61 - 70 , Editor: P. Colauti , Italy .

ACKNOWLEDGEMENTS

I would like to express my sincere gratitude to Dr. D. P. Tunstall for accepting to be my formal supervisor; and Dr. D. E. Watt for the fruitful day-to-day supervision, guidance, endless help and encouragement that built confidence in my work . I wish also, to extend my thanks to all my research colleagues in the Radiation Biophysics Unit, School of Physics and Astronomy at University of St. Andrews, especially to I. C. McDougall for his continuous encouragement and discussion; and to the highly technical staff of the mechanical and electrical workshops of the School of Physics and Astronomy, in particular to: G.S. Radley; J. Lindsay; P. Aitken; A. Barman and S. Balfour, for their unbeatable patience in helping with the construction of my experimental device . Thanks are also, to the staff of the store of the school of Physics, namely to Ian McLaren .

I am very grateful to the Sudan University of Science and Technology and the Ministry of Higher Education for financial support without which my progress would have not been possible . Thanks are also due to all my staff colleagues of the College of Medical Radiological Sciences, in Sudan University of Science and Technology for their endless moral support and encouragement .

Finally, thanks are due to any one contributed, by any means in the success of my research .

DEDICATIONS

To:

MY FATHER:

Yousif Tamboul Yousif

MY MOTHER:

Zainab Tawir Yassin

MY WIFE:

Sadia Omer Turkawi

MY DAUGHTERS:

Sarah; Islam and Eiman

For your continuous encouragement, patience, moral support and understanding.

ABSTRACT

Application of ionizing radiations in different aspects of human life needs to be properly balanced by appraising their respective benefits and hazards . The necessity for proper measurement of physical and biologically related parameters, which are predictive and descriptive of radiation effects then arises . In the current system of dosimetry, the energy transfer at macroscopic and microscopic levels is taken to be the most basic mechanism involved in radiation action, but no satisfactory proof has been given in support of the assumption . There are, also, many well known limitations to these conventional systems of dosimetry .

In this work, the intensive review made of the previous works shows that many diverse attempts have been made to specify these parameters in terms of values capable of better unifying data for different radiation types (Watt,1989b; 1997) . Of these values, the mean free path for primary ionization λ, is recognized as the most fundamental . This review revealed also, that there is increasing support for the view that matching of λ, with the double-stranded DNA segment (i.e 2 nm) is the dominant mechanism for radiation action in mammalian cells . Therefore, there is a strong belief that if a physical detector can be designed, with a response function which can sim ulate that of the DNA to radiation (Pszona, 2000), then absolute dosimetry of ionizing radiation in a unified system becomes feasible .

A critical review has been made of different radiation measuring systems to appraise and recognize the characteristics which are convenient for the practical implementation of the above findings . This investigation reveals that the operational characteristics of the gas-filled ionization chambers and proportional counters are the most appropriate system for simulation of radiation action on the mammalian cells at the level of the DNA bio-molecules .

In the light of the above, a gas-filled , tissue equivalent (TE) gridded parallel plate proportional counter has been designed, constructed and tested . The device, operates at low pressure pure propane or propane based tissue equivalent gas to

simulate the radiation action on the mammalian cells at the level of nanometric biological targets (DNA segment) . At the pressure of 1 torr of pure propane gas, the simulating sensitive volume has a mean chord equivalent to 1.85 nm at unit density, with a response function for ionizing radiation simulating that of the double-stranded DNA segment . The detector is operated with large internal amplification of more than 10^6, with effective background signal discrimination, therefore, it can detect single and plural electron charges . The observed ADC spectra are processed by applying a deconvolution technique combined with a least squares fitting routine to determine the mean number of charges per event, and clusters of integral, 1, 2, 3, etc charges can be resolved . The detector (Tamboul and Watt, 2001) can record simultaneously, both charged particle fluence and bio-effect cross-section, the key parameters for nanodosimetry .

A successful test of the nanodosimeter operation has been made for an internally mounted α-particle source and laboratory external source of operational radiations, such as Cf-252 spontaneous fission neutrons and low energy photon from a Mossbauer source of Co-57 . Detailed results are presented, where the experimentally derived bio-effect cross-sections are compared with the effect cross-sections for biological damage to mammalian cells found in the literature .

A method of interpreting the output signal of the device is described and directly related to the bio-effect cross-section for mammalian cell inactivation, which in turn, can be converted into radiation risk by using the cancer risk coefficients recommended by the International Commission of Radiological Protection. However, this proves that the device can be applied as an absolute radiation measuring unit, in any field of ionizing radiation .

Although the results obtained using the nano-device are favourable and convincing, yet further future improvements are required so that the instrument sensitivity can be made better and expansion of the operation of the system from a single target volume unit to simulate the response for the well known multiplicity of targets in mammalian cell nuclei .

TABLE OF CONTENTS

CHAPTER ONE

GENERAL INTRODUCTION

1.1 Introduction 1

1.1.1 Methods of control 2

1.1.2 Limitations of the current dosimetric system 3

1.2 The need for an alternative system of dosimetry 4

1.3 The objective of the project and the scope of the thesis 5

1.3.1 The objective and aims of the project 5

1.3.2 The scope of the thesis 6

CHAPTER TWO

THE CONVENTIONAL SYSTEM OF DOSIMETRY

2.1 Introduction 11

2.2 Historical background of radiation quantity and quality 13

2.2.1 Radiation quality parameters 13

2.2.1.1 Half-value layer (HVL) as a quality parameter 13

2.2.1.2 The mean ion number as quality parameter 14

2.2.1.3 Linear energy transfer (LET) as quality parameter . . 15

2.2.1.4 Restricted linear energy transfer L_{Δ}, as quality parameter 16

2.2.1.5 LET distribution and its averages 17

2.2.1.5.1 Track length distribution, t (L) 17

2.2.1.5.2 Dose distribution, d(L) in LET 18

2.2.2 Radiation field quantities 20

2.2.2.1 Radiation fluence and fluence rates 20

2.2.2.2 Interaction cross-section and coefficients 21

2.2.2.2.1 Mass attenuation coefficient (μ/ρ) 22

2.2.2.2.2 Mass energy transfer (μ_{tr}/ρ) 23

2.2.2.2.3 Mass energy absorption coefficient (μ_{en}/ρ) . 24

2.2.3 Dosimetric quantities 24

2.2.3.1 The absorbed dose (D) 24

2.2.3.2 Kerma (K) and Kerma rates 26

2.2.3.3 The exposure (X) and exposure rate 27

2.2.3.4 Cema (C) 28

2.2.4 Quantities in Radiation Protection and Radiobiology 29

2.2.4.1 The relative biological effectiveness (RBE) 30

2.2.4.2 The quality factor (Q) 31

2.2.4.3 Dose Equivalent (H) 32

2.2.4.3.1 The ambient dose equivalent, $H^{*}(d)$ 33

2.2.4.3.2 The directional dose equivalent, H'(d, Ω) . . . 34

2.2.4.3.3 The personal dose equivalent, H_P(d) 34

2.2.5 Quantities based on mean values 34

2.2.5.1 Mean absorbed dose in an organ (D_T) 35

2.2.5.2 Mean quality factor (Q_T) 35

2.2.5.3 Quantities used for limitation purposes 35

2.2.5.3.1 The organ dose equivalent 35

2.2.5.3.2 The Effective Dose (E) 36

2.2.6 Microdosimetric quantities 37

2.2.6.1 Energy deposition event 39

2.2.6.2 Lineal energy (y) 39

2.2.6.3 The specific energy imparted (z) 41

2.3 Limitations of the conventional dosimetric quantities 43

2.3.1 Limitations in the linear energy transfer (LET) 43

2.3.2 Limitations in the absorbed dose (D) 46

2.3.3 Limitations in the relative biological effectiveness (RBE) 47

2.3.4 Limitation in the quality factor (Q) 48

2.3.5 Limitations in Dose Equivalent (H) 48

2.3.6 Limitations in the conventional microdosimetric quantities 49

2.3.7 Limitations in the weighting quantities 51

CHAPTER THREE

APPROACHES FOR UNIFIED DOSIMETRY

3.1 Particle track and damage mechanisms 55

3.1.1 Effect cross-section (σ_e) 57

3.1.2 Relative Biological Effectiveness (RBE) 59

3.1.3 Basic physical data of ions and electrons 60

3.1.4 The intrinsic efficiency for radiation damage 61

3.1.5 Cumulative probability and damage mechanism 66

3.2 Biophysical modelling for radiation action 69

3.2.1 Types of radiation damage models 70

3.2.1.1 Hit and target model 71

3.2.1.2 Two component models 72

3.2.1.3 Dual action model 73

3.2.2 A model for the absolute bio-effectiveness of radiation 74

3.2.2.1 The Absolute Biological Effectiveness (ABE) 76

3.2.2.2 Calculation of the absolute bio-effectiveness 76

3.2.2.3 Testing the absolute bio-effect model 79

3.2.3 Bio-effectiveness and fluence-based risk control 82

3.3 Characteristics of the detector for absolute dosimetry 83

3.3.1 General requirements for absolute detectors 85

3.3.2 The physical characteristics of the desired detector 87

3.4 Possible approaches for absolute detection system 89

3.4.1 Solid based detectors 90

3.4.1.1 Organic scintillators for nanodosimetry 90

3.4.2 Liquid based detectors 93

3.4.3 Gas based detectors 94

3.4.3.1 Gas scintillation counters 95

3.4.3.2 The gas-filled and multi-step avalanche detectors 95

CHAPTER FOUR

CRITICAL REVIEW OF GAS-FILLED DETECTORS

4.1 Introduction 98

4.2 Electric fields in gas-filled ionization detectors 101

4.3 Characteristics of the gas-filled counters 103

4.3.1 Ionization chamber 103

4.3.1.1 Pulse formation in ionization chambers 105

4.3.2 Proportional counter 107

4.3.3 Geiger Müller (G. M) counter 111

4.3.4 Parallel-plate and cylindrical ionization chambers 112

4.3.5 Constructional problems of ionization radiation detectors 115

4.3.5.1 Insulators 115

4.3.5.2 Guard ring 115

4.4 Gridded ionization chambers 118

4.4.1 Grid Inefficiency in shielding the collector 118

4.4.2 Pulses across the collector electrode 123

4.4.3 Pulse on the grid of the chamber 123

4.4.4 Brief review of work with the gridded ionization system 129

4.5 Transport properties of charges in gas-filled counters 133

4.5.1 Ion mobility 133

4.5.2 Electron mobility 134

4.5.3 The behaviour of ion-pairs in gas counters 137

4.6 The role of some phenomena in operation of ion chambers 139

4.6.1 Diffusion of charge carriers in gases 140

4.6.2 Recombination of charges in gas-filled counters 141

4.6.2.1 Types of recombination of ions 142

4.6.2.1.1 Electron recombination 142

4.6.2.1.2 Ion and volume recombination 143

4.6.2.1.3 Initial (geminate) recombination 143

4.6.2.1.4 Preferential recombination 144

4.6.2.1.5 Columnar recombination 144

4.6.2.1.6 Wall recombination 145

4.6.3 Charge transfer and electron attachment 145

4.6.3.1 Charge transfer 145

4.6.3.2 Electron attachment 145

4.6.4 Electrical breakdown and corona discharge 147

4.6.4.1 Electrical breakdown 147

4.6.4.2 Corona discharge 148

4.6.5 Polarity effect in gas-filled ionization counters 149

CHAPTER FIVE

EXPERIMENTAL WORK

5.1 Introduction 151

5.2 The detection system 152

5.2.1 Design configuration and construction of the detector 152

5.2.1.1 The design of the initial prototype nano-detector . . . 153

5.2.1.2 The design of the final prototype nano-detector 160

5.2.2 The counting gas, evacuation and the gas filling system 163

5.2.2.1 The counting gas 164

5.2.2.2 The evacuation and gas-filling system 165

5.3 The operation of the nano-detector 165

5.3.1 Experimental set-up of the nanodosimeter 166

5.3.2 The test charges, intrinsic sensitivity and calibration 167

5.3.2.1 Consistency check for the device measurements . . . 174

5.3.3 Size of the sensitive volume 178

5.3.4 Maximum intrinsic gain of the detector 180

5.4 Detection and resolution of single charges 183

5.5 Measurement and results 185

CHAPTER SIX

INTERPRETATION OF THE RESULTS;

CONCLUSIONS AND FUTURE PROSPECTS

6.1 Interpretation of the results 191

6.2 Conclusions 196

6.3 The future prospects and recommendations 198

6.3.1 The hybrid chambers 200

6.3.2 Multi-volume system 203

LIST OF TABLES

Table 2.1 : Specified quality factor-LET (Q-L) relationship 33

Table 2.2 : radiation weighting factors (w_R) 36

Table 2.3 : Tissue or organ weighting factors 37

Table 6.1 : Characteristics of a hybrid photodiode compared to that of two conventional ionization chambers 201

LIST OF FIGURES

Figure 3.1: A typical observed dose-survival curves used for the extraction of the basic data for the study of the radiation action in mammalian cells . . 58

Figure 3.2: The cumulative probabilities of different types of radiation damage to different types of targets plotted against the mean free path for primary ionization 67

Figure 3.3: Bio-effect cross-sections for inactivation of mammalian cells by different types of radiations, as a function of the mean free path λ, for linear primary ionizations . Marks A, N, and G; are the experimental data of the present nanodosimeter for α-particles, neutrons and photons irradiation respectively (see section, 5.5) 81

Figure 3.4: The bio-effectiveness per unit equillibrium charged particle fluence plotted as a function of the energy of different radiations .This permits the ICRP weighting factors to be superposed for the comparison. 84

Figure 4.1: Diagram of the curve relating the output pulse of a gas-filled detector and its applied voltage . A, is the recombination controlled region; B, is the ionization chamber region; C, is the proportional counter region; D, is the limited proportionality region and E, is the Geiger-Mueller region 99

Figure 4.2: Gas multiplication factor M, versus collector voltage in a proportional counter . The factor M, strongly depends on the applied voltage, pressure and type of the gas used in the counter (Tsoulfanidis, 1983). 109

Figure 4.3: The role and function of the guard ring in electrodes of an ionisation

chamber a) A guard ring for the collector electrode only. The size of the high tension electrode is approximately twice that of the collector b) Guard rings are used for the collector and the high tension electrodes, and the electrodes are of the same size 117

Figure 4.4: Schematic drawing of a grid ionization chamber. Electrons and positive ions are produced at the position Q, near the cathode, A . The grid G, of parallel wires screens the collector P, from the effect of the positive charges at Q , through the electric field extending from Q, to, G, and then to, P (Bunemann et al, 1949) 119

Figure 4.5: Curves of constant grid inefficiencies σ, plotted as a function of r/d, versus, d/p; where r, is the radius of the grid wire; d, is the separation between the grid wires, and p (= a), is the separation distance between the collector and the grid (Bunemann et al, 1949) 121

Figure 4.6: The fraction (1 - λ) of the electrons collected by a collector versus the ratio of the field between the grid and the collector; and that between the grid and the cathode. λ, is the fraction of the electrons collected at the grid (Wilkinson, 1950). 121

Figure 4.7: Schematic view of a double-gridded ionization chamber. Signals can be taken from both the collector C, and the first grid, G1 . Grid G_2, screens the collector from the effect of the positive charges (ogawa and Doke, 1961 126

Figure 4.8: Electron drift velocities in three different gases (Fulbright, 1979)136

Figure 4.9: Electron drift velocity in methane-carbon dioxide mixtures (0% to 20% CO_2); (Morgan and Turner, 1973) 136

Figure 4.10: Electron drift velocity in argon-nitrogen (Morgan and Turner, 1973) 138

Figure 4.11: Electron drift velocity in various gases (Knoll, 1989) 138

Figure 5.1a: Schematic diagram of the electrode system of the initial version of the prototype nanodosimeter 154

Figure 5.1b: A schematic block diagram of the experimental set-up of the initial version of the prototype nanodosimeter 155

Figure5.1c: A photograph featuring the initial version of the prototype nanodosimeter 156

Figure 5.2a: Inefficiency of the grid used in the present nanodosimeter versus the ratios of the spaces between the electrodes. 158

Figure 5.2b: Ratios of the voltages V_{ag}/V_{gc} versus the ratios of the distances between the electrodes (d_{ag}/d_{ac}) . Where, a = Anode, g = grid, c = cathode 158

Figure 5.3a: A schematic drawing of the final, single grid, version of the nano-detector, with electrode assembly 161

Figure 5.3b: An enlargement of the electrode assembly of the final version of the nano-detector 161

Figure 5.4a: ADC spectra for alpha particles of Am-241, at pressure of 1 torr of propane gas for different collector voltages. Centroids of the spectra depend on the voltages 168

Figure 5.4b: Centroids of the spectra in fig. 5.4a plotted as a function of the collector applied voltages . Exponential relationship can be noticed. 168

Figure 5.4c: ADC raw spectrum obtained for the gamma-rays from Cs-137

source. 169

Figure 5.5a: Background corrected raw ADC spectrum for external Cf-252 spontaneous fission neutron source. 171

Figure 5.5b: Deconvoluted spectrum of fig. 5.5a to give the calculated frequence distributions of the LSQ Fit compared with the experimental data. . . 171

Figure 5.6: Count rates of primary electron clusters for α-particles extracted from the sensitive volume of the nano-device plotted as a function of the extractor voltages .The optimum extraction voltage is +10 volt, and -20 volt is required to significantly suppress the extraction. 173

Figure 5.7: Experimental probability density distributions of primary electron charge for 1, 2, 5 and 10 torr pressure of propane gas as a function of the primary charges 173

Figure 5.8a: Simulated geometry of the nanodosimeter for Monte-Carlo calculations to which the experimental data of the device were compared for the consistency check (Grosswendt et al, 2000) 176

Figure 5.8b: Calculated frequency distribution $f(N_c)$ as a function of cluster size, N_c, produced by α-particles of energy 5.4 MeV in a pressure, P, of pure propane gas for the simulated geometry of fig. 5.8a. 176

Figure 5.8c: The measured and calculated frequency distribution $f(N_c)$ are compared as a function of cluster size, N_c, produced by the α-particles in fig. 5.8a 177

Figure 5.9: The plateau of integral count rates of α-particle in the initial version of the prototype nano-detector as a function of the extractor voltages whilst keeping the fields, in regions other than between the cathode and the

extractor, constant 181

Figure 5.10: The intrinsic gain of the nanodosimeter as a function of gas pressure and the reduced electric field . The maximum gain is limited by the average number of the primary charges n_{AV}, released in the sensitive volume. 181

Figure 5.11a: An ADC spectrum for α-particles of an internally mounted emitted Am-241 source, measured by the nanodosimeter . Extractor = +10 V; Grid = 210 V; Anode = 500 V; pressure = 1 torr propane gas . the spectrum is corrected for the background 186

Figure 5.11b: The data in fig. 5.11a is processed and deconvoluted to give the integer of the experimental frequency distribution. 186

Figure 5.12a: A raw ADC spectrum produced in the nano-detector by a Mossbauer source of Co-57 emitting low energy x-rays and γ-rays . The source is externally mounted to generate an equilibrium electron field in the sensitive volume of the device 190

Figure 5.12b: The data in figure 5.12a is deconvoluted to give the experimental frequency distributions. 190

Figure 6.1: Zeroth, first and second moments of the observed experimental distributions for lineal primary charges (q/d) generated by α-particles in the nanodosimeter at the pressure of 2 torr pure propane gas 194

Figure 6.2: Schematic diagram of the expected combination of the gridded parallel plate nanodosimeter and the hybrid photo-diode 202

LIST OF ABBREVIATIONS AND NOTATIONS

β	The velocity of an ion
λ	Mean free path for primary ionization
μ	Linear attenuation coefficient
σ	Microscopic cross-section
σ_B	Radiation Bio-effect Cross-section
σ_{DNA}	Geometrical cross-section of DNA segment ($\approx 3\ \mu m^2$)
σ_e	effect cross-section
σ_g	Geometric cross-section
σ_R	Intrinsic efficiency for radiation damage
Φ	Particle Fluence
ADC	Analogue-Digital Convertor
Ar	Argon
$C_3 H_4$	propane
CH_4	Methane
DNA	Deoxyribonucleic Acid
eV	Electron-volt
GBq	Giga-Becquerel
H	Dose equivalent
HVL(T)	Half Value Layer (Thickness)
ICRP	International Commission on Radiological Protection

ICRU	International Commission on Radiation Units and Measurements
keV	kiloelectron-volt
L_Δ	Restricted Linear Energy Transfer
LET	Linear Energy Transfer
LSQ	Least square
mbar	Millibar
MBQ	Mega-Becquerel
MeV	Megaelectron-volt
MWPC	Multi-wire proportional counter
N_A	Avogadro's constant
nm	Nanometre
P	Probability of interaction per unit radiation fluence or pressure
PC	Proportional counter
PTFE	Polytetrafluoroethylene
Q	The quality factor
RBE	Relative Biological Effectiveness
TE	Tissue equivalent
TMS	Tetramethyl Silane
w	Mean energy require for the production of an ion pair
w_R	Radiation weighting factor
w_T	Tissue or organ weighting factor
z	The Effective Charge on an ion
ε	Actual energy deposited by ionizing radiation in a volume of interest

CHAPTER ONE

GENERAL INTRODUCTION

1.1 Introduction

In common with most of scientific development in modern life, the benefits derived have to be balanced against the hazards . Thus the application of ionizing radiations in different aspects of human life needs to be properly balanced by appraising their respective benefits and hazards . Very significant advantages are obtained by the use of these radiations such as in radiotherapy, nuclear medicine and industrial uses, such as in food processing and large scale sterilization . However, there are also disadvantages, mainly the small stochastic possibility of inducing fatal damage in humans . Consequently the benefits and advantages of radiation as well as their disadvantages should be assessed so that an appropriate balance can be kept between them .

In radiological protection, for example, the basic objective is to protect individuals and mankind as a whole from the deleterious effects of ionizing radiation, while still allowing necessary applications that are advantageous but from which radiation exposure might result . Accordingly, the knowledge of the effectiveness of radiation as a damaging agent in living organisms, particularly in humans, is very important so that precise radiological protection programmes can be scheduled and accurate planning for medical use of radiations in radiotherapy and nuclear medicine can

be made . However, radiological protection is the field which is concerned with the control of radiation exposure to the population to ensure that any harmful effects are no more serious than those of other hazards encountered in normal life . This means that there should be reliable means of control of planned or accidental exposures to ionizing radiations .

1.1.1 Methods of control

For radiological protection, the accuracy in prediction of risk needs to be only about 30 % . Consequently, relatively crude physical and biological parameters can be used to describe the processes leading to the critical damage in tissue and hence the prediction of cancer risk (ICRU, 1970) . On the other hand, the mechanism of radiation damage should be precisely understood so that radiation may be usefully applied in radiotherapy and nuclear medicine where more critical criteria are required due to the fact that, for successful treatment, the estimate of damage must be accurate to better than 5 % .

In the presently accepted system of radiation dosimetry, the attempt to achieve the control of radiation exposure and accuracy required for radiotherapy and nuclear medicine is made by the accurate measurement of the quantities currently accepted as radiation quality specifiers, the absorbed dose, D (section 2.2.3.1), and the use of an empirical quantity, the relative biological effectiveness, RBE (section 2.2.4.1) . In radiological protection, the attempt to control the radiation exposures for different radiation types is made by the use of scaling factor called

the quality factor, Q (section 2.2.4.2) . This quantity is selected always to exceed the measured RBE by an arbitrarily chosen safety factor . However, there are many limitations in the present method of control of radiation exposures as many arguments can be made concerning the validity of the currently accepted parameters used for quantification of radiation effects .

1.1.2 Limitations of the current dosimetric system

There are many anomalies which can be observed in the present methods of control used for radiation exposures . These anomalies are the consequences of the severe limitations in the present system of dosimetry (section 2.3) . First, there is the requirement of contriving quality factors, or the use of the empirical values, RBEs combined with the need to know the radiation type . Secondly, particles of different types but with the same LET (section 2.2.1.3) do not have the same RBE . Furthermore, no allowance is made for the size and multiplicity of critical biological radiosensitive sites known to exist in cell nuclei, nor for the stochastic nature of the particle interactions .

In the current system of dosimetry, the energy transfer at macroscopic and microscopic levels is taken to be the most basic mechanism involved in radiation action, but no satisfactory proof has been given in support of the assumption .

A powerful method for exploring the appropriateness of the fundamental parameters used in any system is to test if damage data for any specified

biological end-point can be unified into a single response curve, independently of radiation type (Simmons and Watt, 1999) . A single unified curve is essential if convincing devices are to be designed and produced for practical implementation of the system .

As it must be designed for known types of radiations and particles, the instrumentation used in the traditional system of dosimetry is severely limited in its capabilities . Furthermore, its instruments measure the physical quantities, such as the absorbed dose, consequently, they do not measure the desired quantity, the bio-effectiveness.

1.2 The need for an alternative system of dosimetry

In the light of the foregoing, and because of the persisting difficulties in specifying radiation quality adequately well for the estimation of biological effects, and the arguments that can be made against the suitability of energy-based parameters for quantification of the radiation fields, it is desirable to find a better and more meaningful method to predict, quantify and measure the probability of occurrence of the effectiveness of radiation in mankind, from measurements in the initial radiation fields of exposure .

The main problem is to find a method of predicting, with scientific justification, the probability of occurrence of the deleterious effects from the knowledge of relevant physical parameters, as well as the confirmation of the

relevance of these parameters . Hence, the necessity arises, for proper measurement of physically and biologically related parameters, which are predictive and descriptive of radiation effects .

Many diverse attempts have been made to specify these parameters in terms of single values capable of better unifying data for different radiation types (Watt,1989b; 1997) . Of these values are the restricted LET, (L_{Δ}) (Harder et al, 1988); the square of the ratio of the effective charge on the ion to its velocity, z^2/β^2 (Katz, 1972; Watt et al, 1994); and the mean free path for primary track interaction, λ . Note, however that, the mean free path for primary ionization is the most fundamental of these parameters and it is the 'zeroth moment' of energy transfer . Furthermore, there is increasing support for the view that matching of, λ, with the double strand DNA segment (i.e 2 nm) is the dominant mechanism for radiation action in mammalian cells (Pszona et al, 2000) . Consequently, if a physical detector can be designed, with a response function which can simulate that of the DNA to radiation, then absolute dosimetry of ionizing radiation in a unified system becomes feasible .

1.3 The objective of the project and the scope of the thesis

In section (1.3.1), the objectives and the aims of the project are briefly described, whereas, the scope of the thesis is detailed and discussed in section (1.3.2) .

1.3.1 The objective and aims of the project

The aim of the project is to design, produce, test and then commission a prototype gas-filled nanodosimeter for operational radiation protection, which will have a

radiosensitive volume of nanometre dimension . As the first objective towards the design of the device, it is necessary to identify physical quality parameter(s) which initiate(s) the ultimate bio-effectiveness of radiation tracks and which can be used in the simulation . Fortunately, absolute parameters, based on the bio-effect cross-sections, the equilibrium charged particle fluence and the mean free path for primary ionization, have been already identified by the research group in Radiation Biophysics Unit, at the University of St. Andrews (Chapter Three) .

Therefore, the aim of the present work is to pioneer nanometre instrumentation for the practical implementation of the findings of this research group . Although, many attempts have been made towards such an objective, none have been successful, specially the design and production of a device which can simulate the response of the lower nanometric volumes of the radiosensitive targets .

1.3.2 The scope of the thesis

To make the aims and the objectives of the project stated above true, an attempt is made to back-up the experimental work, which is the ultimate aim of this research, by the theoretical background . This is described through the chapters of the thesis in a sequential manner .

In chapter two the relevant aspects of the conventional system of dosimetry is

critically discussed to outline the features that necessitate the requirement for an alternative system of dosimetry . Therefore, a historical background of the radiation quantity and quality parameters used in the currently accepted system is given . This enables logical criticism to identify the characteristics of the parameters as well as the limitations . This will then assist to decide the extent of dissatisfaction incurred in the present system of radiation dosimetry .

In the light of the outcome of chapter two, it is necessary to review, in chapter three, the different approaches suggested by the research group at the University of St. Andrews (Watt et al, 1985) . The dominant determinants of radiation damage are identified . To investigate the radiosensitive sites responsible for radiation damage, the role of the particle track as a probe to explore radiation damage mechanisms, is studied . Three basic parameters are assumed to be the key factors for the new proposed system . These are ; the bio-effect cross-section σ_B, for the particular biological end-point; the equilibrium charged-particle fluence Φ_{eq}; and the mean free path for linear primary ionization, λ . These parameters are deduced from the major findings that the radiation bio-effects are mainly caused by the spatial correlation of track interactions with sites in each strand of the double-stranded DNA, to induce double strand breaks .

It will be briefly discussed in chapter three also, the biophysical modelling for radiation action proposed on the basis of the above findings . It will be shown that the key factor for this model is the fluence-based system that has been proposed for unified dosimetry (Watt,1997) .

The characteristics and requirements of the detector desired for absolute dosimetry are given as well, including the possible approaches for the absolute detection system . Consequently the potentials of different detection systems will be appraised to explore the most appropriate system for the unified, absolute radiation dosimetry . Very brief remarks are given about some examples of these detection systems and a few are critically described . It transpires that, the gas based detection system is the most attractive system for practical use in the unified system of dosimetry . Therefore, it has been appraised and adopted in this work for practical implementation of fluence-based nanodosimetry . A use of organic scintillators for nanodosimetry is a possible alternative may be suitable for simulation of the absolute bio-effectiveness .

Due to the outcome of chapter three that the gas-filled, multi-step avalanche detection system is the favoured system, chapter four is dedicated to a critical review of gas-filled detectors . An intensive and detailed review is made to explore the potentialities and characteristics of gas-filled detectors suitable for nanodosimetry . This includes the investigation into the various features that govern the operation of these detectors . Of these, the nature of electric fields needed for the desired operation of the device is a significant feature . The characteristics of the gas-filled detectors are studied for each of the common three categories constituting them, viz, ionization chambers; proportional counters; and Geiger Muller counter .

Chapter four Included also, a special reference to the parallel-plate ionization chamber . A comparative study of the parallel-plate ionization chamber versus the traditional cylindrical proportional counter is made . The gridded ionization chamber, which is the system adopted in the experimental work of this project, is described in details focussing on the characteristics desired for the practical implementation of the unified system of radiation detection and measurement . A brief review of works with gridded ionization systems, in the literature, is made . Constructional problems of ionization radiation detectors are stated for possible account for their role when they have to be dealt with practically .

The transport properties of the charges produced in the detector and The role of some physical phenomena in the operation of the ionization chambers, as an example for the gas-filled detectors, are investigated to account for their role in the design and construction of the desired detector for the absolute dosimetry.

Up to this stage of the thesis it will be clear that the double-strand breaks in the intra-nuclear DNA, are the precursors leading to the deleterious effects of ionizing radiations in mammalian cells . It will be already concluded that if detectors can be designed to have an instrumental response which simulates that of the DNA in cells, then there is the possibility of developing unified system of dosimetry which will be independent of radiation type (Watt et al, 1995) . Although various approaches have been proposed to achieve the desired detector, yet, there is no physical instrumentation which can give an absolute measure of the initial

biological effectiveness of unknown ionizing radiation .

Therefore, chapter five is dedicated for the main part of the project, which is the experimental work that deals with the objective of devising conceptually new practical instrumentation for measurement of the absolute bio-effectiveness of radiation at the level of nanometre volumes .

The design, construction and operation of the detector is described, including the evacuation and gas filling system of the detector . The response function of the device is discussed . The experimental set-up of the instrumentation system is described together with the preliminary experimental results .

The interpretation of these experimental results is given in chapter six . They are interpreted using a convolution/deconvolution method (Obileć and Srdoč, 1998). Also given in chapter six are the conclusions of the work performed as well as future prospects and recommendations .

CHAPTER TWO

THE CONVENTIONAL SYSTEM OF DOSIMETRY

2.1 Introduction

The objective of radiation dosimetry, in general is to provide procedures, techniques and concepts for the determination of the amount of ionizing radiation which is quantitatively related to the induced biological effects (Attix, 1986) . The dosimetry in radiation protection is thus concerned with the practical aspects of developing internationally accepted concepts, quantities and methods which are suitable for radiation risk assessment and can be used for controlling exposures and specifying exposure limits for the radiation workers and the public .

The history of radiation measurement in general, and radiation protection in particular, is also the history of a succession of different quantities and unit . Historically, the main physical difficulty that has emerged is the specification of the radiation quality . Soon after the discovery of X-rays by Rontgen, 1895, many of the radiation effects induced by X-rays, including biological effects, were used for radiation measurements . The photographic effects of the radiation was one of the early methods suggested for measurements and definition for units of radiation . The history of standardization of radiation measurement and the methods used, then went through continuous upgrading and replacement utilizing the different radiation effects such as chemical and photoluminescence effects . However, the

most important physical radiation effect used initially for proper standardization of radiation measurement was the ionization effect .

Following the adoption of the rontgen as the unit of radiation quantity in 1928, the International X-ray and Radium Protection Commission agreed on the exposures that could be tolerated by a person in normal health (IX-RRPC, 1934) . However, the limitations of these recommendations became apparent by the late 1940s and as a result of the collaboration between the International commission on Radiation Units and Measurement (ICRU) and the International commission on Radiation Protection (ICRP), new sets of proposals were agreed in 1950 (ICRP, 1950, ICRU, 1950) . Since then, a succession of different units have been introduced and used to define radiation protection quantities . These are continuously updated by the ICRU and the ICRP (ICRU news (1), 1995), a situation which has created confusion, given the whole system instability and caused a loss of confidence in the measuring systems for radiation protection as well as in radiobiology (Pelliccioni and Silari, 1993) . In addition, the determination of radiation protection quantities often involves significant uncertainties due to the inherent limitations of the parameters used such as the LET and its distributions (ICRU, 1978) . Finally, a variety of approximations must be made for relating physical measurements to biological effects caused by radiation .

In the following sections, a historical background and brief definitions and descriptions will be given for the successive quantities defined and used for

specification of parameters in radiation measurement up to the current situation. These reviews are meant to clarify the progress made in determination of the quantities and the relation between them . Accordingly, the degree of limitations of these quantities as parameters for effective and absolute radiation measurement in the present dosimetric system can be assessed . The difficulty of relating these quantities to the real biological effectiveness produced can then be evaluated .

2.2 Historical background of radiation quantity and quality

In general, two types of physical information are required to specify the radiation benefit or advantage .These are the quality of radiation field and its quantity. The correlation of these information together give the useful application of the radiation fields .

2.2.1 Radiation quality parameters

The quality of radiation represents the damaging or penetrating power of the radiation . Historically, development of the meaning of the term quality lead to a series of definitions intended to express the damage ability of the radiation type (ICRU, 1970) . This historical development started with the most simplest parameters leading to more sophisticated ones .

2.2.1.1 Half-value layer (HVL) as a quality parameter

Although the term quality strictly refers to the radiation only, independently of the

medium irradiated, the distribution of events produced in a medium can also be used to describe radiation quality . The half-value layer is the simplest quality parameter used historically to specify quality of radiation in a given material (ICRU, 1962b) and it was used to specify the various energies of x-rays and gamma rays used in radiotherapy . It simply specifies the penetrating power of these radiation when they pass through a medium . The HVL is defined as the thickness of an absorbing medium that reduces the intensity of radiation by one half (Turner, 1986) . For monoenergetic photons, HVL can be estimated from the well known exponential attenuation of the radiation passing through a medium . The limitation of the HVL as a quality parameter was that it can be used only for x-rays and γ-rays .

2.2.1.2 The mean ion number as quality parameter

The mean number of ions per unit charged particle track is used as a quality specifier to account for the inappropriate definition of the half-value layer of the types of radiations other than x-rays and γ-rays . Thus :

$$\bar{n} = \frac{E_i}{R_i . W} \qquad (2.1)$$

Where $\bar{n}$, is the mean number of ion pair per unit charged particle track; R_i , is the mean range of an electron with initial kinetic energy E_i, and W is the mean energy required for the production of ion pair (ICRU, 1979) . To account for the wide energy spectrum of electron tracks which would occur in any small region in

an irradiated medium, the mean linear ion density is used as an improved version of application of the mean number of ion pairs per unit track of the charged particle (ICRU, 1983) . Thus the mean linear ion density is equal to the total ion density per unit volume divided by the total length of electron track .

However, the ion pair formation is a stochastic process . For example, for each alpha particle of a fixed energy 5.30 MeV, there are numerous ways in which the energy may be partitioned into ionization events and into non-ionization events throughout the total collision processes . Therefore, the actual number of ion pairs produced by each alpha particle in this process, may differ from one particle to an other . In other words, there are stochastic fluctuations in the number of ion pairs generated . These fluctuations set a theoretical limit to the precision of the energy for a single particle by ionization measurement .

Another problem which may affect the number of ion pairs produced in a medium due to radiation, such as the alpha particle above, is the possibility of collateral ionization in the process due to conversion of neutral excited species into ion pairs through thermal collisions .

2.2.1.3 Linear energy transfer (LET) as quality parameter

The use of ionization as a measure of radiation quality was confronted with the difficulty of accurate measurement and calculation of the ionization produced in condensed, biological media . Another problem was that no account was taken of

the other possible processes such as excitation or charge transfer (section 4.6.3.1) which could create radiation effects also . Linear energy transfer LET, equivalent to the linear stopping power, was used as a quality parameter (Zirkle et al, 1952) .This is defined as the ratio of the energy dE, transferred to the medium by a charged particle traversing a distance, dl . LET emphasises the importance of the transfer of energy to the medium rather than the energy loss in collision by the particle (ICRU, 1970) . Because LET takes into account all possible interaction process, it is taken as applicable to all the types of charged particles .

2.2.1.4 Restricted linear energy transfer, L_{Δ}, as quality parameter

A related quantity to the LET is the restricted linear energy transfer, L_{Δ}, of charged particles in a medium . This is used to account for the spatial distribution of the track structure by separating those δ-rays which have energies greater than, Δ (usually, $\Delta \geq 100$ eV) and treating them as separate tracks (ICRU, 1968) . The restricted linear energy transfer L_{Δ}, is known also as the restricted linear collision stopping power and its given by;

$$L_{\Delta} = \left[\frac{dE}{dl}\right]_{\Delta} \qquad (2.2)$$

where dE, is the mean energy-loss due to collisions with energy transfer less than some specific value Δ; dl, is the distance traversed by the particle . Although the use of energy cut-off has the advantage of simplifying theoretical calculation, the use of a distance cut-off is more convenient in experimental work (ICRU, 1970) .

2.2.1.5 LET distribution and its averages

To distinguish between the local and distant losses of energy by the charged particles in their tracks, a more sophisticated parameter is introduced in the form of distribution in LET . The change in the LET of the charged particle when it passes through a medium can be expressed either in the track length distribution t (L) or in the absorbed dose distribution d (L) .

2.2.1.5.1 Track length distribution, t (L)

Track distribution t (L), is used when thin layers of a medium are penetrated by mono-energetic charged particle radiation, such as in thin biological target . In such track-segment experiments with radiation, only a narrow distribution of LET is involved . Thus the track length distribution t(L) , t(L)dl is the fraction of the total track length T, which has values of LET between L, and L+dl (ICRU, 1970). Hence, in its differential form, the track length distribution d(L) is given by;

$$t(L) = \frac{dT(L)}{dL} \tag{2.3}$$

and its integral form of distribution T(L), is the fraction of the total track length which have LET up to the value L, and is given by;

$$T(L) = \int_0^{\infty} t(L)dL \tag{2.4}$$

The track average LET, $\overline{L_T}$ is the mean LET associated with the track distributions and it is given by;

$$\bar{L}_T = \int_0^{\infty} t(L) L \, dL \qquad (2.5)$$

The differential distribution in LET, t(L), in equation (2.3) is appropriate for evaluation of cross-sections such as the effect cross-section σ_e, for specific biological target . Then;

$$\sigma_e = \int_{L_{min}}^{L_{max}} t(L)\sigma(L) dL \qquad (2.6)$$

where σ_e, is the total effect cross-section; σ(L), is the cross-section for production of a specified effect at LET value, L .

2.2.1.5.2 Dose distribution, d(L) in LET

The dose distribution in LET, d(L) is the fraction of the incident energy deposited as absorbed dose at a given LET . It is given by;

$$d(L) = \frac{dD(L)}{dL} \qquad (2.7)$$

where d(L), d(L)dL is the fraction of the absorbed dose, D, delivered between LET values L, and L + dL . The integral form of dose distribution D(L), is the fraction of the total absorbed dose which is delivered at a value of LET up to, L. Hence,

$$D(L) = \int_0^{\infty} d(L) dL \qquad (2.8)$$

The dose average LET, $\bar{L}_D$ is the mean LET associated with the dose

distribution and can be calculated as;

$$\bar{L}_D = \int_0^\infty d(L)LdL \qquad (2.9)$$

For the studies where relative biological effectiveness RBE, is involved, the differential form of the absorbed dose distribution is the most appropriate quantity (section 2.2.2.4.1) .

The track distribution in LET, t(L) and dose distribution, d(L) are inter-related by the following formula;

$$d(L) = \frac{Lt(L)}{\bar{L}_T} \qquad (2.10)$$

This stage was the first use of a distribution in specifying the radiation field quality parameter, a stage which could be considered as a fruitful development of the previous stages . It is clear that the initially simple ideas about the specification of radiation quality developed into much more complex definitions involving distributions and averages .

However, the concept of LET and its distributions and averages have inherent shortcomings (section 2.3.1) as radiation quality parameters in the fact that, LET, is a statistical mean value that does not adequately describe actual energy concentration in target sites in microscopic volume or less (ICRP, 1989) . Furthermore, the LET is subject to the choice of the cut-off energy rather than distance cut-off .

2.2.2 Radiation field quantities

The other physical information required to measure a radiation field, is the quantity. There are different and numerous quantities which are used for measurement and calculation of the radiation fields in radiation protection . These physical quantities are often interrelated in simple relationships such as products or quotients . A coherent system of physical quantities are used in the present system of radiation field measurement in radiation protection . Of these; radiation fluence and fluence rates; interaction cross-sections and coefficients are briefly described in the following sections .

2.2.2.1 Radiation fluence and fluence rates

Radiation fields of all types of radiation are characterized by the radiometric quantities which include the particle fluence Φ, which is defined as the quotient of the number of particles dN , by the cross-sectional area, da, of a sphere on which the particles are incident, hence;

$$\Phi = \frac{dN}{da} \qquad (2.11)$$

The distribution of particle fluence in time, energy or direction give the more specific radiometric quantities of the fluence rates (Greening , 1985) . In dosimetric calculation, the fluence is often considered as the track-length density at a point (ICRU News, 1992) . Thus;

$$\phi = \frac{dl}{dV} \qquad (2.12)$$

where dl, is the sum of the track lengths of particles in the volume, dV .

2.2.2.2 Interaction cross-section and coefficients

Radiation quantities include the microscopic cross-section σ , which represents the probability of the specific interaction with the target entity . The microscopic cross-section of radiation interaction for indirectly ionizing radiation, such as neutrons, is the basic radiation interaction coefficient and it is the probability P, of interaction per unit particle fluence (Greening, 1985) . thus,

$$\sigma = \frac{P}{\Phi} \qquad (2.13)$$

When the microscopic cross-section of interaction σ , is multiplied by the number of interaction centres N, per unit volume, such as the nuclei, it could be converted into the macroscopic cross-section Σ, (Knoll, 1989), thus;

$$\Sigma = N\sigma \qquad (2.14)$$

The macroscopic cross-section of interaction Σ, for non-ionizing radiation has the physical interpretation of the probability per unit path length for the specific process of interaction described by the microscopic cross-section, σ . Since, by definition σ, is equal to the probability of interaction per unit particle fluence (Φ), and with number of interaction centres N, the number of interactions would be NσΦ, per unit path length, that is NσΦdl , in a length dl . The fractional change in the particle fluence (dΦ/Φ) in path length dl, then becomes -Nσdl, hence;

$$\frac{d\Phi}{\Phi} = -N\sigma dl \qquad (2.15)$$

Here Nσ, is the macroscopic interaction cross-section Σ, for indirectly ionizing particles (such as neutrons) . This has the same significance as the linear attenuation coefficient μ, such as that used for gamma rays . Thus ,

$$\frac{d\Phi}{\Phi} = -\Sigma_{tot} dl = -\mu dl \qquad (2.16)$$

and;

$$\Phi_l = \Phi_0 \exp(-\mu dl) \qquad (2.17)$$

where Φ_0, is the initial fluence, and Φ_l, is the fluence after traversing a path length, l . This indicates that the different types of interaction coefficients are also used in the specification of radiation field quantities with their specific definitions (ICRU News, 1993) . The interaction coefficients are important parameters because they characterize the degree of radiation interaction with matter and they are, together with the particle fluences, used to derive the interaction cross-sections for particular radiation fields which are the basic and fundamental elements of interpretation for the absolute measurements of radiation bio-effectiveness . The following are examples of such interaction coefficients with brief definition and descriptions (Attix,1986) .

2.2.2.2.1 Mass attenuation coefficient (μ /ρ)

The mass attenuation coefficient of a material for ionizing radiation is the fraction of particles, dN/N, that experience interactions per traversed distance, dl, in a

material of density ρ, hence;

$$\frac{\mu}{\rho} = \frac{dN}{N} \cdot \frac{1}{\rho dl} \qquad (2.18)$$

where μ, is the linear attenuation coefficient which depends on the density, ρ, of the absorbing medium . Consequently μ, depends on the physical conditions and states of the medium . This dependence on the density is avoided by using the mass attenuation coefficient . However, the reciprocal of the linear attenuation coefficient μ, is known as the interaction mean-free-path for the uncharged particles . It represents the average distance travelled by a particle of specific energy, between successive interaction with the target in the medium . The mean-free-path is a significant physical quantity for unification of radiation quality parameters (Cannell and Watt, 1985 ; Watt et al, 1990) .

2.2.2.2.2 Mass energy transfer (μ_{tr} / ρ)

Mass energy transfer is the fraction of the incident radiant energy dR_{tr}/R, that is transformed to kinetic energy of charged particles by interactions in traversing a distance, dl, in a medium of density ρ, thus;

$$\frac{\mu_{tr}}{\rho} = \frac{dR_{tr}}{R} \cdot \frac{1}{\rho dl} \qquad (2.19)$$

where R_{tr}, is the part of the incident radiant energy R, which is transferred to the medium .

2.2.2.2.3 Mass energy absorption coefficient (μ_{en} / ρ)

Mass energy absorption coefficient μ_{en}/ρ, of a medium for uncharged ionizing particle is the product of the mass energy transfer coefficient μ_{tr}/ρ, and (1 - g), where g, is the fraction of the energy of secondary charged particles lost in the medium, thus,

$$\frac{\mu_{en}}{\rho} = \frac{\mu_{tr}}{\rho}(1-g) \qquad (2.20)$$

The coefficients described above, can all be expressed in terms of cross-sections from the fact that the linear attenuation coefficient μ, is equal to the product of the number of the particles N,in the medium and the total cross-section, σ .

2.2.3 Dosimetric quantities

The radiation fields are further specified using the dosimetric quantities which are quantities for physical measurement at a point or in a region of interest which correlates with the actual effects of ionizing radiations . Dosimetric quantities can be derived using the radiometric quantities that describe the radiation fields . That is by applying the interaction coefficient, and yet they can be defined directly by the way they are usually measured (ICRU, 1993) . Of these quantities, the following are briefly described and defined .

2.2.3.1 The absorbed dose (D)

The absorbed dose, D, is the fundamental dosimetric quantity used in the present conventional radiation measurement . It is defined as the mean energy $d\varepsilon$,

imparted by ionizing radiation to the medium of mass dm, thus,

$$D = \frac{d\varepsilon}{dm} \tag{2.21}$$

The energy imparted ε, is a stochastic quantity (ICRU, 1993) and it is given by:

$$\varepsilon = \varepsilon_{in} - \varepsilon_{out} + \Sigma Q \tag{2.22}$$

where ε_{in}, is the radiant energy incident on the volume of interest as the sum of the energies of all charged and uncharged ionizing particles which enter the volume ε_{out}, is the sum of the energy of all charged and uncharged particles which leave the volume ΣQ, is the sum of the changes in the rest mass energy of nuclei and elementary articles in any nuclear transformation that occurs in the volume . These changes in the rest mass energy of the particles could be positive or negative . The mean energy imparted $\bar{\varepsilon}$, is a non-stochastic (deterministic) quantity (ICRU, 1980) .

The absorbed dose D, is originally defined so that it could be allowed to be specified at a point . In ICRP Report 60 (ICRP, 1991), it is defined as the dose average over a tissue or organ . Although the absorbed dose is a fundamental quantity, it is a limited concept (section 2.3.2) . This is true for many reasons one of which is that its value determines only the mean energy absorbed per unit mass

in an irradiated medium . Another limitation is that the absorbed dose does not account for the microscopic distribution of the absorbed energy in the medium of interest which may influence the cellular effects .

2.2.3.2 Kerma (K) and Kerma rates

The Kerma K, is the sum of the initial kinetic energy dE_{tr}, of all charged particles released by indirectly ionizing particles in a volume of material per unit mass dm, of the matter in the volume (ICRU, 1977), hence,

$$K = \frac{dE_{tr}}{dm} \qquad (2.23)$$

Although Kerma has the same dimensions and units as absorbed dose, it has the advantage that it is independent of the complexity of the energy transferred by charged secondary particles . Kerma has further advantage that unlike the absorbed dose, it has a defined value for infinitesimally small sample of material in another medium . Therefore, it is often convenient in the conventional dosimetry to refer to a value for kerma or kerma rate for a particular material at a point in a different medium, such as the value of the tissue kerma at the point P, in a water phantom . The kerma rate $\dot{K}$, is the increment of kerma dK, per time dt , that is,

$$\dot{K} = \frac{dK}{dt} \qquad (2.24)$$

In conventional calculations, the kerma K, is expressed usually in terms of either spectric energy fluence Ψ_E, or the spectric fluence Φ_E, of uncharged particles of specified type . Thus the kerma, K, is the integral of the product of the spectric energy fluence Ψ_E, of such particles and the mass energy transfer

coefficient $\mu_{tr}(E)/\rho$, of these particles in the material (ICRU News, 1993), hence;

$$K = \int_E \psi \frac{\mu_{tr}(E)}{\rho} dE = \int_E E\Phi_E \frac{\mu_{tr}(E)}{\rho} dE \qquad (2.25)$$

and,

$$\frac{K(E)}{\Phi(E)} = E\frac{\mu_{tr}(E)}{\rho} \qquad (2.26)$$

Expression (2.26) is termed as the kerma factor for uncharged particles of energy E, in the particular material . However, kerma is meant to be an intermediate dosimetric quantity that can be used as a substitute for the absorbed dose whenever no high spatial resolution is required . But at higher energies, especially of photons, the kerma is often not a satisfactory approximation to absorbed dose (ICRU News, 1994) .

2.2.3.3 The exposure (X) and exposure rate

The exposure (X) is a dosimetric quantity that depends on the ionization property of the radiation . It is defined as the quotient of the absolute value of the total charge Q, of the ions of one sign produced in air when all the electrons (positive and negative) liberated by photons in air of mass dm, are completely stopped in the air (Greening, 1985) thus;

$$X = \frac{dQ}{dm} \qquad (2.27)$$

With the present dosimetric techniques, it is difficult to measure exposure when the

photon energies involved lie above a few MeV or below a few keV.

The exposure can be alternatively defined related to the energy fluence Ψ , the mass energy absorption coefficient μ_{en}/ρ, the elementary charge, e, and the mean energy w, expended in air in production of an ion pair (ICRU, 1980), hence;

$$X = \Psi \frac{\mu_{en}}{\rho} \cdot \frac{e}{w} \qquad (2.28)$$

The quotient of the exposure increment dX, by the time dt, gives the exposure rate.

2.2.3.4 Cema (C)

Cema is an intermediate dosimetric conversion quantity, as the kerma, used in absorbed dose calculations (Kellerer et al, 1992) . It is defined relative to the energy dE_c, expended by ionizing particles other than delta rays in electronic collisions in a mass of specified material (ICRU News, 1993), thus;

$$C = \frac{dE_c}{dm} \qquad (2.29)$$

This quantity is usually expressed in terms of the spectric fluence Φ_E, of the primary charged particles and the linear energy transfer L (E), as the integral of their product , thus;

$$C = \int_E \Phi_E \frac{L(E)}{\rho} dE \qquad (2.30)$$

where ρ, is the density of the specific material . L (E) is the same as the

collisional stopping power S (E) . Cema is frequently used in calculation of S, as an approximation to absorbed dose .

The relation between the kerma (K) and cema (C) is that while the kerma is the sum of the kinetic energies of the energetic particles produced by uncharged ionizing radiation in a medium, Cema is the energy dissipated, per unit mass, by the charged particles with the kinetic energies accounted for kerma . The energy accounted for in cema is further transported by delta rays (ICRU News, 1994) .

Although there are clear differences between the quantities kerma (K) and absorbed dose (D) in a medium, the difference between cema (C) and absorbed dose (D) is often very small and in most cases the latter two quantities may be considered equal .

2.2.4 Quantities in Radiation Protection and Radiobiology

At the present time, constant efforts are made to provide a coherent system of quantities and units for use in radiation protection dosimetry . The intention of these efforts is for the purpose of measurements and calculation in the assessment of compliance with dose limitations (ICRU, 1993) . In conventional dosimetry, the biological effectiveness of the radiation fields is assessed using absorbed dose as a quantity specifier, whereas the quality is expressed in terms of relative biological effectiveness (RBE) for radiobiological and therapeutic purposes, and as the quality factor Q, for radiation protection affairs (Watt, 1989).

2.2.4.1 The relative biological effectiveness (RBE)

The relative biological effectiveness (RBE) is the quantity used to express the quality of radiation in radiobiology and radiation therapy . It is defined as the ratio of an absorbed dose of low-LET reference radiation to the dose of radiation that produces the same quantitative and qualitative biological response (ICRP, 1989) . However, in general, the relative biological effectiveness (RBE) of any radiation A, with respect to the reference radiation R, is defined as the ratio of an absorbed dose D_R, in a tissue to the dose D_A, that causes a quantitatively and qualitatively equal effect, hence;

$$RBE_A = \frac{D_R}{D_A} \tag{2.31}$$

The differential form of the absorbed dose distribution in LET, d(L), in equation (2.7), section (2.2.1.5.2) is the most appropriate quantity for the studies of RBE and its evaluation, hence;

$$RBE = \int_{L_{min}}^{L_{max}} d(L) . r(L) . dL \tag{2.32}$$

where, r (L) is the RBE for radiation field deposited a fraction of dose, d(L).dL. The RBE, here, is for the whole dose distribution in LET . In practice the degree of biological response is very often taken as 37 % survival, and the dose to produce this effect is denoted by, D_{37} .

Although the RBE of the high-LET radiation is normally larger than unity, RBE's less than unity have been observed for high-LET radiation (ICRU, 1989) to some

molecules, such as proteins and to some structures in cells such as membranes. Two classes of radiation effects are considered when estimating the relative biological effectiveness (RBE) values . These are the stochastic and deterministic effects . The stochastic effects are the most important for setting the dose limits. The severity of these effects are not dose dependent while its frequency increases with dose without threshold . The deterministic effects, on the other hand, are dose-dependent in their severity and their frequency . Therefore, it is necessary to define two types of relative biological effectiveness values for radiation protection purposes . These are RBE_M, values for stochastic effects and RBE_m, for deterministic effects . In radiological application, the choice of the type of reference radiation in the definition of RBE is important due to the fact that, not all the low-LET radiation have an equal biological effectiveness (ICRU, 1989) .

2.2.4.2 The quality factor (Q)

The quality factor Q, is a dimensionless quantity used to weight the absorbed dose for the biological effectiveness of the charged particles (ICRU, 1986) . It is the relative measure of radiation quality in radiation protection and it is meant to take account of the relative effectiveness of the different types of ionizing radiation at the low exposure levels encountered in routine radiation protection practice . The quality factor Q, is a functional dependent of unrestricted linear energy transfer (L_∞) in water, which is equal to the linear collision stopping power . The great majority of protection measurements involve only photons and electrons, and for these, the quality factor Q, is unity at LET $\leq$ 3.5 keV/μm . Because of the way they

have been derived, values of the quality factor are only applicable for routine radiation protection purposes and should not be used in assessing the effects of accidental doses .

In case of mixed radiation fields or radiations other than photons and electrons to be measured, a range of values of quality factor Q, arises and a mean value $\bar{Q}$,

weighted by absorbed dose is employed . This is known as the effective quality factor (ICRU, 1993) and it is given by;

$$\bar{Q} = \frac{1}{D}\int_0^\infty Q(L)D(L)dL \qquad (2.33)$$

where D(L)dL, is the absorbed dose deposited by radiation having linear energy transfer lying between, L and L + dL .

Although the initial recommendation of ICRP for the relationship between the quality factor Q(L), and the unrestricted LET was such that the ranges of Q, were from 1 for $L \leq 3.5$ keV/μm, to 20 for $L \geq 175$ keV/μm, these have been modified to reflect the higher RBE_M values for stochastic effects of intermediate energy neutrons . These modified and specified Q-L relationships are given in table 2.1 (ICRP Report 60, 1990) .

2.2.4.3 Dose Equivalent (H)

The dose equivalent H, is the product of the quality factor Q, and the absorbed

dose D, at a point, hence;

$$H = QD \tag{2.34}$$

In radiological protection, additivity of the effectiveness of mixed radiation fields is achieved in conventional dosimetry through the summation of the partial dose

Table 2.1 : Specified quality factor-LET (Q-L) relationship

L_∞ (keV.μm^{-1})	Q (L_∞)
< 10	1
10 - 100	$0.32L_\infty - 2.2$
> 100	$300 / \sqrt{L_\infty}$

equivalent H, for the radiation types involved . Therefore H, represents an attempt to correlate the effectiveness of any radiation field in a unified way (Watt et al, 1987) . There are however, serious limitations to its application both in theory and practise due to various reasons (section 2.3.5) . The original definition of the dose equivalent H, included an additional factor N, as a product of all weighting factors that might modify the potentially harmful biological effects of the absorbed dose D.

Different operational quantities have been defined, based on the dose equivalent H, at a point, for practical measurements, both for area and individual monitoring (ICRU, 1993) . Example of these quantities are given in the following sections;

2.2.4.3.1 The ambient dose equivalent, $H^*(d)$

The ambient dose equivalent is defined at a point in a radiation field as the dose

equivalent that would be produced by the corresponding expanded and aligned field, in the ICRU sphere at a depth, d, on the radius opposing the direction of the aligned field . For highly penetrating radiation, a depth of 10 mm is currently recommended where the ambient dose equivalent is $H^*(10)$. For weakly penetrating radiation, a depth of 0.07 mm for the skin is employed .

2.2.4.3.2 The directional dose equivalent, H'(d, Ω)

The directional dose equivalent at a point in a radiation field, is the dose equivalent that would be produced by the corresponding expanded field, in the ICRU sphere at a depth d, on a radius in specified direction, Ω . For the directional dose equivalent statement, specification of the reference depth, d , and the direction Ω, should be included .

2.2.4.3.3 The personal dose equivalent, $H_p(d)$

The personal dose equivalent is the dose equivalent in tissue, at an appropriate depth d, below a specified point on the body .

2.2.5 Quantities based on mean values

Both the absorbed dose and the quality factor depend on the position in the body and on its orientation in the radiation field . Therefore, the mean-value quantities are averaged over an extended mass, and formulated as integral . These are;

2.2.5.1 Mean absorbed dose in an organ (D_T)

The mean absorbed dose D_T, in a specified tissue or organ equals the ratio of the energy imparted ϵ_T, to the tissue or organ and the mass m_T, of the tissue or organ . In its integral form D_T, is given by;

$$D_T = \frac{1}{m_T}\int_{m_T} D dm \qquad (2.35)$$

where D, is the absorbed dose in the mass element, dm .

2.2.5.2 Mean quality factor (Q_T)

The mean quality factor Q_T, in a specified tissue or organ is given by,

$$Q_T = \frac{1}{m_T D_T}\int_{m_T} Q D dm \qquad (2.36)$$

where D_T, is the mean absorbed dose to the tissue or organ of mass m_T; Q, is a quality factor and D, is the absorbed dose in the mass element, dm . Q_T, is based on the type and energy of the radiation existing in the organ of interest, but when the energy is not known, the Q_T, in any organ can be approximated by a conventional mean quality factor (ICRU, 1986) .

2.2.5.3 Quantities used for limitation purposes

Two limiting quantities have been recommended by ICRU (ICRU, 1977) . These are organ dose equivalent and effective dose (E) .

2.2.5.3.1 The organ dose equivalent

The organ dose equivalent is defined as the mean dose equivalent in specified

tissue or organ and is given by the product of $Q_T D_T$, where Q_T, is the mean quality factor in the organ (section 2.2.5.2) and D_T, is the mean absorbed dose to the organ (section 2.2.5.1) . The organ dose equivalent has been replaced by the equivalent dose H_T, in tissue or organ (ICRP, 1991) . H_T, is based on the radiation weighting factors and is given by;

$$H_T = \sum_R w_R D_{T,R,} \qquad (2.37)$$

Table 2.2 : radiation weighting factors (w_R)

Radiation type and energy range	Radiation weighting factor (w_R)
Photons of all energies	1
Electrons and muons, of all energies	1
neutron, energy < 10 keV	5
10 keV - 100 keV	10
> 100 keV - 2 MeV	20
> 2 MeV - 20 MeV	10
>20 MeV	5
Proton, other than recoil protons, energy > 2 MeV	5
α-particles, fission fragments and heavy nuclei	20

where $D_{T,R}$, is the mean absorbed dose in the tissue or organ T, due to radiation, R, and w_R, is the corresponding radiation weighting factor . ICRP, have collated specified values for w_R, which are shown in table 2.2 (ICRP 60, 1991) .

2.2.5.3.2 The Effective Dose (E)

The Effective Dose is given by,

$$E = \sum_T w_T H_T \qquad (2.38)$$

where H_T, is the equivalent dose in the tissue or organ T; and w_T, is the corresponding tissue weighting factor . Some examples of the recommended values of w_T, are shown in table 2.3 (ICRP 60, 1990) .

Table 2.3 : Tissue or organ weighting factors

Tissue or organ	Tissue or organ weighting factor (w_T)
Gonads	0.20
Red bone marrow	0.12
Colon	0.12
Lung	0.12
Stomach	0.12
Bladder	0.05
Breast	0.05
Liver	0.05
Oesophagus	0.05
Thyroid	0.05
Skin	0.01
Bone surface	0.01
Reminder	0.05

2.2.6 Microdosimetric quantities

If we have to improve our understanding of radiation effects, concepts must be developed which relate some of the principal features of interaction of ionizing radiation with matter, to the size and the nature of the structure being affected . Different concepts and ideas, such as the LET and target theory, are utilized to explain cellular radiation effects (ICRU,1983) . It has now become clear that most of the concepts used are suffering from severe limitations (section 2.3), such as the different limitation to the LET concept . The impossibility to measure LET

distributions and the limitation to the LET in explaining relative biological effectiveness reflects limitations not of the experimental techniques, but the inherent limitation of the LET concept itself . The recognition that the measured spectra of energy deposited are more directly related to the biological effects of ionizing radiations than the LET distributions has led to the definition of microdosimetric quantities which are stochastic in nature and correspond to the actual energy deposited in microscopic sites.

In general, microdosimetry is the study of the relationship between stochastic quantities, intended to describe the physical action of the radiation field and the observed biological effects . Theoretical considerations are given to the expression of the actual energy losses in biologically relevant volumes in terms of probability and spectral distributions . The degree of success attained with these theoretical considerations is then assessed and determined by experimental tests .

The advantage of the microdosimetric concept is that it involves the selection and setting of new physical parameters, derivation of distributions of these parameters, the design of instrumentation for measurement of the relevant distributions and comparison of the experimentally and theoretically determined physical data that represent the action of the radiation field and the biological effects produced . Brief definitions and descriptions for the fundamental microdosimetric quantities are given below.

2.2.6.1 Energy deposition event

The energy deposition event is the actual deposition of energy in the volume of interest, such as the cell, by statistically dependent ionizing particles such as recoil protons . This energy is independent of fluence rate or absorbed dose rate . However, it depends on the radiation quality and the size and shape of the atomic composition of the region of reference (ICRU, 1977) .

2.2.6.2 Lineal energy (y)

The lineal energy, y, is the ratio of the actual energy, ϵ , deposited in a volume of interest, during energy deposition event, to the mean chord length $\bar{d}$, through that volume, thus;

$$y = \frac{\varepsilon}{\bar{d}} \qquad (2.39)$$

The mean chord length $\bar{d}$, of the volume is the average length of randomly oriented chords in that volume . It is calculated according to the shape of the volume, so that for a convex body, it is equal to 4V/a, where V, is the volume, and a, is the surface area of the body; and it is equal to 2d/3, in the special case of a sphere of diameter, d (ICRU, 1977) .

The lineal energy y, is a stochastic quantity analogous to the deterministic quantity linear energy transfer, LET . It deals with the energy deposited by individual

particles and its defined only for single energy deposition events . It is, therefore, independent of the absorbed dose or dose rate . The lineal energy y, compared to its analogous LET, has significant features that make it more reliable radiation measuring system so far . The lineal energy y, is subject to the geometrical cut-off unlike the LET which is subject to the energy cut-off .The lineal energy y, is defined without reference to track structure, therefore it is applicable even to tracks with ranges less than the mean chord $\bar{d}$, whereas the LET applies to a differential track element which is small compared with the range of the directly ionizing particle .

In analogy to the two types of distributions in LET (section 2.2.1.5) two different distributions of lineal energy, y, can be defined . These are the distribution of the frequency of events in y, (y_F), and the distribution of absorbed dose in y, (y_D) . If F(y) is the distribution function of y, and is the fraction of events which lead to values of lineal energy up to y; then the probability density f(y), is the derivative of the sum of distribution, F(y) with respect to y, (i.e differential distribution of y), hence,

$$f(y) = \frac{dF(y)}{dy} \qquad (2.40)$$

f(y) is also known as the lineal energy distribution and it is independent of absorbed dose or its rate (ICRU, 1983) .

The expectation value of the lineal energy $\bar{y}_F$, which is also called the frequency-

mean lineal energy, is deterministic quantity and it is given by;

$$\bar{y}_F = \int_0^\infty y f(y) dy \qquad (2.41)$$

similarly, the dose distribution of lineal energy can be defined as the dose probability density d(y) . It is the derivative form of D(y), the fraction of absorbed dose delivered with lineal energy less than or equal to y, hence;

$$d(y) = \frac{dD(y)}{dy} \qquad (2.42)$$

Similarly, the expectation value $\bar{y}_D$, of the dose distribution in y, can be derived

the same as in equation (2.41) . This is known also as the dose-mean lineal energy and it is a deterministic quantity .

2.2.6.3 The specific energy imparted (z)

The specific energy imparted z, is the energy ε, imparted by ionizing radiation to a region of interest in a matter divided by the mass m, of the matter in that region, thus;

$$z = \frac{\varepsilon}{m} \qquad (2.43)$$

The specific energy is a stochastic quantity analogous to the deterministic quantity the absorbed dose . Values for distribution and averages similar to that of linear

energy transfer (section 2.2.1.5), can be defined for the specific energy, z .

Relations between the lineal energy y, and the specific energy z, as well as between their distribution and averages, can be derived for the same size of energy deposition events such as the same single event . Thus, using equations (2.39) and (2.43);

$$y = \frac{m}{d}.z \qquad (2.44)$$

Now it is clear from the definitions of the above microdosimetric quantities that microdosimetry provides a means to obtain experimentally defined and measurable quantities which can be utilized in place of the ones which cannot be so defined and measured, such as LET and absorbed dose . This is an objective criterion that cannot be dismissed . Therefore, when the dosimetric calculations are restricted to idealized situations which are out of touch, the conventional experimental microdosimetry contributes effectively as a check against the calculations and as an independent means of verifying the validity of a particular calculation system (Kliauga, 1990) .

Furthermore, in the case of a practical application where the radiation is usually not well known in terms of type and flux of all particles making up the field, the experimental microdosimetry is invaluable as a means of characterizing the radiation field in question in terms of microdosimetric quantities . This can be done with a single measurement of a microdosimetric spectrum as opposed to multiple

measurements required to identify energy, type and flux of all particles constituting the radiation field needed for calculation of track structure .

Although within the historically well known limitations of the experimental microdosimetry are the inability to make useful measurement in simulated tissue regions smaller than about 200 nm, and the restriction to measurements in gas phase, it is possible now to extend measurements down to less than 5 nm simulated target site sizes (Grosswendt et al , 2000) and in operational gaseous nanodosimeters down to the DNA level (Tamboul et al, 2000) . This simply means that the primary experimental difficulties of the conventional microdosimetry are different from those encountered in extending such measurement to regions of the order of nanometres (Kliauga, 1990) .

2.3 Limitations of the conventional dosimetric quantities

There are several serious limitations to the present system of dosimetry (Watt, 1990) . These limitations are mainly due to the limitations in the fundamental quantities used as the specifier parameters for quality and quantity of radiation . Of these, the most primary parameters are the linear energy transfer LET, dose D, relative biological effectiveness RBE, and the quality factor, Q .

2.3.1 Limitations in the linear energy transfer (LET)

The limitation of the concept of linear energy transfer LET, as a radiation quality specifier, has been recognized and debated for a long time . It has become

apparent that the concept of LET distributions of dose has certain limitations, such as statistical fluctuation in its values, change in the LET along the track and lateral extension and curvature of tracks which is assumed to be linear according to the definition of LET that states a linear value of loss of energy locally absorbed . Rossi has discussed these limitations as early as 1959 (Rossi, 1959) .

The inherent limitations of the LET concept itself is also reflected through the impossibility to measure its distributions using experimental techniques (ICRU, 1977) . The difficulty with the LET spectra is that it does not contain information on the rate of change of LET along the track and there is no unique relationship between fluence and LET distributions when several types of particles are present (ICRU, 1970) . Therefore, and due to the fact that the fluence spectrum contains more information than a whole set of LET spectra, the distribution of fluence in energy is more fundamental than LET distribution as a basis for theoretical analysis of radiation studies .

LET and its distributions serve only as an approximate specification of quality . It has been shown that different radiations with the same d(L) do not produce the same biological or chemical effects . This is due to the fact that LET is defined on the idealized assumption that particles travel in straight tracks of negligible width with continuous deposition of energy (ICRU, 1986) . In practice, deposition of energy is discrete, the tracks are not straight and they make curvatures at their ends, specially for electrons . This affects the mean energy deposition that either

increases if the radius of the curvature is comparable to the dimension of the sensitive volume site, or the LET concept becomes meaningless if the radius of curvature is comparable to the interaction mean free path .

LET is an average quantity, and as a quality parameter, it does not allow for the variation of the path length of the particles passing through the volume of interest . The LET concept does not allow also for energy straggling along the particle track .

The LET concept as a quality parameter, does not allow for fluctuations in the number of particles which may penetrate a sensitive structure when a medium is irradiated . The fluctuations may be also due to the discrete nature of radiation energy deposition events . LET and its distributions which are based on the continuous slowing down approximation, do not make allowance for these stochastic processes which become important particularly when very small biological sensitive sites are involved in the process (ICRU, 1978) .

Although the manner by which the energy is transferred, such as in elastic collisions and transfer of energy by ionizing collisions, can cause biological effects, LET as well as the other energy based parameters, do not consider this fact . This makes the LET for a specified radiation, non-single valued parameter . As an example, the energy transferred through elastic collision differ clearly from that transferred by ionizing collision even for particles of

the same type and the same LET (ICRU, 1970) .

However, the LET represents the first moment of the energy transfer in a collision, where as the dose weighted restricted LET ($L_{D,100}$) is a second moment of the restricted energy transfer (Watt, 1994) . $L_{D,100}$, is related to the specific ionization density, which is a volume density quantity . Therefore, the LET and its distributions are volume quantities and are not suitable parameters for quality specification although the LET is indirectly incorporated in the currently recommended system of dosimetry.

2.3.2 Limitations in the absorbed dose (D)

The absorbed dose as the central parameter for radiation field quantity specification in the present system of radiation dosimetry, is also a limited concept . Its value determines only the mean energy absorbed per unit mass in an irradiated medium (ICRU, 1977) . Thus, the absorbed dose is one of the dosimetric quantities which are physical point functions that vary continuously in space and time (ICRU, 1978) .

Furthermore, the specification of the absorbed dose does not account for the microscopic distribution of the absorbed energy . The discrete nature of radiation necessitates the use of stochastic quantities that represent some values of quantity for a small region of irradiated material . However, since the dose is simply the product of the LET and charged particle fluence, any arguments against LET

are equally valid against dose (Watt et al, 1994) . Therefore, it is widely accepted that the dose is an inadequate parameter for quantification of biological effects of ionizing radiations .

2.3.3 Limitations in the relative biological effectiveness (RBE)

As the definition of the relative biological effectiveness RBE, is related to the absorbed dose D, of the low-LET radiation, it always involves ambiguity in radiological consideration . That is because all the low-LET radiations do not have an equal biological effectiveness . This makes the choice, of the type of radiation employed as a reference radiation in the definition of RBE very important (ICRP, 1989) .

The RBE of a given type of radiation depends on the distribution of LET and on a variety of factors, mainly related to the absorbed dose involved, which may influence the actual value of RBE observed . In neutron radiotherapy, the specification of radiation quality related to low-LET radiation has practical limitation due to the dependence of RBE on neutron energy .

The most prominent limitation of the parameter RBE, as a radiation quality specifier, is that it cannot be correlated, for different biological end-points, onto a single curve when expressed as a function of LET . Consequently, different quality factors are required for different radiation types (Watt and Kadiri, 1990) . In general, if the LET and the absorbed dose are inappropriate parameters for

quantification of radiation effects, then the relative biological effectiveness, RBE, must also be inappropriate .

However, for better representation of the biological effectiveness of radiation, the RBE, which is given as the ratio of the radiosensitivity of the test radiation with respect to the reference radiation for the same biological end-point, could be replaced, advantageously, by the ratio of the respective cross-sections for induction of the end-point of interest (section 3.1.2) .

2.3.4 Limitation in the quality factor (Q)

Referring to the way the quality factor Q, has been defined relative to the absorbed dose (section 2.2.4.2), and thus to the LET parameters, it can be noticed that Q, was chosen arbitrarily from a synthesis of RBE values for a given radiation (ICRU, 1983) . It was also empirically fitted to a functional relationship with the unrestricted linear energy transfer L_∞, in water, that has no fundamental basis . This means that other choices of Q, values dictated by different higher values of RBE at low doses will necessitate different empirical relationships . Furthermore, the selection of Q values for different types of radiation, is a matter of judgement taking into account appropriate value of RBE values (ICRP, 1989) .

2.3.5 Limitations in Dose Equivalent (H)

In section (2.2.4.3) it has been stated that although the quantity dose equivalent, H, represents an attempt to correlate the effectiveness of any radiation field in a

unified field, still there are serious limitation to its application both theoretically and practically (Watt et al, 1987) . These limitations are due to various reasons such as to the subjective judgement involved in the degree of in-built safety factor; the requirement that the radiation type be known; the necessity for different types of dose equivalent instrumentation for different types of radiation fields, the relative nature of Q, and RBE; the generally poor unification achieved because different particle types with the same LET, and therefore the same Q values, can have different biological effects .

All these reasons hinder the use of dose equivalent as a parameter for absolute radiation dosimetry .

2.3.6 Limitations in the conventional microdosimetric quantities

Historically, the limitations in the conventional microdosimetry are well known . One of these is the inability to make useful measurements in simulated tissue regions smaller than about 200 nm (Kliauga, 1990) . The traditional microdosimetric quantities in their present applications, are limited to irradiated regions of down to 1 μm . Therefore, measurements are not possible for regions substantially smaller than 1 μm, unless good understanding of the mechanisms of radiation action down to nanometric target site sizes is achieved (ICRP, 1989)

Another limitation in the conventional microdosimetry is the restriction to the

measurements in gas phase . However, the reasons usually given that an ordinary proportional counter will not operate at pressures low enough to simulate some tens of nanometres, are well known . These are the inadequate gain and an extension of the avalanche region into an appreciable fraction of the collection volume . The difficulties of the gain can be solved, now, using a multi-step avalanche, parallel plate system (Tamboul et al 2000) . The system can effectively solve both the gain and avalanche problems and for the first time enables single and multiple charges, released in a 2 nanometre sensitive volume, to be assessed in an operational instrument .

Since the employment of microdosimetry, as applied conventionally in biology, is linked to the assumption concerning target size, target structure and radiation mechanism of action, the limitations in the application of microdosimetry are mainly due to shortcomings in the model and are probably not due to inadequacies in the basic concepts of microdosimetric quantities themselves . These microdosimetric parameters provide information not easily available from a knowledge of absorbed dose and LET alone . Their greatest value is that they can make possible predictions concerning the size of critical structures when experimental biological data for different radiations are taken into account and thus help in the identification of the mechanisms of radiation action (ICRU, 1970).

Although the reported dependence of target sensitive site size on radiation type

casts doubt on the general validity of microdosimetry, as an attempt to surmount these problems, the role of the number and type of interactions has been investigated rather than the gross transference of energy (Cunningham et al, 1982) .

2.3.7 Limitations in the weighting quantities

The new quantities introduced and defined by the ICRP as weighting factors such as the tissue weighting factor w_T, and radiation weighting factor w_R, are meant to replace quantities and factors which are already being defined relative to either the absorbed dose or LET . These new quantities are intended for use by ICRP in specifying dose limits . However, they cannot be used in a coherent system of quantities or in accurate calculations . This is due to the introduction of the weighting factors, such as w_R, (section 2.2.5.3) which numerical values are specified with reference to the radiation incident on the body, taking no account of the location of the organ in the body or its orientation (Jennings, 1994) . Furthermore, the indirect relation of these weighing factors to the generally inappropriate parameters LET and dose, make them questionable factors as the specifier of parameters for radiation protection .

As a conclusion to the limitations reviewed above, one can note that there are several serious limitations to the present system of dosimetry (Watt, et al, 1990; Simmons, 1992) . The consequences of these limitations can be summarized in the following points;

i) there is necessity for quality factors as dose-modifying factors due to the lack of knowledge about the exact nature of radiosensitive sites and physical mechanism of radiation damage .

ii) Correlation of RBE's for different biological end-points onto a single curve is not possible when expressed as a function of LET .

iii) The absence of a single-response characteristic hinders any attempt to design a universal, absolute dosimetry, and construction of instrumentation that would be used in any field of radiation without any foreknowledge of the radiation type . The physical instrumentation used in the traditional system of dosimetry is severely limited in its capabilities, as it must, always be designed for known types of radiation or particles . Dosimeters so designed and constructed, they typically measure physical quantities such as absorbed dose and effective dose . They do not measure the bio-effectiveness, which is the desired quantity in radiation protection or radiobiological applications .

iv) Although the current system of dosimetry can be useful and adequate for particular purposes, such as for external radiation exposures, it is inapplicable in the case where damage by inhaled or incorporated radionuclides needs to be expressed . Furthermore, in the present system of radiation measurements, no allowance is made for size and multiplicity of the critical biological radiosensitive sites known to exist in cell nuclei nor for the stochastic nature of the particle interaction .

To overcome these serious limitations in radiation dosimetry, first a proper understanding of radiation action on radio-sensitive targets is needed . Then a reliable approach is required, which could suggest a suitable radiation damage model that can be translated into an absolute measurement system for the biological effectiveness of the ionizing radiation .

The following chapter reviews the different approaches which have been suggested towards a satisfactory means of radiation measurement, leading to a unified method of radiation dosimetry .

CHAPTER THREE

APPROACHES FOR UNIFIED DOSIMETRY

In the preceding chapter it has been shown that the energy based parameters are seriously limited, with regard to their role in quantification of the bio-effectiveness of the ionizing radiation . Such limitations in the conventional dosimetry system create inherent difficulties in adapting the conventional dosimeters for use as absolute detectors within a unified system . These difficulties emphasise the unsatisfactory nature of the basic premises involved in the present system of dosimetry and raises significant doubts about the validity of the scientific basis of the system . If the validity of these long established quantities is to be questioned, then it is necessary to explore for better alternatives (Watt, 1988) .

The difficulties with the currently accepted system of dosimetry lie in our lack of knowledge of the basic mechanisms of radiation action and our consequent inability to specify the radiation quality in absolute terms (Watt et al, 1987) . If this could be done, the construction of a unified system should be relatively easy although its practical implementation may not be as simple . Design of new instrumentation will then be required to comply with the fundamentally new concepts . Therefore, a better system of specification of radiation action would be required . Hence, identification of the main physical mechanisms responsible for radiation damage is necessary to improve our understanding of radiation effects

in radiation biology, protection and therapy .

In the following sections of this chapter, first, an alternative method of quantification of radiation effects will be discussed, followed by a review of some of the different approaches suggested for the achievement of a unified system of radiation bio-effectiveness and its measurement . Also included in this review are brief critical remarks on modelling the relevant radiation action leading to an appraisal of the most response function for instrumentation which should be capable of the absolute measurement of radiation bio-effects .

3.1 Particle track and damage mechanisms

An effective method of quantifying the bio-effectiveness of the radiation action, is to use the charged particle tracks in the radiation field to explore the radiosensitive structures of nanometre size within the mammalian cell nuclei to identify physical track structure parameters which are descriptive of the quality of the ionizing radiation of interest . The results can be combined into a unified model of absolute bio-effectiveness which can be applied to any type of ionizing radiation (Watt, 1997) . The test criterium used here is the ability to unify bio-effect data onto a single curve for a wide range of radiation types for any specified biological end-point .

In an attempt to identify the physical quantities which are appropriate for the specification of radiation quality in biological systems, Watt and co-workers have

conducted a series of investigations by re-analysing published information on the biological effects of different types of radiation . To obtain guidance on the most appropriate means of specifying the quantity and quality of the radiation field for radiation protection, Watt et al, 1980 and Cunningham, Al-Kazwini and Watt (Cunningham et al 1982) have investigated the role of the number and the type of interaction rather than the gross energy transference . To achieve such objectives, they studied the effect of low-energy ion interactions on enzymes in the dry state under vacuum . These studies were a continuation of investigations performed by Watt and Sutcliffe, (1975) on ribonuclease inactivation by slow heavy ions. The cross-sections for inactivation of different enzymes normalized by their geometric cross sections were correlated onto a single representative curve when plotted versus the mean chord length, $\overline{d}$, through the enzyme molecule and versus the ratio of the square of the effective charge on the particles and their velocity (i.e. z^2 / β^2) .

Parallel to their investigation on the effect of ions on the enzymes, Cunningham and collaborators have also re-analysed published radiation damage data for viruses and bacterial spores aiming for guidance on parameters which are likely to be descriptive of radiation damage to mammalian cells . They have found that, for low-energy electron irradiation, the damage is related to the number of primary events . This led to the conclusion that the radiosensitivity could be related to the mean chord length of charged particles for x-rays, gamma rays and alpha particles That was a good indication for the importance of the track-structure concept and

that the track length of the primary and secondary particles expended in the target is an important parameter .

Following the guidance of the earlier work on enzymes, viruses and bacteria, Watt and a group of his researchers (Watt et al, 1985) continued re-analysis of the published data for inactivation of enzymes, viruses, yeast and higher cells (mammalian cells) by accelerated ions, x-rays and gamma rays . The philosophy of the approach was guided by the earlier works on hit and target theory (Watt, 1975) . Intensive investigation was made and the basic data were calculated . These basic data are illustrated in figure 3.1 and described briefly in the following sections .

3.1.1 Effect cross-section (σ_e)

The microscopic effect cross-sections for the induction of the radiation effect were extracted from the dose survival curves with the assumption of unit density and the use of the formula;

$$\sigma_e = \frac{1.6x10^{-9}\bar{L}_T}{D} \qquad (3.1)$$

where $\bar{L}_T$, is the track average LET in keV/μm for the relevant charged particle energy spectrum; and D is the absorbed dose in gray taken either with reference to a percentage survival fraction, such as 37%, or taken as the value of D_0, the slope of the dose-response curve at high doses .

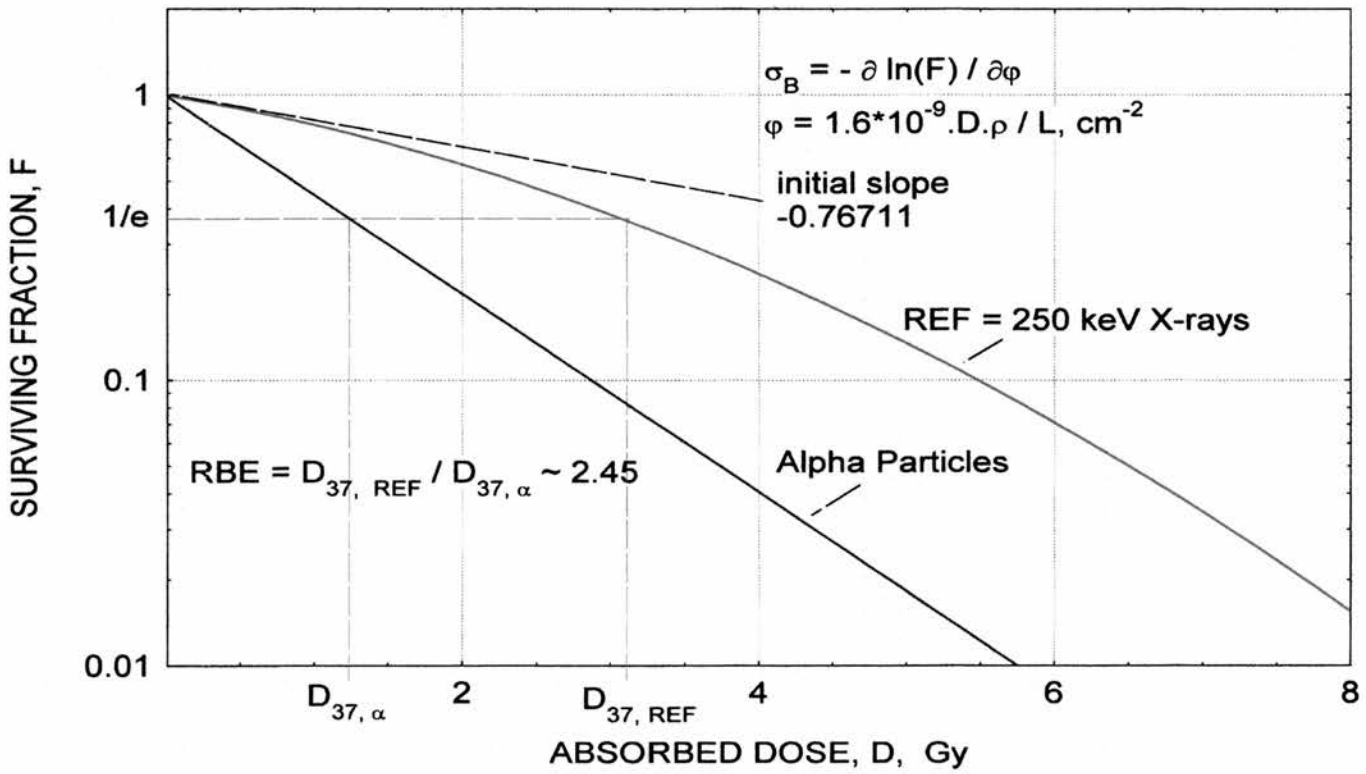

Figure 3.1: A typical observed dose-survival curves used for the extraction of the basic data for the study of the radiation action in mammalian cells .

The effect cross-section is an absolute measure of bio-effectiveness for the end-point of interest at a point (Simmons and Watt, 1999) and it is related to the slope of the survival curve at that point so that,

$$\sigma_e = -\left(\frac{\partial \ln F}{\partial \Phi} \right) \tag{3.2}$$

where F, is the survival fraction $\partial\Phi$, is the charged particle fluence at equilibrium, which is related to the absorbed dose at a point through the formula,

$$\Phi = 6.25 \times 10^8 \frac{\rho D}{\overline{L}_T} \tag{3.3}$$

where ρ, is the density of the medium (g/cm^3)affected by the radiation and it is taken as unity for soft tissues .

Equations (3.1) and (3.2) show that the effect cross-section (probability of lesions per unit fluence) can be expressed either as a function of absorbed dose or the fluence .

3.1.2 Relative Biological Effectiveness (RBE)

In the preceding chapter (section 2.3.3) it has been stated that for the limitation of the RBE concept, it would be possible that the definition of RBE be replaced by the ratio of the respective effect cross-section for induction of the particular end-point of interest . Watt et al, 1985 have calculated the RBE of radiation type 1 with respect to the reference radiation type 2 using the formula;

$$RBE_{1,2} = \frac{\sigma_1}{\sigma_2} \cdot \frac{\bar{L}_{T,2}}{\bar{L}_{T,1}} \qquad (3.4)$$

The ratio of the average track LETs reintroduces the dependence of RBE on energy deposition . However, the simple ratio of effect cross-section is a more fundamental measure of relative effectiveness of radiation . Indeed, in practice, the effect cross-section by itself serves as an absolute measure of the effect per unit fluence and making equation (3.4) redundant .

3.1.3 Basic physical data of ions and electrons

The results of data for the accelerated ions and electrons were calculated for liquid water of unit density . The linear primary ionization I_i, is one of the vital parameters for specification of quantities for unified dosimetry . For the accelerated fast ions, it can be deduced, to a good approximation over the whole energy range, using the following formula (Watt et al, 1985);

$$I_i = \frac{L_\infty}{(\bar{T}_\delta + w)} \qquad (3.5)$$

Alternatively, it can be calculated using the formula,

$$I_i = k\frac{z^2}{\beta^2}\left(\frac{1}{I_1} - \frac{1}{T_{\delta,max}}\right) \qquad (3.6)$$

where w, is the mean energy required to produce an ion pair, and I_1, is the mean

ionization potential for water . The value of both w, and I_1, are taken to be 30 eV for water . $\overline{T}_\delta$, is the frequency weighted average energy for the delta ray spectrum z, and β, are the effective charge and velocity of the ions respectively; and k, is a constant equal to (0.0153 Z/A) where Z/A, is the ratio of the atomic number of the accelerated ion to its mass number .

The linear primary ionization I_i, for electrons at energies greater than 10 keV is calculated as,

$$I_i = \frac{0.3387}{2\beta^2} \ln(2.325 x 10^4 \beta^2) \qquad (3.7)$$

The progress which has been achieved in experimental and theoretical studies of charged particle track interaction has enabled accurate calculations down to energies (~ 15 eV) at the end of the particle range . Therefore, the prediction of radiation effects at low energies became possible .

3.1.4 The intrinsic efficiency for radiation damage

As the biophysical mechanism of radiation damage to mammalian cells by fast ions has been already investigated by Cannell and Watt (1984), Chen and Watt (1986) have extended their investigation and re-analysed published survival data for X-rays and gamma-rays, ranging from 1.25 MeV to 300 eV, to gain information on the intrinsic efficiency for damage per particle track of electrons in mammalian cells . They calculated in this investigation various basic data including the charged particle effect cross-section for X-rays and γ-irradiation of various types of

mammalian cell .

The effect cross-section is calculated using equation (3.1) and utilizing the collated track average LET for the electron equilibrium and the absorbed dose, D_0. Here, the effect cross-section values were normalized to a compromised numerical nominal value of 5×10^{-7} cm^2 taken for the geometrical cross-section, σ_g, of the radiosensitive sites in the cell nuclei . This normalization gives the ratio (σ_e / σ_g) of the effect cross-section to the geometrical (or saturation) cross-section to represent the intrinsic efficiency σ_R, for the particular damage . Therefore, the geometrical cross-sections σ_g, are normalizing factors representative of the radiosensitive sites for killing of the different cells and bio-molecules . For example, for simpler targets such enzymes σ_g, is taken as the whole bio-molecule. For viruses it is assumed to be the whole system less the projected area of the surrounding protein coat (Cunningham, 1982) . For highly organized cells, such as yeast, plant and mammalian cells σ_g, is an uncertain quantity . However, Watt et al (1986) and Watt (1989) have taken this geometrical cross-section σ_g, to be the projected area of the intra-nuclear DNA .

The logarithmic graphical representation for the intrinsic efficiency for damage of the photons of all energies versus the track average LET, or the mean linear primary ionization $\bar{I}_s$, gave a linear relationship indicating that either of the latter two parameters is a satisfactory quality parameter . However, when comparing

these results with those for heavy fast ions, (Cannell and Watt, 1985), the linear primary ionization is clearly superior to the track average LET .

Although good correlation can be obtained of electrons, photons and neutron data with dose restricted LET (Virsik et al 1983), which bears a proportional relationship to specific primary ionization, it is in the wrong dimensional units to permit direct identification of the idea of the critical spacing between the strands of the double stranded DNA bio-molecule (Chen and Watt, 1986) .

The intrinsic efficiency per delta ray yield (or per primary ionization) σ_R/I_s, have been also calculated for the equilibrium electron spectra . The results of this calculation and the collation showed that the intrinsic efficiency for damage per delta-rays generated by electrons entering the cell nucleus is approximately constant independent of both the track average LET and the mean primary ionization . This shows that electrons cannot produce significant damage unless they are at the end of their tracks and if they come to rest in the cell nucleus (Bartels and Harder, 1990) .

An example of the basic survival data calculated by Chen and Watt (1986) for various mammalian cells irradiated by X-rays and γ-rays is given in table (3.1) . The content of the table which has been adapted for the purpose of the review here, contains some of the basic data they obtained by re-analysing survival data for V79 cells from different references found in the literature . It can be noticed that

while the calculated data of the intrinsic efficiency, σ_R, shows progressive changes with the change in the energy of the photons, the efficiency per delta ray yield, σ_R/I_S, approximately remains constant . This confirms that the bio-effect of delta-rays is not significant .

Jawad and Watt, 1987; Watt and Younis, 1987 have extended their investigation to include inactivation of metalloenzymes by characteristic X-rays and Younis and Watt, 1987 and 1990 have studied the quality of ionizing radiation emitted by radionuclides incorporated into mammalian cells first in 1989, and then into E.colli and bacteriophages in 1990 .

Table 3.1: The basic survival data for V79 cell (Effect cross-section σ_e, intrinsic efficiency σ_R (i.e σ_e/σ_g), track average LET, L_T, linear primary ionization I_s, and the ratio of the efficiency per delta-ray yield (σ_R/I_s) . The data are adapted from Chen and Watt, 1986 .

E_{hv} (keV)	D0 (Gy)	LT (keV/μm)	Is (μm-1)	σe (10-8cm2)	σ_e/σ_g ($x10^{-2}$)	σ_R/I_s (nm)
1252	1.97	0.88	11.5	0.071	0.143	0.124
662	1.75	1.40	18.5	0.128	0.256	0.138
120	1.67	6.2	88	0.594	1.188	0.135
100	1.45	7.6	13	0.834	1.677	0.148
95	1.33	8.0	125	0.962	1.925	0.154
80	2.21	9.3	150	0.673	1.347	0.09
40	1.54	12.7	250	1.319	2.639	0.106
1.5	1.04	22.8	680	3.508	7.015	0.103
0.3	0.79	25.6	700	5.180	10.37	0.148

The subsequent and successive investigations by the St. Andrews radiation biophysics research group have continued for further verification of their approaches towards the unified system of dosimetry . However, up to date, progressive and intensive re-investigations were made on a wide range of data on the action of different types of radiation, such as electrons, X-rays, γ-rays, neutrons and accelerated heavy ions on various types of biological targets such as enzymes (Watt, et al, 1981); viruses and bacteria (Cannell and Watt, 1985); yeast (Jin, Watt and Kobayashu, 1994); plant (Watt,1989a) and mammalian cells (Chen and Watt 1986; Watt 1987) .

The biological effects of the radiation on these targets were re-analysed and re-interpreted for different end-points such as cell inactivation and mutation (Kadiri and Watt, 1987); chromosome aberration and dicentrics (Alkharam and Watt, 1997) and oncogenic transformation .

The outcome of these intensive studies is that , damage to the DNA by direct radiation action is the common precursor for the production of all the above mentioned end-points of radiation actions . It is concluded that the mechanism of radiation action is predominantly single track action which is most efficient when the spacing of ionizations along the track matches the spacing of the critical structure within the DNA to produce double-strand breaks (Watt and Hill, 1994).

This concludes that the mechanism of radiation damage to biological targets

depends on the numbers and spacing of paired correlated events and not on the energy imparted .

3.1.5 Cumulative probability and damage mechanism

It has been stated earlier (section 3.1.4) that the ratio of the effect cross-section, σ_e, to the geometric cross-section σ_g, of the target or the sensitive site to the radiation track gives the intrinsic efficiency σ_R, for radiation damage to the targets. However, this ratio is also known as the average cumulative probability P, of damage for induction of the biological end-point by an individual track in the relevant charged particle spectrum (Watt et al, 1985) .

To express the radiation damage mechanism in a unified system, the ratio representing the cumulative probability of damage is made using the projected area, σ_{DNA} , of the DNA content in the nucleus combined with the mean number, n_0, of DNA segment (as targets) at risk along a mean chord traversal . This combination of, σ_{DNA}, and n_0, constitutes the saturation cross-section σ_s, (section 3.2.2.2) for induction of the biological effect (Simmons and Watt, 1999) .

In figure 3.2, the cumulative probability P, of damage by a wide range of radiation, such as X-rays, γ-rays and various heavy particles is plotted against the mean free path for primary ionization which represents the mean spacing of ionization. The obtained curve gave quantitative comparison of the radiation effectiveness in

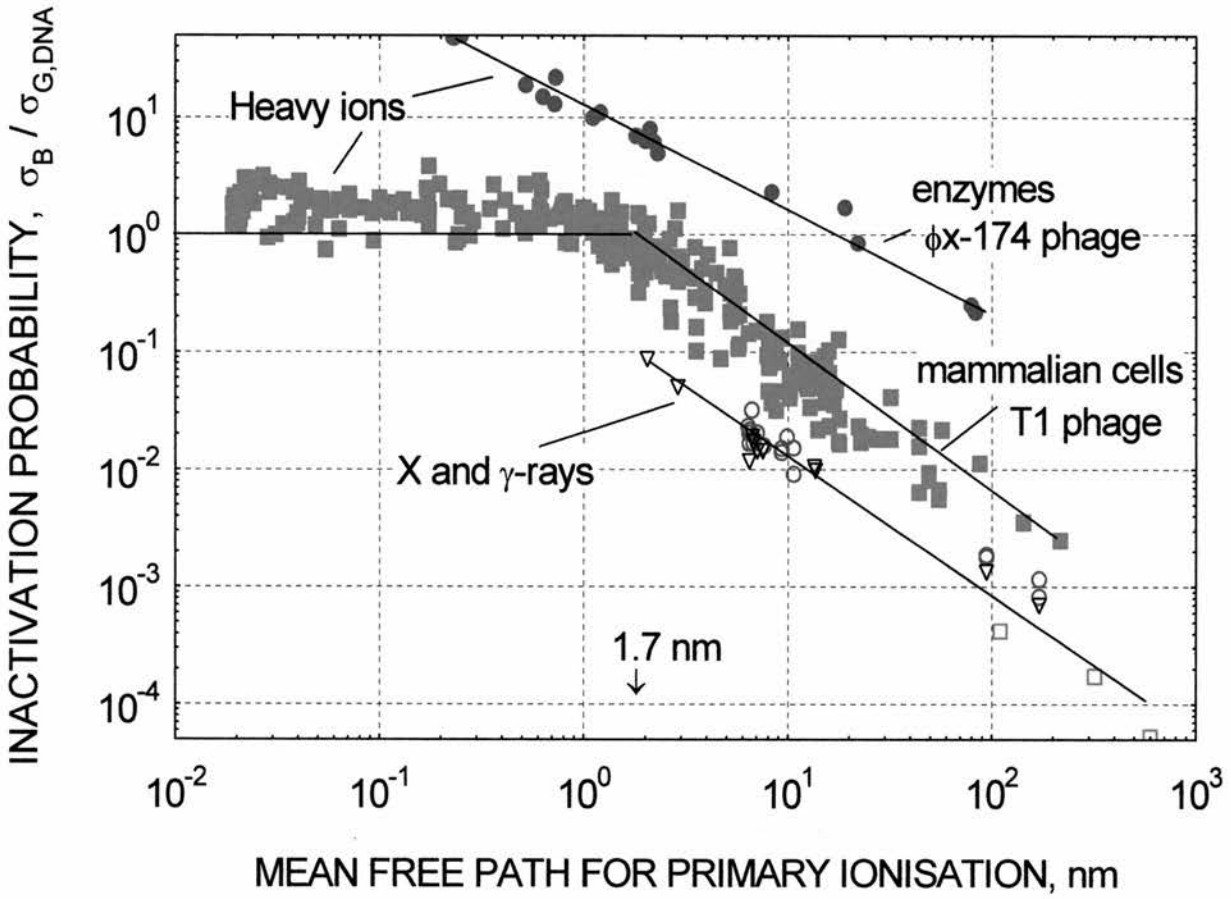

Figure 3.2: The cumulative probabilities of different types of radiation damage to different types of targets plotted against the mean free path for primary ionization .

a wide range of biological material such as enzymes, different types of bacteria, viruses and mammalian cells .

The examination of curves and data for different targets in figure 3.2, reveals three main features;

i) There is a distinct change of slope in the curve for the targets that contain double-strand DNA (mammalian cells and T1-bacteriophage) with a common nature of the point of inflection at mean free path for primary ionization of about 2 nm, a dimension that can be associated automatically with the mean chord distance across a segment of the double-stranded DNA molecule .

ii) There is no sign of structure for the curve representing the group of targets known to suffer single hit inactivation or to have single-stranded DNA, such as the enzymes, viruses and ΦX174 phage . This group represents the single-hit radiation kinetics group (section 3.2.1.1) . The cumulative probability of damage for inactivation of targets for this group, decreases with the increase in the interaction mean free path without any characteristic physical features .

iii) The intrinsic efficiencies (or the cumulative probabilities) for inactivation observed for targets containing double-stranded DNA, are much smaller compared to those observed for targets not containing double strand DNA. This suggests a more complex hit-target mechanism for the damage in double-stranded DNA targets such as the mammalian cells and T1phage.

All of these features give strong evidence that the dominant damage mechanism is caused by intra-track action in which the key lesions are double-strand breaks in the intra-nuclear DNA, the concept that has long been supported in different conceptual interpretations (e.g. Bryant, 1985 and Frankenberg, 1994) .

From these findings, it seems that the application of effect probability to the interpretation of radiation mechanisms has proved to be a very powerful technique for linking the fundamental physical processes with the biological end-point of interest and could make an important contribution to applications of radiation in various fields particularly in radiation protection, radiotherapy and radiobiology (Watt et al, 1987) .

On the basis of the foregoing results, a simulation model of radiation effects can be devised, and which can be tested against experimental data taken from the literature .

3.2 Biophysical modelling for radiation action

A model for radiation damage is a means of analysing the radiation effects on matter mainly biological material (cells) . An effective, useful model should permit the understanding of the radiation action mechanism and enable prediction of effects at low-radiation doses using data of radiation at high doses .

An important objective of modelling the radiation action is to assess the radiation

risk of biological injuries from low doses of radiation to which the population may be exposed . It enables also, to relate the biological effects in a biological system to physical parameters that help to investigate properly , the basic mechanisms of radiation action . The biophysical modelling of radiation action helps also to suggest new experimental approaches to test new ideas and predictions in various fields where the radiations are utilized such as in radiotherapy, nuclear medicine, industrial use of radiation and in radiation protection (Psilocin, 1995).

Because of the persisting difficulties in specifying radiation quality adequately well for estimation of biological effects, and the arguments that can be made against the suitability of parameters used for quantifying the radiation field, the re-evaluation of the fundamental processes involved in the damage mechanism seems always appropriate and necessary (Watt and Alkharam, 1994) . This permits progressive simulation models of radiation action to be suggested leading to a very large number of these models in the literature . In fact, the very existence of many simulation models is further support of the need for revised approaches towards a unified model for radiation effects, particularly on biological targets .

3.2.1 Types of radiation damage models

There is a large number of varied biophysical models of radiation action found in the literature, but none of these many models have been adequately successful.Of these types of models are the ones which are applied to the biological targets represented by their basic units, the mammalian cells . Most of the recent models

of the radiation actions are related to the contents of the biological cells, for example, to the DNA in the nucleus of the cell . In 1995, Psilocin reviewed different types of such biophysical models . A brief summary of some of them is given here because of their important role in the theory of the radiation action modelling and their roles as guiding tools for unified instrumentation for absolute dosimetry which is the interest of this work .

3.2.1.1 Hit and target model

For inactivation of a biological system, this model assumes particular targets in the system that must be hit (Dertnger et al, 1969) . The historical importance of this model theory relies on the fact that it is the basic component of almost all the subsequent radiation action models . It uses simple Poisson's statistical treatment and it is further categorized into single hit, single target where one hit of one target is required for inactivation . The survival fraction $F_{1,1}$, of the target population subjected to irradiation is given by;

$$F_{1,1} = \exp(-h) \tag{3.8}$$

where h, represents the mean number of hits the target has suffered, and it may be given as the function of the absorbed dose D; or the particle fluence . Thus, h = D/D_{37} = k.D, where k, is the radiosensitivity . h, may be equal to $\sigma.\Phi$, where Φ is the particle fluence and σ, is the action cross-section which is equal to $1/\Phi_{37}$, where Φ_{37}, is the charged particle fluence at 37% survival .

The second category of the hit and target model is when multiple targets are present in the cell and one hit is required to inactivate the cell . that is, Single hit, Multi-target model . The survival fraction $F_{1,m}$, for this category is given by;

$$F_{1,m} = [1 - \exp(-h)^m] \quad (3.9)$$

where m, is the number of targets .

The hit and target model may, further, be categorized as Multi-hit, Multi-target model if multiple hits are required for each of the many targets found in the cell so that its inactivation can occur . The survival fraction, $F_{n,m}$, of the irradiated population for such a model is given by;

$$F_{n,m} = 1 - (1 - F_{n,1})^m \quad (3.10)$$

where;

$$F_{n,1} = \exp(-h).\sum_{r=0}^{n-1} \frac{h^r}{r!} \quad (3.11)$$

which represents the Poisson probability of a single target surviving up to n, hits. This means that n, is the number of hits required for each of m, targets in the cell and h, is the mean number of hits per target .

3.2.1.2 Two component models

In two component model, the action of the radiation on the cells is categorized into low-LET and high-LET components .

In the low-LET component of the model, the response is assumed to follow single

hit multi-target kinetics . Here, sigmoidal survival curve is produced due to the delta-rays surrounding the track . The damage may be repairable .

In the high-LET component of the two component model, the response is expected to follow single hit single target style of action, and it is representative of a semi-empirically defined track core with pure exponential survival characteristic which is due to non-cumulative, irreparable radiation damage (Katz, 1972) . Due to the fact that, this model involves parameters depending on the LET and on radiation type and biological end-point, it is of limited value and impractical to achieve a unified system .

3.2.1.3 Dual action model

In dual action models, two different types of radiation interactions take place for the production of primary radiation effect .The first is due to intra-track action of radiation which causes the radiation lesion to be produced along an individual particle track . This is a linear component of the dose or energy deposition .

The second component of the dual action model is the quadratic action of radiation dose which is due to inter-track action where the lesion is produced by separate particle tracks each producing a sub-lesion . The yield of legions , for the dual action model can be written as;

$$Y = \alpha . D + \beta . D^2 \qquad (3.12)$$

where α, and β, are constants or coefficients . This relationship means that the intra-track action of the radiation here is directly proportional to the dose D , where as for inter-track, the radiation action is proportional to the dose squared, D^2 . The survival fraction F, for the dual action model is given by;

$$F = \exp[-(\alpha.D + \beta.D^2)] \qquad (3.13)$$

The dual action model is used for a variety of applications, depending on the target structure accounted for, such as in modelling the chromosome aberration on the basis of LET, taking the DNA as a primary target (Neary, 1965); and in the molecular theory of radiation biology for modelling the double-strand breaks in the DNA (Chadwick and Leenhouts, 1973) . Despite the fact that the model has been used for a variety of these applications, still the dual action model suffers from serious limitations and some forms of these limitations have been discussed by Simmons and Watt, 1999 . One example of the limitations they discussed, concerning the dual action models, is the dependence of the constants and coefficients such as, α, and, β; on the radiation quality mainly for the factors and parameters which are expressed as functions of LET or dose-weighted mean values, such as the specific energy, z_D, in the distance model of the dual action of radiation used in microdosimetry (Kellerer and Rossi, 1978) .

3.2.2 A model for the absolute bio-effectiveness of radiation

Many attempts have been made to improve the understanding of the basic mechanisms involved in radiation damage to mammalian cells by developing

theoretical models but with only limited success . If a model is to be of value in guiding the design and specification of instrumentation, it must be able to express the action of a wide range of radiation types for a variety of biological end-points in unified manner which enables logical physical simulation of the real biological response .

Following the foregoing results of their investigation, Watt and his researchers have made simple initial attempt to model the process of radiation damage in the light of their findings . In devising this initial model, no account was made for variation of sensitivity during the cell cycle, indirect action or temperature effects (Watt, 1988) . The models devised were first for direct action of the radiation (Watt, 1989a) and mainly for low dose of heavy particles and neutrons . However, the successively followed modelling of Watt's group have been extended on a conceptual basis where the radiation damage to double-stranded DNA by single charged particle track are presumed to be induced by three mechanisms (Younis, 1989);

i) Direct primary interaction with two neighbouring strands (spaced 2 nm) in the DNA segment .

ii) Direct action on one strand combined with indirect action on the other strand due to chemical species diffusing from the track (mixed action) .

iii) Indirect effects on both strands due to diffusing species from a track in close proximity to the sensitive targets (Watt and Hill, 1994) .

3.2.2.1 The Absolute Biological Effectiveness (ABE)

The absolute bio-effectiveness of radiation on any type of biological cells, such as the mammalian, can be defined in terms of the effect cross-section, σ_e (section 3.1.1) . The product of the effect cross-section and the equilibrium fluence of charged particles Φ_{eq}, defines the absolute bio-effectiveness B, (Watt, 1989a), hence;

$$B = \sigma_e \Phi_{eq} \tag{3.14}$$

B, also represents the mean number of unrepaired double-strand breaks per cell produced in the DNA by the charged-particle radiation .

The survival fraction of the irradiated cells can be obtained by combining the factors above using Poissons relationship, that is;

$$F = \exp(-B) \tag{3.15}$$

3.2.2.2 Calculation of the absolute bio-effectiveness

The absolute biological effect of the radiation can be defined from the proposed model in terms of three biological parameters; the geometrical projected cross-sectional area of the DNA; the cell cycle time; and a mean recovery time for the double strand breaks in the DNA; and two physical parameters, viz, the charged particle equilibrium fluence and the average mean free path for primary ionization for the equilibrium energy spectrum of charged particles .

For the calculation of the bio-effectiveness in the extended model of radiation action suggested by Watt and co-workers, the model is in more general form applicable to three common types of irradiation situations (Watt and Kadiri, 1990);

i) External irradiation by charged-particle beams .

ii) Internal irradiation by α-, β-, and γ-emitters homogeneously distributed in the medium or as radionuclides incorporated into cells .

iii) External irradiation by indirectly ionizing radiations under the conditions of charged particle equilibrium .

In the latest version of Watt's model of radiation action (Watt, 1997), additional factors were taken into account, that are generally considered to govern the shape and magnitude of the survival curves . These factors are, the duration of irradiation; the nature of the cell population, whether it is synchronised or asynchronised; and the link to the position in the cell cycle that decides the changing radiosensitivity in progression through the cycle .

To calculate the biological effectiveness of radiation damage to mammalian cells, the unrepair function $U(z,t_m,t_r,t_i)$, is expressed for synchronised and asynchronised cell population, for specified damage fixation time t_m; repair time t_r; and irradiation time t_i, then;

a) For synchronised cell population;

$$U(z,t_{m,r,c,i}) = \frac{1}{t_i}\int_{t_c}^{t_c+t_i} Z(F,t)\exp\left[-\frac{(t_m-t)}{t_r}\right]dt \qquad (3.16)$$

b) For asynchronised cell population;

$$U(z,t_{m,r,i}) = \frac{1}{t_i}\frac{1}{t_m}\int_0^{t_i}\int_0^{t_m} Z(F,t_j)\exp\left[-\frac{(t_j - t)}{t_r}\right]dt_j dt \qquad (3.17)$$

Z(F,T), is an approximate function which takes into account the change in radiosensitivity during cell cycle (Sinclair, 1972) . it is a function that represents a modifier to the mean number of DNA segments at risk per unit fluence [given by U(Z,t).$\sigma_{g,DNA}.n_0$]; t_i, t_m, are respectively, the irradiation time and the time (at mitosis) at which damage is considered fixed; t_r, is the mean time taken to repair 63% of the lesions and it is equal to (1 - 1/e); t_c, is the time into the cell cycle, at which the irradiation begins and it applies to a synchronised cell population only .

For the conceptual calculation of the model, the absolute biological effectiveness can be expressed using equation (3.14), that is; $B = \sigma_B.\Phi_{eq}$, where B, is the absolute bio-effectiveness; Φ_{eq}, is the charged particle fluence at equilibrium condition; and σ_B, is the effect cross-section which is given by;

$$\sigma_B = \sigma_s.\varepsilon_{dsb}(\bar{\lambda}).U(Z,t) \qquad (3.18)$$

and;

$$\sigma_s = \left[\sigma_{g.DNA}.n_0.\frac{\bar{R}}{\bar{d}}\right]; \qquad \frac{\bar{R}}{\bar{d}} \le 1 \qquad (3.19)$$

where σ_s, is the saturation effect cross-section (section 3.1.5); $\sigma_{g,DNA}$, is the projected geometrical cross-sectional area of DNA (about 3 μm); n_0, is the

number of double-stranded DNA segments at risk per track traversal (about 15); R , is the mean projected range of the relevant tracks; d , is the mean chord length through the cell nucleus (about 7 μm); $\varepsilon_{dsb}(\lambda)$, is the efficiency for production of double strand breaks in the DNA by direct and indirect actions and it is given by;

$$\varepsilon_{dsb} = \left[1 - \exp\left(-\frac{(2\Lambda + s)}{\lambda}\right)\right]^2 \qquad (3.20)$$

where Λ, is the mean diffusion length in the immediate vicinity of the DNA molecule for active radicals (indirect action); s , is the thickness of a single strand of DNA (approximately 1 nm); λ, is the mean free path for linear primary ionization .

The bio-effect cross-section can be written as the cumulative probability, P, which is the ratio of the effect cross-section σ_B, and the saturation cross-section, σ_s (Watt, 1997) .

3.2.2.3 Testing the absolute bio-effect model

To test the validity of the model, the single-track damage mechanism is put under test . The values of the absolute bio-effect cross-sections, calculated using equation (3.18), were compared with the experimental measurements randomly selected from the literature . These measurements were made at different laboratories for different types of radiation, such as X-rays, gamma-rays, accelerated heavy ions and neutrons .

The extent of unification achieved in this comparison was tested graphically by using the calculated absolute bio-effect cross-section as a function of the mean free path for linear primary ionization λ, for the charged particle spectrum of interest . The best unification was obtained in this comparison when lambda λ, is used as the quality parameter instead of the traditionally accepted quality factors including the track average LET .

Figure 3.3 illustrates the degree of correlation attainable between the bio-effect cross-sections for some types of mammalian cells (Chinese hamster, V79 cells) and the mean free path for primary ionization as quality parameter . The figure shows that the data is found to be separated into two curves, one for electrons and photons; and the other for heavy particles including neutrons . Interpretive argument can be made that the two curves are linked by the multiplicity of biological targets at risk for a charge particle traversal of the cell nucleus (Simmons and Watt, 1999) .

In figure 3.3 the ratio of bio-effect cross-section (the absolute radiation quality) for heavy charged particles to that of electrons is seen to be approximately 15 to 1 for the same frequency weighted spacing, λ . Allowance for this multiplicity of sensitive sites at risk, enables all the data for mammalian cells to be unified into a single curve .

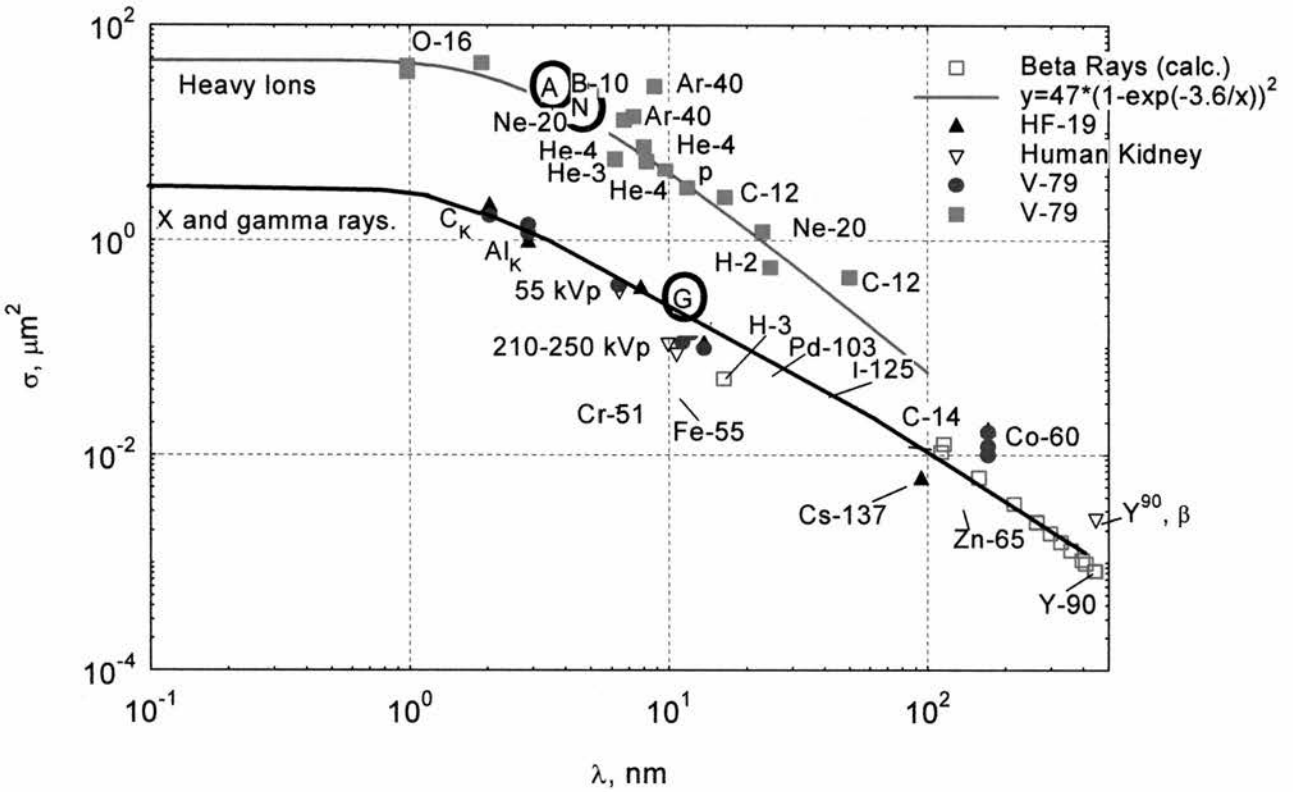

Figure 3.3: Bio-effect cross-sections for inactivation of mammalian cells by different types of radiations, as a function of the mean free path, λ, for linear primary ionizations . Marks A, N, and G; are the experimental data of the present nanodosimeter for α-particles, neutrons and photons irradiation respectively (see section, 5.5) .

Although the points of the experimental data are, somewhat dispersed, the solid curves described by the equation (3.18) represent a suitable response function for the desired radiation detector, the nano-detector (section 6.1) . So as to make comparisons between these results and that of the experimental measurements made using the present nanodosimeter, the points A, N and G are marked, coinciding to the experimental data for α-particles, neutron and photon irradiation respectively (section 5.5) .

3.2.3 Bio-effectiveness and fluence-based risk control

From the conclusion reached in the foregoing analyses, the fluence-based approach constitutes a system in which the field quantities to be measured are the equilibrium charged particle fluence, and the bio-effect cross-section . Both of these quantities can be determined simultaneously by designing appropriate instrumentation with the correct response function that will simulate the response of the double-stranded DNA segment .

On the basis of the bio-effectiveness and fluence system proposed for the unified system of dosimetry in radiation protection, an improved system of dose limitation based on fluence can be devised for better radiation risk control . To compare the new risk control system proposed for radiological protection, Watt, 1997 has transposed the effect cross-section into radiosensitivity by dividing the effect cross-section by the kerma factor, which can be calculated using equation 2.26, and plotted against particle and photon energy . This permits the ICRP weighting factor

be superimposed for comparison . The significant differences in the effectiveness per unit equilibrium fluence as a function of photon energies for X-rays, γ-rays, fast electrons and neutrons is appropriately quantified in figure 3.4 .

However, it can be noticed that the new system of risk control gives a smooth curve compared with the ICRP step function . The new system has also additional advantages such as its scientific validity, offering unified dosimetry and absolute measurement . Above all, the system has got the privilege of the scalability from inactivation to other biological end-points (Alkharam and Watt, 1997) . The applicability of the system in radiotherapy, nuclear medicine and radiological protection permits absolute measurement without the need to know the radiation type .

As a conclusion to the prospect of defining the new unified fluence-based system of dosimetry, a conceptually new instrumentation design and construction will be necessary to have a radiation response simulating that of the nanometre sites (Colautti, 1994), possibly a segment of the DNA . The system would then be more rigorous and meaningful than the currently accepted system of dosimetry . A new family of desired detectors could be defined with particular optimum physical characteristics .

3.3 Characteristics of the detector for absolute dosimetry

In the light of the foregoing findings, attention should be focussed on the design

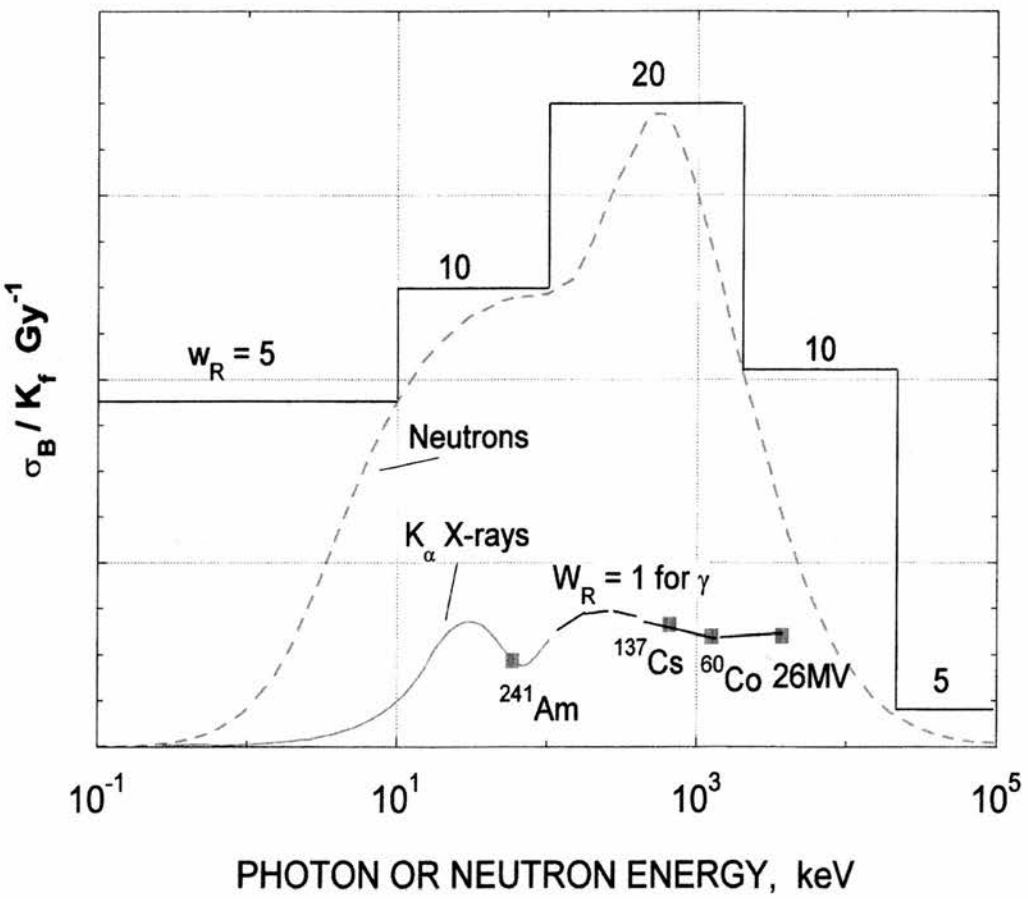

Figure 3.4: The bio-effectiveness per unit equillibrium charged particle fluence plotted as a function of the energy of different radiations .This permits the ICRP weighting factors to be superposed for the comparison.

of instrumentation with a response function which, in principle, should enable direct measurements of absolute bio-effectiveness . Such desired detectors have general requirements and physical characteristics that would make them true simulators of radiation bio-effectiveness in mammalian cells .

3.3.1 General requirements for absolute detectors

More realistic measurements can be made if the absolute detector can record the frequency of events that result from interaction of radiation with the biological targets such as the number of double strand breaks in DNA . Thus, ideal detectors for absolute dosimetry measure stochastical numbers of events and not energy imparted.

For operation and implementation in absolute dosimetry, the desired detectors should provide pulse height spectra . The pulse height of the individual event, in this case, should be proportional to the ratio of the observed bio-effect cross-section to the saturation effect cross-section (σ_e/σ_s), which represents the cumulative probability of radiation damage (section 3.1.4 and 3.1.5) . The number of events per pulse height interval corresponds to the cumulative probability represented by the ratio (σ_e/σ_s) per interval of (λ_0/λ) . The integral of the response spectrum (IRS) of such detector to radiation of mean free path λ, is given by;

$$IRS = \Sigma \frac{\sigma_B}{\sigma_s} \left| 1 - \exp\left(-\frac{\lambda_0}{\lambda}\right) \right| \Phi_s \qquad (3.21)$$

where λ_0, is the mean chord through the double-stranded DNA segment, and it is equal to 1.8 nm; Φ_s, is the charged particle fluence related to the saturation effect cross-section.

Accordingly, the integral of the area under the peak of the single radiation spectrum depends on its mean free path λ, and charged particle fluence . For radiation beam composed of more than one component, multiple response peaks will be produced superimposed on each other resulting in a more broadly-peaked spectrum . When $\lambda = \lambda_0 = 1.8$ nm, the cumulative probability can be made equal to unity, thus making the integral of the response spectrum of an ideal detector to be a direct measure of the absolute bio-effectiveness of particular radiation.

The implication of the foregoing is that the net absolute biological effectiveness of a mixed radiation field must be simply given by the integral of the response spectra . This means that direct additivity of the net biological effectiveness should be possible without foreknowledge of the constituents of the mixed radiation field .

To simulate the response of the double-stranded DNA segment to ionizing radiation, within mammalian cell nuclei, ideally paired sensors would be required each of dimension 3 nm X 1 nm, and spaced at 2 nm . Each sensor must be capable of detecting single ionization . These sensors may be, for example, the sensitive volumes of the gas-filled detector or the scintillation centres in the

scintillators system . The events for which coincidences occur in each strand of the paired sensors are the significant events .

The mean number of paired sensors at risk along a mean chord track through the dimension of 6 micron, which is the diameter of the cell nucleus, should be about 15 . A simulated array of cells may be required to compensate for the extrinsic efficiency of such detector .

Due to the probable practical difficulties in the design and operation of such detectors, some interpretive scaling may be needed when the detector is allowed to operate in single sensor detection mode .

3.3.2 The physical characteristics of the desired detector

The desired detector for the absolute measurement of bio-effectiveness should satisfy particular physical requirements so that it can be suitable for simulation of the effects of radiation on the DNA segment (Kadiri, 1990) .

a - The interaction of the ionizing radiation with this simulating volume(s) in the detector should produce charges which should be properly controlled, oriented, conveniently processed such as being amplified and then collected ensuring sufficient resolution to the obtained useful signal .

b - If the threshold level of radiation interaction with the unified dosimeter is supposed to be 30 eV (Watt et al, 1985), for double strand break (dsb), the noise level and the associated background of the device should

be far less than this value so that all the interaction of radiation equal to or below this threshold should be detectable . However, external amplification of the signal obtained and internal multiplication increase signal-to-noise ratio for the detector .

c - One of the most essential physical requirements of the detector desired for the absolute dosimetry is that the signal or the result obtained at the collection points of the detector should be related linearly to the interaction events occurring in the simulating volume .

d - A high degree of uniformity would be required in the detector where the interaction processes take place so that with the stochastic processes of radiation interactions, the ultimate resolution of the detector could be obtained (Alkhazov, 1970) .

e - The interaction coefficient of the detector medium through which the charged particle should pass to be detected, must be equivalent to that of the tissue namely, the DNA bio-molecules . This is to ensure that the detector operation will be under the charged particle equilibrium conditions .

f - For a meaningful simulation of the response of the DNA to radiation, the response of a desired detector should be reasonably fast to correspond to the very short time that will be required for the radiation to traverse the nanometric segments of DNA . Therefore, coincidence resolving times, when applying the coincidence techniques with such detectors, should be within the nanoseconds or even less .

g - The unified, absolute dosimetric system desired here is supposed to be an operational system in radiation protection and therapy fields . Portability, reproducibility, good tensile strength and readiness and simplicity of its operation are therefore some of the desired physical and general properties

These general requirements and physical characteristics for the desired detector should be met by the choice of a suitable detection system . The potentialities and abilities of various detecting approaches are briefly discussed and assessed in the following sections in an attempt to compare and match their potentialities to the required characteristics of the detector for unified dosimetry .

3.4 Possible approaches for absolute detection system

To fulfil the requirements of the desired detection system for absolute dosimetry, Watt and co-workers have considered various approaches of detection system that could be possibly utilized for the unified system of dosimetry proposed here . The detectors can be broadly categorized into; solid based; liquid based or gas based detectors . As a guide for the design and production of instrumentation for absolute measure of bio-effectiveness of radiations, very brief accounts and remarks will be given in the following sections on some examples of these categories of detection systems . Detailed accounts, description and remarks will be given for few of them, that may be much or less related to the present work . The objective here is to realize the suitable and appropriate parts of their potentialities for the absolute nanodosimetry (Baum, 1974) .

3.4.1 Solid based detectors

The solid based radiation detectors are the instruments that use solids as their detection media . Some technical areas have been suggested and developed by Watt and his research group so that they may be applied successfully to the design and construction of radiation detectors that can meet the need of simulating nanometric volumes in the solid phase . Examples of these areas are; the amorphous semi-conductors; supper-conducting junction devices and organic scintillators .

As most of these suggested nanometric device approaches require specialist expertise with expensive technological facilities, the organic scintillators may be the most convenient approach . It has, therefore, been briefly described as an alternative for the gaseous nano-devices adopted in this work .

3.4.1.1 Organic scintillators for nanodosimetry

Studies have been conducted by Watt and his group of researchers to investigate the potentials of the solid organic scintillators for absolute dosimetry (Watt and Alkharam, 1995) . The object is to utilize the scintillation properties of fluor molecules in organic (plastic) phosphors to simulate the response of mammalian cells to ionizing radiation . The mean of the random distance between the active centres in the crystalline lattice of the scintillators can be modified to simulate the sensitive sites of nanometre volumes, such as the DNA segments in the mammalian cells .

The competition of the sensitive sites in scintillators for production of scintons and excitons is analogous to the competition in production of double strand breaks by the direct radiation action and indirect radiation actions through the diffusion of radicals in mammalian cell nuclei .

To simulate the yield of initial radiation damage by double strand breaks in the DNA, Watt and Alkharam, 1995 have determined the scintillation photon yields and the distribution of activated centre pairs in a scintillators, and their relationship to the biological effectiveness . The efficiency for double strand break production ε_{dsb}, has been determined so that;

$$\varepsilon_{dsb} = \frac{Y_{pr}}{Y_{hv}} \tag{3.22}$$

where Y_{pr}, is the total yield of scintillation photon pairs from the scintillators, analogous to the double strand breaks in the DNA; Y_{hv}, is the total yield of photons from the scintillators .

The cross-section for induction of simulated biological effect, σ_B, is determined by a simple ratio of the average yield of photon pairs from the scintillators, that represents the double strand breaks in the DNA segments, to the total equilibrium particle fluence, hence;

$$\sigma_B = \frac{Y_{pr}}{\phi_i \Sigma_k w_k \mu_{tr,k} \Phi_{T,eq,k}} \tag{3.23}$$

where $\phi_i w_k \mu_{tr,k}$, is the concentration of electrons generated by an initial incident photon fluence ϕ_i; and $w_k \mu_{tr,k}$, is the fraction by weight w_k, of the mass energy transfer coefficient for the constituent element type k, of the phosphor material; $\Phi_{T,eq,k}$, is the total equilibrium fluence per unit concentration of primary electrons produced by the interaction of X-rays and γ-rays in component element of k, of the phosphor .

Although the approach of the scintillators for the absolute dosimetry is a promising one, there are some problems to be surmounted before the real success could be declared . Of these;

i) The difficulty to detect single photons above instrumental noise and backgrounds .

ii) The difficulty in the use of minimal thickness so that the stochastics of the emitted signal will permit identification of the number of photons required (1 to 20) for proper simulation .

iii) The dependency of light output on the particle type may lead to difficulty in absolute and unified simulation of radiation damage arising from different types of radiation .

iv) Detailed studies and investigation are required on the optimum concentration and distribution of fluor molecules to improve simulation of the key radiosensitive features and separation of the components of event sizes for estimation of the probability that two hits will occur on the sensors

pair of the scintillators to produce simulated equivalent of double-strand break .

However, the scintillation choice is the most probable alternative approach for an absolute system of radiation measurement . Furthermore, there is a good possibility of combining the gaseous detection system of approach adopted in this work with the scintillation method of detection that can be applied at the signal collection stage of the gas-filled gridded proportional counter used as the approach for absolute nanodosimetry here (section 6.3.1) . This is particularly promising approach due to the possibility of including the hybrid diode in the combination for precise detection of single electron signals .

3.4.2 Liquid based detectors

Liquid based radiation measuring devices are not uncommon, since liquid ionization chambers have been widely used in the study of charged particle transport in liquid inert gas and organic liquid (Capollini et al, 1977) . Chaar, 1998, has intensively investigated the principles of liquid radiation detectors and the possibility of their application in absolute radiation nanodosimetry system . Tetramethylsilane (TMS) is a familiar example of the organic liquid di-electrics used for radiation dosimetry (Nakamura et al, 1980) . Tetramethyl pentane is another liquid of particular interest in making liquid ionization chambers and proportional counters because it is almost tissue equivalent for photons and neutrons and it has high dielectric strength, electrons with relatively long lifetimes

in the range of microseconds and high velocities of about 3 X 10^5 cm/s .

Despite the fact that the liquid based radiation detectors would be claimed as the most appropriate approach for the simulation of tissue equivalent conditions and the condensed phase requirements, there are well-known limitations to liquid based radiation measurement devices . This is true, in particular, if it is to be suggested as the basis for absolute measurements of bio-effects of radiation . Of these limitations are;

i) Difficulty in saturation collection of charges due to recombination problems (section 4.4.2), which is more prominent in liquids .

ii) The difficulty in the permanent maintenance of the purity of the liquid combined with the need for high purity of the liquid for the improvement of charge transport and to avoid the loss of electrons in impurity traps .

iii) The presence of polarisation traps associated with the large organic molecules of liquid in high applied electric fields . This limits charge transport in the liquid.

3.4.3 Gas based detectors

The instrumentation in this category of detection system uses various types of gases as the detection medium . Examples of this would be; the gas scintillation proportional counters; the traditional gas-filled proportional counters; the multi-step avalanche counters; ion recombination detectors; and variance and variance-covariance detectors . Of these, the first three examples are of greater concern

with the present work, therefore, they are briefly remarked upon here . In particular, the latter two examples of the first three are the core of the approach adopted in this project, hence they have been allocated a separate space (chapter four) where they have been intensively investigated and discussed in detail .

3.4.3.1 Gas scintillation counters

This category of gas based counters is a combination of gas proportional counter with gas scintillators as the counting medium (Policarpo, 1977) . The advantages of the gas scintillators over the solid and liquid scintillators are that the former give better resolution and linear light response with increasing radiation energy .

There are some limitations and disadvantages concerning the gas scintillators systems as an appropriate method for absolute dosimetry . The main limitation of the scintillation system is that very few noble gases are efficient scintillators . Therefore, this hinders and limits the choice of the counter gas and tissue equivalent conditions .Their emission in the UV region of the spectrum causes more complicated wall effects . Accordingly, the gas scintillation proportional counter may not be appropriate for nanodosimetry .

3.4.3.2 The gas-filled and multi-step avalanche detectors

These category of the detectors depend, for their operation, on the basic principles of the traditional gas-filled proportional counters used in microdosimetry. In

principle, all gas based ionization detectors can be used at low-pressure to simulate small volumes such as those of sensitive sites in the mammalian cells .

Although most of the criticisms levelled against the gas based system of detectors are based on the original proportional counters (Rossi's type), most of the disadvantages can now be solved . For example, the criticism of the lack of adequate multiplication and yet with sufficient uniformity of response through out the detector volume can be achieved by different approaches, such as the use of gridded parallel electrode arrangement with uniform applied electric fields instead of the traditional cylindrical proportional counters (section 4.6 and 4.7) .The simulation can be made down to 2 nm, that is, at the DNA level (Tamboul and Watt, 2001) .

The problem of the wall effect commonly associated with gas-filled detectors with solid walls can be effectively overcome by the use of new techniques such as the combination of plane electrode configuration with the use of multi-stage amplification regions . The latter arrangement, in addition to its fundamental role of multiplication of charges (section 4.7), separates the detection region from the multiplication regions, and thus reduces the wall-effect .

However, the multi-step avalanche detectors operated at very large gas-gain can be considered as the modern version of the traditional gas-filled proportional

counters and ionisation chambers and have been successfully applied to radiation measurements (Charpak and Sauli, 1978) .This arrangement has therefore been adopted in the present work for its versatility and flexibility . Accordingly, it will be intensively and critically reviewed in chapter four to explore its applicability in nanodosimetry .

CHAPTER FOUR

CRITICAL REVIEW OF GAS-FILLED DETECTORS

4.1 Introduction

There are different mechanisms whereby measurement of radiation can be carried out . Of these, ionization and excitation in the measuring media such as in gas-filled radiation detectors are typical . These consist of chambers filled either with pure or mixed counting gases located between two or more electrodes . A potential difference is applied between the electrodes so that one, the anode, is positively charged and the other, the cathode, is negatively charged, thereby creating an electric field between the electrodes . The interaction of the radiation with the gas creates ion-pairs so that each detected particle or photon produces a number of electrons and an equal number of positive ions . These charges together constitute a charge pulse, in a pulse type chamber, or a current, in an integrating type chamber . The electrons are attracted to and collected by the anode while the positive ions are collected by the cathode recording one event .

There are many varieties and types of gas-filled counters . The best known are the oldest, traditional gas counters namely, ionization chambers, proportional counters and Geiger-Muller counters . The three detectors are classified according to the well known operational regions of the curve obtained in the study of the relationship between the output of a gas-filled detector and the high voltage applied to its electrodes (Tsoulfanidis, 1983) . Figure 4.1 illustrates the

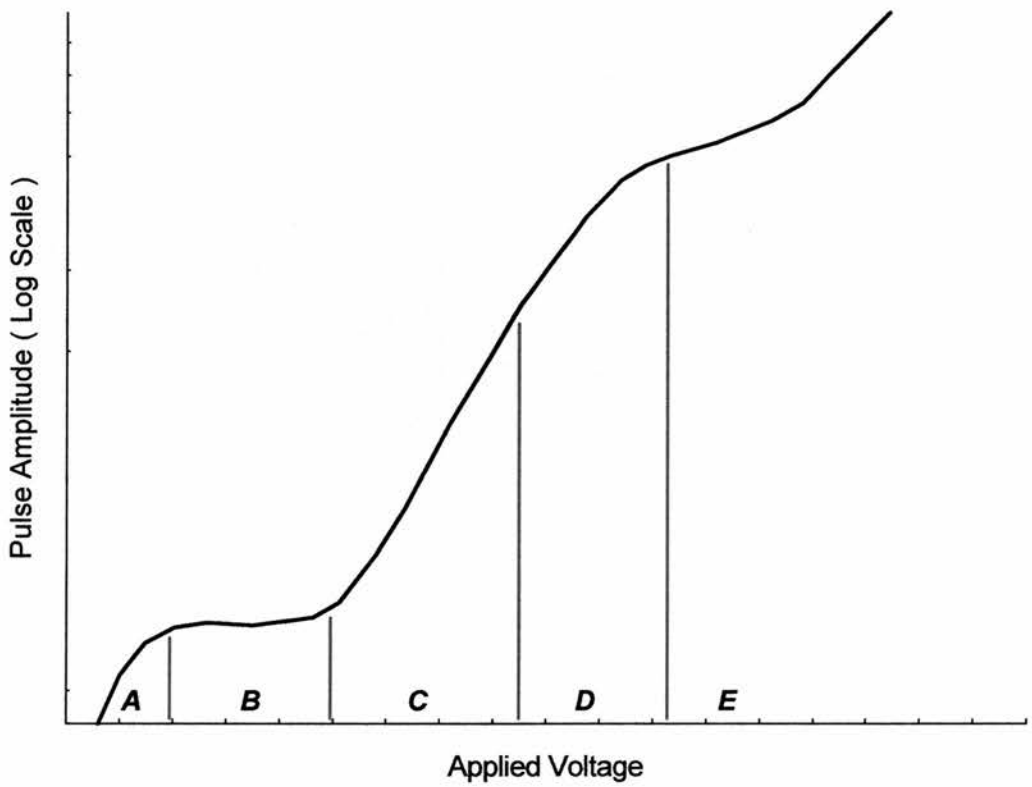

Figure 4.1: Diagram of the curve relating the output pulse of a gas-filled detector and its applied voltage . A, is the recombination controlled region; B, is the ionization chamber region; C, is the proportional counter region; D, is the limited proportionality region and E, is the Geiger-Mueller region.

relationship between the amplitude of the observed pulse from such a detector and the high voltage applied to it . The curve reveals distinctive operational regions .

1- At very low values of the applied voltage, the electric field is insufficient to prevent recombination (section 4.6.2) of the original pairs of charges . Therefore the charge collected is less than that represented by the original ion pairs (region A , figure 4.1) .

2- At region B, the effect of recombination is suppressed with the rise in the applied voltage, and thus the electric field, and a pulse equal to the total collected charge (ion saturation) will be registered . This region represents the operation mode of ionization chamber .

3- Further increase in the applied voltage will create enough electric field that will initiate the multiplication of the primary charges, and eventually the linearity of the gas amplification is reached so that the collected charge is proportional to the number of the original primary ion pairs created by the incident radiation . This region (C, in figure 4.1) represents the operation mode of the proportional counter .

4- Increment of the applied voltage above the true proportionality region will lead to non-linearity which is mainly related to the slow positive ions which are created with each secondary ionization process . These processes alter the electric field which magnitude governs further multiplication . This region of the curve, represented by D, in figure 4.1, is the limited proportionality region . The pulse still increases with the increased number of the initial

pairs of the primary ions, but with the loss of linearity .

5- Region E, in figure 4.1 represents the operation mode of Geiger-Mueller counter . The sufficiently high applied voltage makes the effect of the space charge, due to the positive ions produced in the ionization processes, the dominant determinant of the subsequent output pulse of the device which will then, be of the same size regardless of the number of primary ions formed by the primary particles .

6- Region of continuous discharge follows the Geiger-Mueller region as the applied voltage is increased sufficiently to make the secondary processes continue to discharge giving several pulses in rapid successions instead of single definite pules .

These gas-filled counters can be constructed in any of the three basic geometries, (parallel plate, cylindrical or spherical) each configuration with its own particular characteristics . More detailed consideration of each type of these detectors will be given in section 4.3 .

4.2 Electric fields in gas-filled ionization detectors

The electric field created in the gas-filled detectors depends on the geometry of the particular detector . It is uniform in a parallel-plate chamber with strength E, equal to;

$$E = \frac{V_0}{d} \qquad (4.1)$$

where V_0, is the potential difference between two electrodes with a separation

distance d, between them . In a cylindrical chamber, the voltage is applied to a very thin wire stretched axially at the centre of the cylinder . The wall is usually grounded . The electric field in such a chamber is given by;

$$E(r) = \frac{V_0}{r\ln(b/a)} \qquad (4.2)$$

where a, is the radius of the central wire; b is the radius of the counter; r is the axial distance from the centre of the counter . Equation (4.2) shows that the electric fields inside a cylindrical counter can be very strong close to the central wire . Therefore charge multiplication can be more easily achieved in a cylindrical gas counter than in a simple parallel plate one .

In a spherical gas counter, the voltage is applied to a small sphere located at the centre of the counter . The wall of the counter is usually grounded. Then the electric field is given by;

$$E(r) = V_0\left(\frac{ab}{r^2(b-a)}\right) \qquad (4.3)$$

where a, is the radius of the central sphere; b, is the radius of the counter; r, is the axial distance from the centre of the counter .

A strong electric field could be produced in a spherical counter, but a detector of this type of geometry is not popular due to the construction difficulties . A counter with a gas at a particular pressure may be operated at any region of the familiar characteristic curve of the gas detector, depending on a combination of the following parameters :

1- dimension of the counter cathode .

2- dimension of the central anode wire of the cylindrical counter.

3- The type of counting gas used .

4- The gas pressure at which the counter is operated .

5- The magnitude of the voltage applied to the detector .

4.3 Characteristics of the gas-filled counters

It has been mentioned in section 4.1 that there is a wide variety of gas-filled counters, most of which are of traditional design . Of these, the ionization chambers, proportional counters, and Geiger-Muller counters are typical categories . Each of these relies principally on derivation of an electronic output signal which originates from the motion of the ion pairs formed by the ionizing radiation in the gas filling of the detector . Each category of detectors does this in somewhat different ways. In the following sections, the properties of the three categories of gas-filled detectors will be discussed with the intention of identifying features which will have the potential of development as nanodosimeters and which will have the capability of serving as absolute devices for the measurement of the radiation bio-effectiveness (chapter 5) .

4.3.1 Ionization chamber

Ionization chambers have been used to observe ionizing radiations since the 1900's . They have been used to detect and to measure the intensity of UV radiation, X-rays, cosmic rays and all kinds of nuclear radiations. They were an essential tool in the early study of X-rays and they have continued in use for monitoring the ambient flux of radiation to which laboratory workers may be

exposed . Together with proportional and Geiger counters, they were a valuable means of radiation detection in the early days research into nuclear structure . These gaseous detectors declined in importance because of the development of more useful and convenient detectors such as the scintillation counters of the mid-1940's and the solid state detectors of the late 1950's (Fulbright, 1979) . In the 1960's, ionization chambers were principally used in nuclear laboratories to monitor radiation; for routine assay of radioactive samples and for serving simply as energy detectors .

The gas-filled detectors, including ionization chambers, became the typical types of detector needed for application in the new field of heavy ion physics, which had become a lively area of research in the early 1970's, when many accelerators could provide high quality energetic ion beams . Ionization chambers were the most convenient for application in this field for several reasons such as;

1 - The range of heavy ions is small, hence low gas pressures and thin windows are convenient.

2 - Ionization chambers can be made into different sizes, large or small with more freedom in choice of geometry, that is either in parallel-plate, cylindrical or spherical form .

3 - They can be made by standard workshop techniques.

4 - Normally they are not subject to radiation damage.

5 - They are cheap to operate and maintain .

6 - They are stable in operation.

As a consequence of these, many systems of radiation detection with ionization chamber components have been built and successfully used .

4.3.1.1 Pulse formation in ionization chambers

In order to explore the most suitable characteristics of ionization chambers for possible application in the measurement of the radiation bio-effectiveness, it is essential that the way in which the pulse is formed in these devices when exposed to radiation be well understood . The analysis of the formation and shape of the pulse in an ionization chamber is similar for all the geometries i.e parallel-plate, cylindrical or spherical . The results for cylindrical and spherical counters are slightly different because the electric field is not constant in these two as is the case in parallel-plate devices . For derivation of the pulse, many factors should be confirmed such as the electric fields which should be sufficient to avoid recombination of ions (section 4.6.2) .

Consider a parallel-plate ionization chamber, and assume that one electron-ion pair is produced at a distance x_0, from the collector of the chamber . The negative charge of the ion pair should remain as free electrons . When the initial electron and the ion start moving in the electric field of the chamber, the signal for the initial portion of the pulse can be derived, assuming that at this stage, all of the ion pair components drift towards the appropriate opposite electrode (Wilkinson, 1950). The changing voltage output of the chamber V_R, is represented by;

$$V_R = \frac{n_0 e}{dC}(v^+ + v^-)t \qquad (4.4)$$

where n_0, is the number of the original ion pairs; e, is the electronic charge; C, is the capacity of the chamber system and v^+ and v^- are the drift velocities of the positive ions and the electrons respectively and t, is the time during which the ions

drift in formation of the signal . The drift velocity (v^-) of the electron is a few thousand times greater than the velocity (v^+) of the ion . Typical values of these velocities are approximately 10 m/s for ions and 10^6 m/s for electron . Therefore, the typical values of the arrival times of the ion pairs, each to its opposite electrode, are approximately, in milliseconds for the positive ions to reach the cathode and some microseconds for the electrons to reach the anode (Tsoulfanidis, 1983) .

Equation (4.4) shows that the signal voltage (V_R) changes linearly with time . When the electrons reach the collector, all of their charge will be induced on the collector electrode, but due to the fact that the positive ions are not yet all collected, the magnitude of the pulse at the collector will be dependent on the space charge created by the slow positive ions . This magnitude will be equal to the charge collected by the collector minus the induced charge divided by the capacitance of the chamber (Bunemann et al, 1949) . However, when the time it takes the positive ion to reach the cathode is greater than the time it takes the negative electron to reach the collector, the signal is given by;

$$V_R = -\frac{n_0 e}{Cd}(x_0 - v^+ t) \qquad (4.5)$$

When the positive ions reach the cathode, the signal reaches its maximum negative value i.e;

$$V_R = V_{max} = -\frac{n_0 e}{Cd}x_0 \qquad (4.6)$$

The derivation of the pulse obtained above, is carried out under the assumption that all the ion pairs are created at the same distance (i.e $x = x_0$) from the

collector . In fact, in the real situations, the incident radiation track creates ion pairs over a wide range of positions within the chamber . Therefore, the final pulse will be the result of the superposition of many pulses with different electron arrival times at the collector. This means that the pulse heights obtained on the collector due to electron collection, depend on the orientation of the track and the position where the ion pairs are created .

The pulse obtained above is not suitable for counting individual particles, as needed in the nanometric modelling adopted here . That is because it does not decay quickly enough . A pulse type counter should produce a signal that decays faster than the average time between the arrival of two successive particles . Practically, the method used is to "chop off " the pulse at a time equal to the arrival time of the electrons at the anode collector . The signal is then fed to an electronically shaping circuit, which is the first stage of the preamplifier application. The disadvantage of the signal obtained as the result of "chopping off " of the pulse is that its maximum value depends on the position where ionization was produced . This disadvantage and the geometrical dependence of the pulse amplitude can be corrected or reduced to negligible importance by several ways, one of which is the use of a gridded ionization chamber (section 4.4), in which the collector is screened electrically from the entire volume in which the particle tracks are formed.

4.3.2 Proportional counter

The proportional counter is a gas-filled counter in which, when the electric field

exceeds a certain value (Figure 4.1), the electrons moving in such a field acquire, between collisions, sufficient energy to produce new ions which in turn will produce more ions . The net effect then is the gas multiplication, gain or amplification . To achieve the high field intensity needed for gas multiplication without excessive applied voltage, chambers operating in proportional counter mode are traditionally cylindrical with a very thin wire stretched axially at the centre of the counter . Then the electric field of such geometry can be calculated using equation (4.2). The successive avalanche of ionization will be then generated migrating towards the direction of the electric field . The gas multiplication factor M , which is equal to the total number of free electrons produced in the counter when one ion pair is produced by the incident radiation, can be calculated as follows;

$$M = \frac{N}{1 - \delta N} \qquad (4.7)$$

where N, is the total number of electrons set free per primary electron-ion pair; δ, is the average number of photoelectrons produced per ion pair generated in the counter . The gas multiplication factor M, is strongly dependent on the applied voltage and the pressure of the gas in the counter and the type of gas used . Figure (4.2) shows that M, increases almost exponentially with applied voltage (Tsoulfanidis, 1983) . The strong dependence of M, on applied voltage can be reduced by adding a small amount of a polyatomic, organic quenching gas in the counter, e.g a mixture of 10% Methane and 90% Argon . Such quenching gases stabilize the operation of the counter by reducing the effect of the secondary process, that is in addition to the control of the drift velocities in the counting gas . The total charge, Q, produced in a proportional counter is;

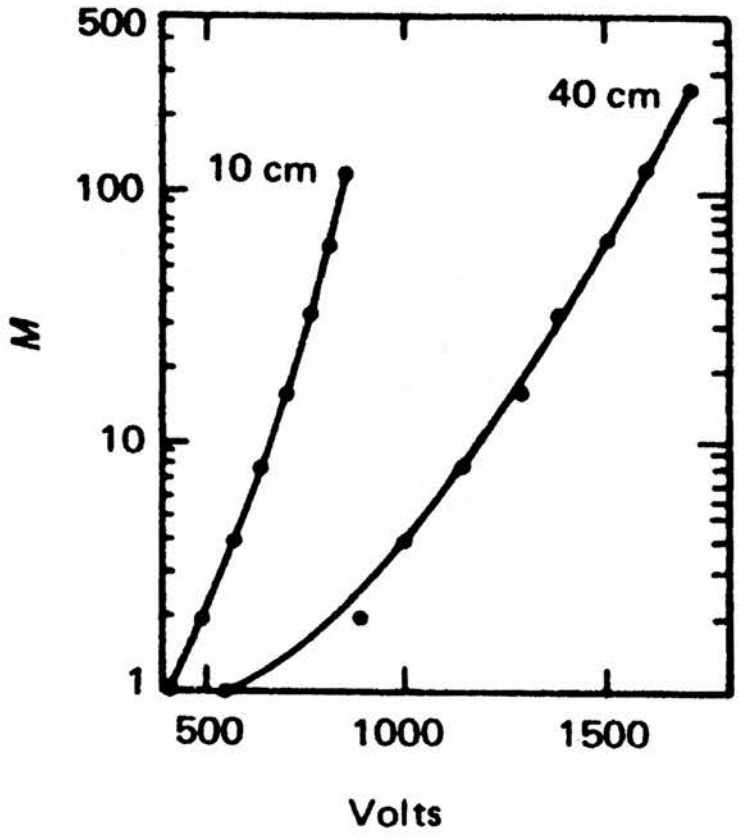

Figure 4.2: Gas multiplication factor M, versus collector voltage in a proportional counter . The factor M, strongly depends on the applied voltage, pressure and type of the gas used in the counter (Tsoulfanidis, 1983).

$$Q = MNe = M\frac{\Delta E}{W}e \qquad (4.8)$$

where ΔE, is the energy of the incident particle dissipated in the counter; W, is the average energy required to produce one ion pair . Equation (4.8) indicates that the output charge Q, is proportional to the number of the original ion pairs (ΔE/W) created by the incident radiation in the counter, leading to the name given to such counters as proportional counters (Knoll, 1983) . This proportionality holds only if the gas amplification factor, M, remains constant, independent of the primary ionization . This is true provided the space charge caused by the positive ions does not modify unduly the electric field formed in the counter . The magnitude of the space charge is a function of the primary ionization and the gas multiplication . If the primary ionization is very small, the value M, may be 10^5 to 10^6 before the space charge affects the proportionality . And if the primary ionization is large, the critical value of M, is small . There is a critical maximum value of the charge produced by the multiplication process beyond which proportionality does not hold. This value depends on the counter size and the type of the counting gas used .

The final multiplication factor M, is statistical in nature and will show statistical fluctuations . The probability P(M), that the multiplication will have the value M, is given by;

$$P(M) = \frac{1}{M}\exp\left(-\frac{M}{\overline{M}} \right) \qquad (4.9)$$

where $\overline{M}$, is the mean multiplication factor .

The phenomenon of the space charge dependency of the output signal of a proportional counter can occur in any geometry of gas counter, such as plane parallel-plate, cylindrical or even spherical counter (Rose, 1941) . The use of a gridded type of counter can help to reduce the effect of such geometrical dependency.

4.3.3 Geiger Müller (G. M) counter

In this type of gas-filled counter, a single initial ion pair is enough to produce a complete discharge, due to high secondary electron cascade, so that the output signal amplitude is no longer a measure of the initial ionization . This type of counter operates at very high, strong electric fields (figure 4.1), so that δN in equation (4.7) is approximately equal to "1" and thus the amplification factor M, becomes extremely high (Tsoulfanidis, 1983) . The GM devices are of great utility that results from their several characteristics, the most important of which are the high sensitivity for use with different type of radiation, wide variety of shapes and windows, large size of the output signal and reasonable cost . However, the independency of the magnitude of its output signal creates the disadvantage that it is not proportional to the primary ionization and therefore, not suitable for the measurement of absolute bio-effectiveness . A more detailed account is given about the successive discharge of GM counter by Wilkinson (1950) . The various methods used to solve the consequent problems of such continuous discharge (e.g the different quenching methods) are discussed also, so that the counter could be useful in application . These disadvantages together with the long dead time of such counters make them unsuitable for the count of single charge

spectra, the method which is the basis of, and the key factor for, nanodosimetry adopted in this work .

The review of the mechanism of pulse formation given in the previous sections, and analysis of the signal produced in gas-filled ionization counters have shown the desirability of having a chamber in which the output signal does not depend on the track position or orientation within it . It has been shown that the phenomenon of the space charge dependency of such output signal is not a desirable one and that the electric field in the counter should be uniform and homogeneous, specially at the charge collection volume of the chamber . Although most of the desirable characteristics mentioned above could be achieved by the use of co-axial cylindrical geometry in proportional counters, it will be shown in section (4.4) that, the most reliable way of creating these is with a parallel-plate chamber incorporating a third electrode (a grid) that will enable the introduction of a multiplication system in the chamber . That will, in turn, satisfy the requirements for the conditions of a proportional counter that can be used to investigate the qualities needed for nanodosimetry .

4.3.4 Parallel-plate and cylindrical ionization chambers

Parallel-plate ionization chambers have been used, historically, for efficient determination of energies of fast charged particles and to obtain information on the orientation of particle tracks (Sikkema, 1970) . This application will be difficult at particle energies below 1 MeV due to amplifier noise and electrical noise picked up from the environment . Such a problem may be overcome by the utilization of

a parallel-plate geometry of ionization chamber instead of the usual cylindrical geometry . This preference arises because, for the measurement of the orientation of particle tracks, it is essential that the electric field be uniform and homogeneous in the gas volume traversed by the particle . The parallel-plate system of ionization chamber offers, readily, such requirement and can be easily and efficiently coupled to the gas amplification as a means to overcome the noise background problems associated with low energy radiation measurements . However, most international recommendations on dosimetry have explicitly recognized the advantages of using parallel-plate ionization chambers for dosimetry of therapeutic beams especially for low energy electrons and photon beams . The design characteristics, mainly regarding the shape and height of the collecting volume, make this instrument theoretically ideal for ionization measurements whenever the uncertainty in the position of the effective point of measurement of the ionization chamber is to be minimized .

A detailed code of practice for the use of a parallel plate ionization chamber in radiotherapy has been published by Shonka (1998) . Expanded knowledge on perturbation and other correction details in parallel plate ionization chamber dosimetry, in addition to constructional details of the chambers, are readily available in more recent research (Shonka,1998; Göpfert et al, 2000) .

Although the cylindrical arrangement of ionization chamber has the advantage that its pulse amplitude represents the total ionization unambiguously at moderately high count rates, there is a major disadvantage that the electric field in the main volume of the chamber is low if multiplication and breakdown effects in the high

field region near the central wire are to be avoided . The low velocity imparted to the electrons allows more time for electron attachment which may decrease the pulse height and spoil the resolution if electronegative impurities are present in the gas . The advantages gained in the use of a gridded parallel plate ionization chamber have long been recognised and their use becomes preferable in such situations (Chase, 1961) .

The polarity effect (section 4.6.5) in a cylindrical ion chamber is much greater than in parallel plate chambers, mainly at lower energies of radiation to be measured and that is one of the major reasons that plane parallel plate chambers are recommended for the measurement of electron beams and photons used in radiotherapy as well as for measurements of heavy particles and ions (Hiraoka et al, 1998) . In addition to the fact that the pulses obtained by electron collection in a parallel plate ionization chamber can give information regarding the energy of the particle, their range; the angle between the tracks and the electric field of the chamber and their range-energy function, a careful design of the parallel plate chamber can make it suitable for the detection of single particles . This is one of the basic requirements for a nanodosimetric system (Sherr and Peterson, 1947).

For a controlled avalanche, in general, the parallel plate ionization chamber method is the most simple, direct and least elaborated to use for high accuracy measurement in determination of the physical parameters needed for absolute measurement of ionizing radiation .

4.3.5 Constructional problems of ionization radiation detectors

There are different design and constructional problems concerned with the ionization radiation detectors . They are chiefly concerned with the attainment of a suitably high electric field in the chamber which produces no severe side effects in its operation. Of these, are the difficulties arising from the use of insulators and guard rings as essential constructional constituents of the chamber .

4.3.5.1 Insulators

One of the major problems related to the attainment of high electric field in an ionization chamber is the type of insulators used . They should be of the highest quality, especially for use in current ionization chambers rather than in pulse chambers . Insulators placed in high electric fields tend to give rise to spurious effects particularly if they are made from plastics, due to polarization and charge distortion of the field due to piezo-electric effect . Tracking or local discharge may occur across the surface .This is the reason why the supporting insulators in an ion chamber should be kept in low electric field regions as much as possible .

Insulators may also suffer from exposure to the ionizing radiations, which can cause changes in the intrinsic resistance of the insulator . After exposure to intense irradiation, long recovery times of the order of days may then be needed.

4.3.5.2 Guard ring

The primary purpose of a guard ring in an ionization chamber is to intercept any leakage current flowing from the high potential electrode, and thus prevent it

reaching the collecting electrode. A secondary purpose is to control the electric field and define, accurately, the active volume of the chamber i.e the volume from which ions can reach the collecting electrode . A final function of the guard ring is to reduce microphonic vibrations in the chamber caused by distortions in the electric field which, in turn, either create spurious voltages at the collector or distort genuine ones .

To avoid electrical leakage between the guard ring and the collector, these electrodes should be maintained as nearly as possible to the same potential . However, the potential of the collector may drift a little above or below that of the guard ring during measurement . This small voltage drift can be avoided by the use of high quality insulators between the guard ring and the collector . Such insulation reduces leakage .

Any change in the collector potential relative to that of its guard ring will distort the electric field near the surface of the collector and may change the active volume of the ionization chamber . The magnitude of such errors have been investigated by Boag (1964) for the parallel plate ionization chamber . The effect of making the collector field more uniform by the guard ring as well as its effect of accurately defining the collecting volume of the chamber can be seen from the illustrative sketches of figure (4.3a) and (4.3b) .

These facts, which feature the problems arising from the application of insulators and guard rings in ionization chambers, often impose severe design and

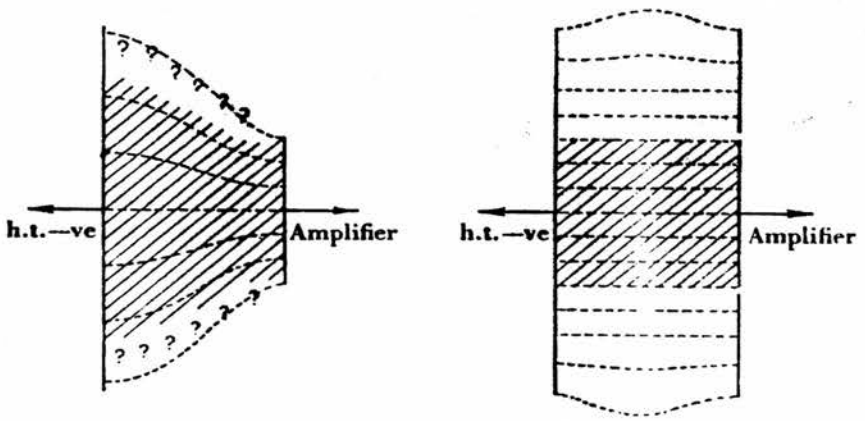

(a)

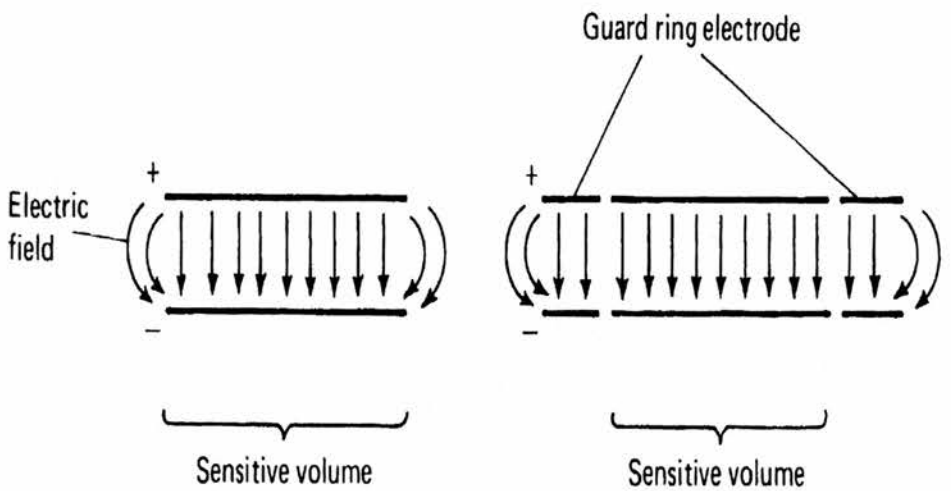

(b)

Figure 4.3: The role and function of the guard ring in electrodes of an ionisation chamber **a)** A guard ring for the collector electrode only, and the size of the high tension electrode is approximately twice as that of the collector **b)** Guard rings are used for the collector and the high tension electrodes, and the electrodes are of the same size.

constructional difficulties . This is particularly true in high pressure ionization gas-filled detectors .

4.4 Gridded ionization chambers

It has been shown in section 4.3 of this chapter that the geometrical dependence of the pulse amplitude and the phenomenon of the space charge dependence can be reduced to negligible importance by the use of a gridded ionization chamber . The collector is screened electrically from the entire volume in which the particle tracks are formed . The simplest type of gridded ionization chamber is the prototype of the Frisch grid (Frisch 1944) which consists of two electrodes comprising the cathode and the collector . Between them is a third electrode, a grid of parallel wires . The grid is maintained at intermediate potential between the two electrodes and is made to be as transparent as possible to electrons . The drifting of electrons between the cathode and the grid does not induce any signal on the collector anode until they pass through the grid .

4.4.1 Grid Inefficiency in shielding the collector

The inefficiency σ, of the grid in shielding the collector represents, essentially, the fraction of the lines of force from Q, (Figure 4.4) to the grid and the collector P, which finish actually on, P . Then the desired information, the charge induced by the positive charges at Q, on the collector P, is given by;

$$Q_{+} = e\sigma\left(1 - \frac{B}{b}\right) \qquad (4.10)$$

where e, is the electronic charge; B, is the separation distance between the

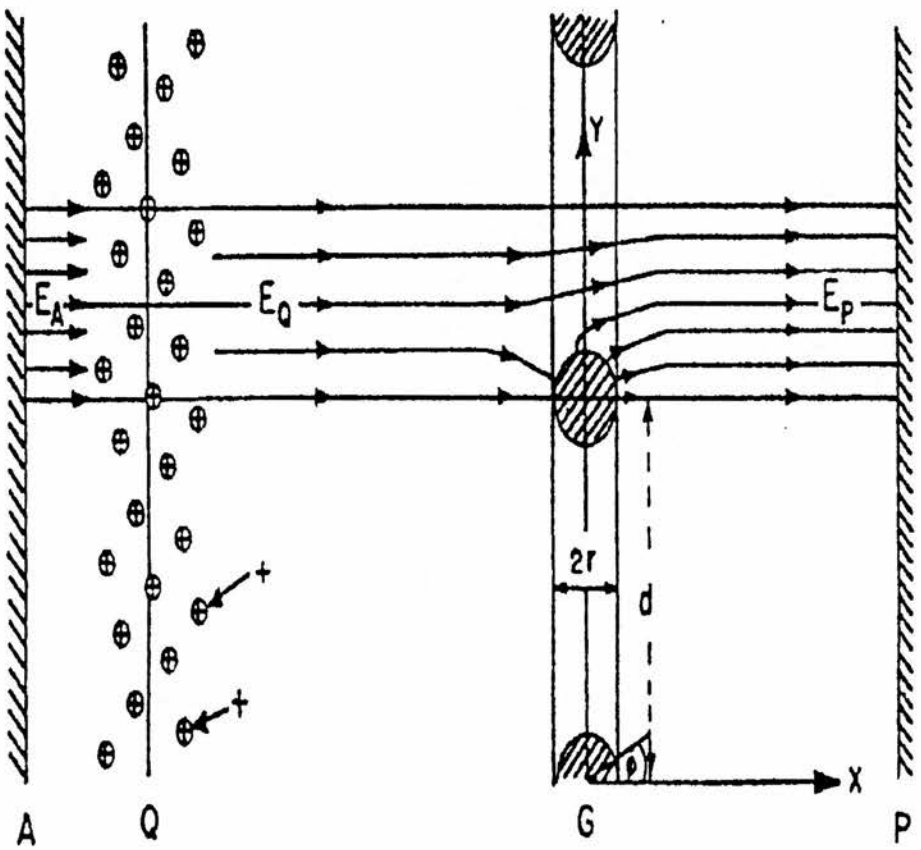

Figure 4.4: Schematic drawing of a grid ionization chamber. Electrons and positive ions are produced at the position Q, near the cathode, A . The grid G, of parallel wires screens the collector P, from the effect of the positive charges at Q , through the electric field extending from Q, to, G, and then to, P (Bunemann et al, 1949) .

position Q, of the production of the charge in the chamber and the grid; b, is the distance between the cathode (A) and the grid (G) . Bunemann, Cranshow and Harvey (Bunemann et al, 1949) have given a variety of formulae which are useful for the design of gridded ionization chambers . The expression for the inefficiency, σ, of the grid is given in its simplest form by;

$$\sigma = \frac{dE_P}{dE_Q} \quad for \quad V_P - V_G = constant \tag{4.11}$$

where dE_P, is the change in electric field between the collector and the grid; dE_Q, is the change in the field between the grid and the point Q, where ion pairs are formed V_P, is collector voltage V_G, is grid voltage . The inefficiency of the grid is calculated as a function of the two geometrical ratios r/d, and a/d, where r, is the radius of the wire of the grid d, is the separation distance between the wires of the grid and a, is the separation between the collector and the grid (Fulbright, 1979; Watt et al, 1964) Thus;

$$\sigma = \frac{d}{2\pi a} \ln \frac{d}{2\pi r} \tag{4.12}$$

Figure 4.5 shows curves of constant σ, and it can be seen that σ, can be made small and the efficiency increased either by choosing a grid-to-collector distance large compared to the separation between adjacent wires (pitch) d, of the grid or by choosing, carefully, the wire radius r, comparable to the pitch . Then, if the ionization can be formed reasonably far from the grid, this method allows pulses of uniform height to be obtained from randomly oriented particle tracks .

The important question in connection with gridded ionization chambers is concerned with the fraction λ, of the electrons collected on to the grid, instead of

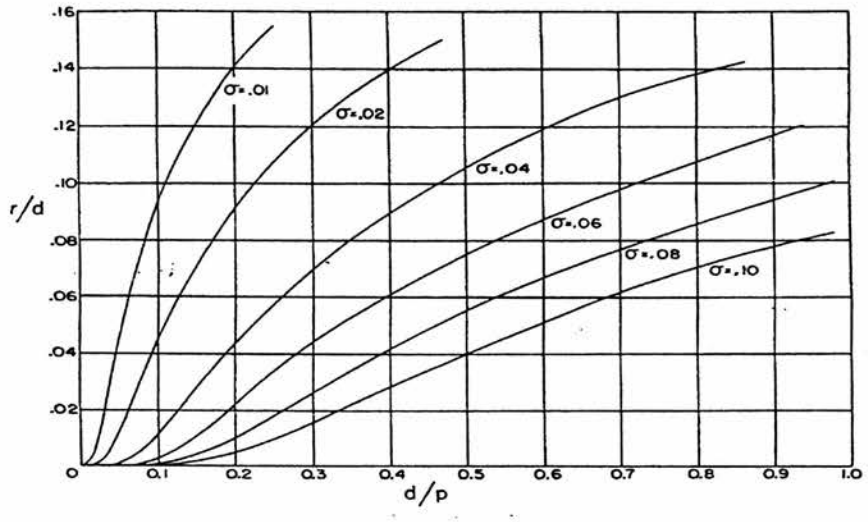

Figure 4.5: Curves of constant grid inefficiencies σ, plotted as a function of r/d, versus, d/p; where r, is the radius of the grid wire; d, is the separation between the grid wires, and p (= a), is the separation distance between the collector and the grid (Bunemann et al, 1949) .

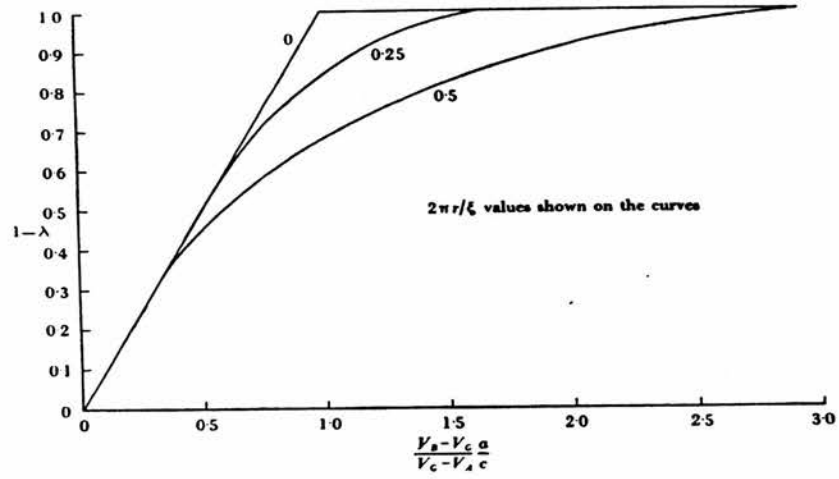

Figure 4.6: The fraction (1 - λ) of the electrons collected by a collector versus the ratio of the field between the grid and the collector; and that between the grid and the cathode . λ, is the fraction of the electrons collected at the grid (Wilkinson, 1950).

on to the collecting electrode and so are lost as far as pulse production is concerned. λ, is not always accurately constant and its value is dependent on the orientation of ionization if it is formed close to the grid (Wilkinson, 1950) . Such an effect introduces an additional variance in the pulse size distribution and the pulse size and the signal-to-noise ratio would be reduced . Therefore λ, should be made small . The fraction "1 - λ" of the electrons collected on to the collector, can be expressed in terms of the ratio of the field between the grid and the collecting electrode to that between the grid and the cathode of the chamber i.e $[(V_P - V_G) / (V_G - V_A)] (a / b)$. Where here a, is the separation distance between the collector (P) and the grid (G); b, is the separation distance between the grid and the cathode (A) . Figure 4.6 shows (1 - λ) as the function of $(dE_{PG} / dE_{GA})(a/d)$. The complete collection of electrons by the collector electrode of the ionization chamber can occur when the following condition is fulfilled;

$$\frac{E_a}{E_b} \equiv \frac{V_P - V_G}{V_G - V_A} \cdot \frac{a}{b} \geq \frac{1 + \frac{2\pi r}{d}}{1 - \frac{2\pi r}{d}} \qquad (4.13)$$

where E_a, is the electric field between the collector and the grid E_b, is the field between the grid and the cathode of the chamber; V_P, is the collector voltage; V_g, is the voltage of the grid and V_A, is the cathode voltage (Volkle, 1974) .

In addition to the screening advantage given to the collector signal in gridded ionization chambers, the modern application of such kind of chambers showed that a pulse can be extracted efficiently from the grid . This may be conveniently used as a signal containing information on the orientation of the tracks of, for

example, α-particles emitted from the cathode of the chamber .

Bochagov; Vorob'ev and Komar (Bochagov et al, 1957) have investigated the gridded ionization chamber as a pulse ionization chamber instrument for simultaneous study of the energy and angular distribution of charged particles . The magnitudes of the voltage pulses at different stages of acquisition and at different sites in the chamber are given . Some of these are described in the following sections .

4.4.2 Pulses across the collector electrode

The magnitude of the pulse arising from the electronic collection at the collector of the gridded ionization chamber is shown to be independent of the direction of the particle thus;

$$V_C = - \frac{Ne}{C_1} \qquad (4.14)$$

where N, is the original number of ion pairs created proportional to the energy of the particle passed through the chamber; C_1 , is the capacitance between the collector and the earth potential; e, is the electronic charge (Knoll, 1989) .

4.4.3 Pulse on the grid of the chamber

It can be shown that during their motion towards the collecting electrode, the electrons induce a charge on the grid as well, and a voltage pulse arises on the grid too . When the electrons move between the cathode and the grid, the pulse on the grid has a negative polarity and attains a maximum equal to;

$$V_g = -\frac{Ne}{C_g}(1 - \frac{R}{d_1}\cos\theta) \qquad (4.15)$$

where V_g, is the pulse height of the grid; C_g, is the total capacitance between the grid and the earth potential; d_1, is the separation distance between the grid and the cathode of the chamber; θ, is the angle formed by the track of the particle relative to the normal to the electrodes; R, is the "run" of the particle in the gas of the chamber . Ogawa (1961) represented this quantity R, by R*, as a representative of a length close to the range of the particle so that it could be taken, to a good approximation, equal to it . The magnitude of the grid pulse then changes its sign and at the time when all of the electrons reach the collecting electrode, the magnitude of the pulse becomes;

$$V_g = \frac{Ne}{C_g}.\frac{x}{d_1}\cos\theta \qquad (4.16)$$

where x, is the distance between the ions and the beginning of the particle tack. Bochagov et al (1957) demonstrated that simultaneous measurement of the magnitude of the collector pulse and that of the grid, will make it possible to determine the energy and the escape angle of a given particle from its source .

In view of the versatility of the gridded ionization chamber method, Ogawa (1961) carried out a wave form analysis of the grid pulse in a more general manner than Bouchagov et al, (1957) . They succeeded in deriving an improved pulse height formula and some approximation expressions for the distortion effect of the source thickness and the amplifier band-width on the pulse height distribution . During his analysis, Ogawa found that the original formula proposed by Bochagov et al

became insufficient for accurate work when the drift time t_2, of electrons in the grid-collector region is relatively long that it is not negligible with respect to the drift time t_1, in the cathode- grid region .

In an ordinary single-grid ionization chamber, simultaneous extraction of both the collector and grid pulses generally impairs the shielding efficiency of the grid and results in a serious loss in the energy and time resolution . To overcome this difficulty, Ogawa and Doke (1961) used a double-grid ionization chamber (Figure 4.7) . It consists of a cathode which could either be connected to a high tension or simply earthed . The cathode is followed by grid G1, from which a signal can be taken as well as from the collector, C . An additional grid G_2, serving as a screening grid, is situated between G_1, and the collector C;, and it could be directly grounded or connected to a high tension . The latter version of the gridded ion chamber is extensively used for investigating nuclear reactions, α-particle spectra etc . So as to obtain the optimum results, the voltages applied to each of the electrodes of double-gridded ionization chambers should be chosen so that the relation between the electric field strengths between the electrodes are as follows;

$$E_1 < E_2 < E_3$$

where E_1, is the electric field between the cathode and grid G_1 ; E_2 , is the field between the grids G_1, and G_2; E_3, is the field between grid G_2, and the collector.

For the fact that the grid pulses arising from particles emitted from G_1, G_2, or C, are essentially positive, at least in the first approximation, Ogawa and Doke (1961) were able to reduce the background in the energy spectrum, by a reasonable factor, merely by counting those collector pulses which are accompanied by

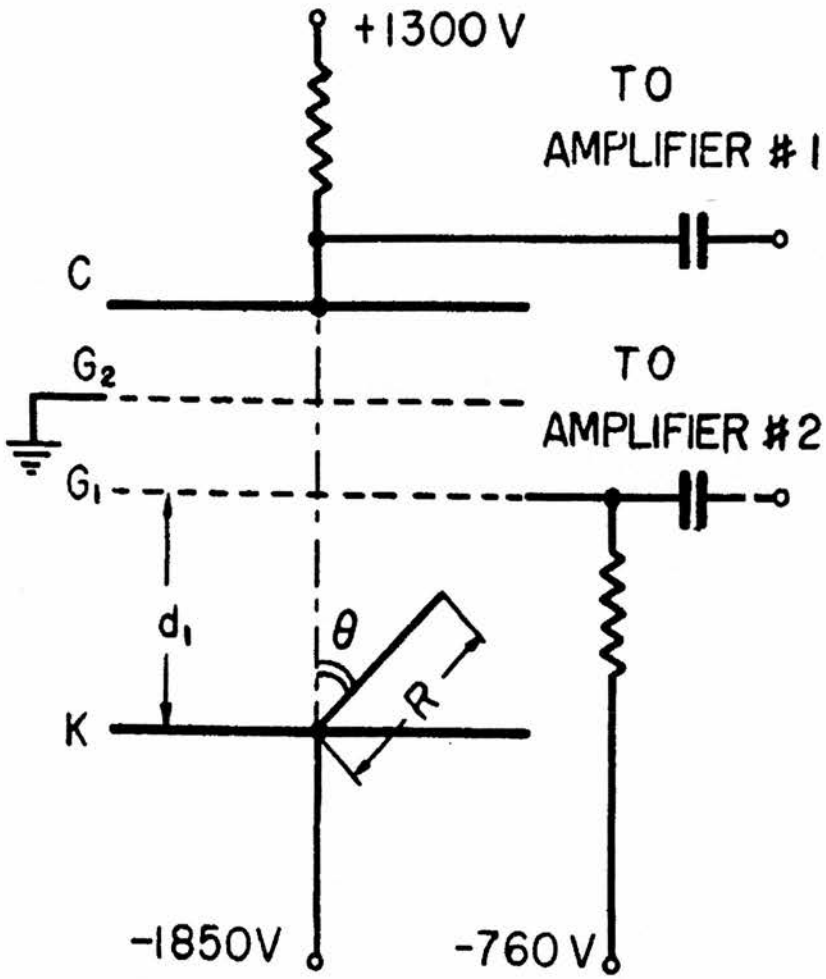

Figure 4.7: Schematic view of a double-gridded ionization chamber. Signals can be taken from both the collector C, and the first grid, G1 . Grid G_2, screens the collector from the effect of the positive charges (Ogawa and Doke, 1961) .

negative grid pulses . In this context, Korolev and Kocharov (1960) have investigated the pulse arising on the grid of a double-gridded ionization chamber and showed the possibility of enhancing the time and energy resolution of ionization chambers . This evolution in the ionization chambers made it possible to use pulses from different electrodes in various combinations such as coincidence and anti-coincidence . This made it possible to record the energy of particles as well as their angular distribution and point of emergence . The modern system of the gridded ion chambers allow even better background radiation discrimination and reduction of signal interference in the detector . Furthermore, Korolev and Kocharov have shown that, in the case of negative grid pulses, the choice of pass-band of the amplifier is particularly important . If the pass-band is not properly chosen, the angular distribution of the pulses may be distorted .

Watt et al (1964) applied, usefully, a double-gridded ionization chamber in investigating the range energy relationships for heavy charged particles in gases. The chamber was especially designed to measure high energy protons and complex neutron spectra at high gas pressures . The formulae derived by Watt et al, particularly, those for the collector output (Equation 4.14) and the maximum voltage induced in the grid of the chamber (Equation 4.15) incorporated the amplification elements A_A and A_G respectively, which proved to be useful elements in the present work (chapter 5) . Then equation (4.14) becomes;

$$V_C = - \frac{Ne.A_A}{C_1} \qquad (4.17)$$

where A_A, is the amplifier gain of the collector pulse. And equation (4.15) concerning the pulse on the grid of the chamber becomes;

$$V_g = -\frac{Ne.A_G}{C_g}(1 - \frac{R}{d_1}\cos\theta) \qquad (4.18)$$

Where A_G, is the grid pulse amplification factor .

The amplifier gain A_A, may include the pre-amplification of the pulse . From equation (4.17) and (4.18) it is clear that any particle energy giving collector voltage V_C, emitted at an angle θ, to the normal, has an associated grid voltage V_G, which is given by;

$$V_g = KV_C(1 - \frac{R}{d_1}\cos\theta) \qquad (4.19)$$

where,

$$K = \frac{C_1.A_G}{C_G.A_C} = constant$$

Relationship (4.19) shows that when θ = 0, V_G, is a minimum i.e;

$$V_{min} = KV_C\left(1 - \frac{R}{d}\right) \qquad (4.20)$$

And when θ = 90, V_G, is maximum; i.e;

$$V_{max} = KV_C \qquad (4.21)$$

It follows that by the measurement of the minimum and maximum values of the grid spectra for a particular value of V_C, the value of the range R, is given directly by;

$$R = d\left|1 - \frac{V_{min}}{V_{max}}\right| \qquad (4.22)$$

where d, is the grid-cathode spacing .

4.4.4 Brief review of work with the gridded ionization system

Since Frisch (1944) first suggested the application of the gridded ionization system, there have been evolutions in different aspects of the system and there have been varieties and wide range of application in different radiation detection fields . Therefore, it is interesting to discuss briefly some examples of work carried out using systems incorporating the gridded ionization methods .

Most of the workers have used gridded ionization systems in measuring angular distribution of particles (Coon et al, 1946) and / or for the measurement of the track angle in the chamber (Sherr, 1946; Facchini et al, 1959) . The devices are used also in measuring the total energy of the particles interacting with the media in them and hence, the measurement of (dE/dx) to discriminate between heavy ions such as He^3 and He^4 (McWhriter et al, 1958) .

Although gridded ionization chambers are usually used in parallel plate geometries, cylindrical geometries are not unfamiliar for grid system detectors . The grid in the latter example of geometry, is utilised between the cathode and the central collector and may be in a form of a helix . Campion (1968; 1971) used such type of gridded cylindrical counter in the study of the proportional counter mechanisms to measure gas gains and the shape of the photon pulses . Sikema (1974) utilised the grid system that constituted a multi-wire proportional counter. It consisted of an ionization or drift volume confined between a flat cathode and a grid, with number of field electrodes between the two to keep a homogeneous electric field for a uniform drift of electrons which are then amplified beyond the

grid and collected by multiple wire collector . The addition of field electrodes for homogeneity of the field shows the simplicity and flexibility at which gridded ionization system can be modified to suit particular requirements for different applications .

The gridded ionisation system is used also by Shapira et al (1975) for detection of heavy ions to measure their total, residual and loss energies as well as to measure the position and angle of incidence for each detected ion .

Breskin and co-workers have established a very efficient and evolutionary basis for the most modern modes of application of the gridded ionisation chambers . In 1979 Breskin, Charpak, Majewsk and Melchart (Breskin et al 1979) investigated a mechanism of charge multiplication in gases using the photon mediated mechanism in an advanced system of the gridded parallel plate ionization chamber. This mode of operation allowed one to obtain a controlled electron avalanche mainly after the electrons have been multiplied and transferred through a succession of amplifying elements thus constituting a multi-step avalanche chamber . Such method of gridded ionization chambers provided remarkable energy, time and position resolution for soft x-rays as well as for charge particles. The method applies the pre-amplification and transfer mechanism that proved to be effective.

Breskin and another group of co-workers (Breskin et al, 1983) have used multi-wire proportional counters (MWPCs) operated at low pressures (0.5 - 3 Torr), with the advantage of offering detection efficiency with low costs and simplicity of

operation with no severe limitation on shape and area . In 1986, a more evolutionary method of the gridded ionization chamber was used by Breskin and Chechik as a multi-step avalanche chamber operating at low gas pressures and was able to efficiently detect and localize single electrons . That is due to the high amplification factor attainable . The system is based on dividing the amplification process into very clear two steps, pre-amplification step limited by parallel grids and further amplification in a second element of parallel grid system. The properties required for the detection of a single electron avalanche were studied in particular detection gases and pressures together with some physical phenomena associated with the operation of the system . Some examples of these properties and physical phenomena are;

- The total amplification factor, which was seen to be very high ($\approx 10^8$) and therefore high detection efficiency for single electrons and cheaper electronics,
- Longitudinal and transverse diffusion,
- Electron drift velocities,
- Secondary effects .

A low-pressure, primary cluster counting detector with a conversion volume region followed by parallel grid stages is used by Malamud, Breskin and Chechik (Malamud et al 1991) . The system is utilized for systematic measurement of ionization density . Various electron transport processes were studied, such as cluster dissociation, cluster overlap and electron attachment or recombination . The impact of these processes on the statistical distribution of the number of counted clusters was investigated .

Pansky and co-workers (1993) have used a detector based on the primary electron counting in a low pressure multistage electron multiplier for an efficient counting of soft X-rays . Two methods were used for recording single electron avalanche-induced pulses . These methods comprised an electronic readout of the charge induced on the collector of the detector and an optical readout of the light emitted during the amplification process .

Breskin et al (1995) have devised a detector based on multi-step proportional counter which utilizes gridded ionization mechanism in its operation . The detector consisted of a sensitive ionization volume of a wall-less (Emery, 1970) millimetric region defined by a properly designed electric field . The system is capable of counting, efficiently, single electrons at low gas pressures . The device was able to measure the primary ionization yield in tissue equivalent as volume of few nanometre equivalent length . The investigation of Breskin et al (1995) into their detection system proved that the gas detectors are capable of performing measurement of charged particle-induced ionization in nanometre volumes . The involvement of the grid ionization system in such mode of application in radiation detection provides strong elements that can support the requirements for absolute detection and measurement of radiation.

The different ways in which the gridded ionization chamber systems have been used and the various applications they supported in the brief reviews given above, make it such a suitable system to be adopted to investigate the basic requirements for the desired response functions for detectors leading to absolute detection and

measurement of radiation needed in radiation therapy and protection . The properties and qualities of the system revealed by Breskin and co-workers such as the high amplification attainable, combined with high resolution pulses, flexible modification in the modes of operation and particularly, its capability to efficiently count the single electrons at low pressures make possible the simulation of radiation actions to equivalent sensitive biological targets, such as the intra-nuclear DNA bio-molecules .

4.5 Transport properties of charges in gas-filled counters

The transport properties of ion-pairs produced in gases have been studied experimentally since shortly after the discovery of x-rays in 1895 and theoretically since 1903 (McDaniel et al, 1973) . Data in mobilities and diffusion coefficients of the ion-pairs in an ionized medium, together with their recombination data are of both theoretical and practical interest . The experimental values of these quantities and their dependency on the ratio (E/N) of the electric field E, to gas number density N; or the reduced electric field E/P, where P is the gas pressure, can provide information that can help in determination of the working conditions of a system where the mechanisms of ionization are involved . Information on both mobility and diffusion is required for a quantitative understanding of electric charges collected at the collector of an ionization chamber .

4.5.1 Ion mobility

The results of the studies of the motion of ions in gases determine that the drift velocity v, (in cm/sec.) of the ions in a given gas at a given pressure P, in torr is

proportional to the applied electric field E, in volts/cm (Morgan et al, 1973), hence;

$$v = 760\mu\frac{E}{P} \tag{4.23}$$

where μ , is the mobility constant of the ion expressed in (m^2.torr/V.Sec) . The mobility of ions is nearly constant over extended range of E/P, for a given ion of a specified charge in a given gas . A typical value of v, for heavy ions is approximately 10 m/sec (Tsoulfanidis, 1983) . For the pressures and E/P, commonly used in detecting instruments utilizing gas ionization, it is usually sufficient to consider the ion-mobility to be constant, leading to a calculated drift velocity proportional to the electric field . However, at very high values of E/P, the mobility μ, cannot be considered constant since at such values, the energy acquired from the field between collisions is no longer small compared with (3/2)kT, which is equivalent to the kinetic energy of the ions in moderate electric fields . k, is the Boltzmann constant; T, is the absolute temperature (Malamud et al, 1991) . The ion velocity at higher values of E/P, approaches;

$$v = constant\left(\frac{E}{P}\right)^{1/2} \tag{4.24}$$

and the behaviour of the mobility as a function of E/P, may become quite complex.

4.5.2 Electron mobility

The electrons which are free behave quite differently from the ions . Their much smaller mass allows a greater kinetic energy to be acquired by the electrons between collisions with the neutral molecules of the gas, and their mobilities are typically 10^3 times greater than that for ions . The drift velocity v, of the electrons

produced in an ionization chamber is a function of the reduced field strength (E/P) . According to classical kinetic theory, it is given by the following relationship (Fulbright 1979);

$$v = \frac{e\lambda E}{muP} \qquad (4.25)$$

where e, is the electronic charge λ, is the scatter mean free path of the electron E, is the electric field strength m, is electron mass u, is the electron rms agitation velocity and P, is the pressure of the detecting gas . From equation (4.25) it is clear that v, is inversely proportional to the agitational velocity . This velocity, in pure noble gases, such as Argon, remains low with increased E/P (Figure 4.8) because u, increases with increase in E/P, whereas in pure polyatomic gases such as methane v, increases with an E/P increment (Figure 4.9) .The electron drift velocity in noble gases can be increased with percent admixture of polyatomic molecules as in the standard gas mixture of 90% Argon + 10% methane (Figure 4.8) . Such increment in the drift velocity v, reduces the collection time of the detector for electrons to the order of microseconds rather than milliseconds which is the normal collection time for the heavy ions . In general, addition of a small percent of hydrocarbons to monatomic noble gases enables saturation in the electron drift velocity .

The drift velocity in pure noble gases and their admixtures, is a function of E/P alone and does not depend on the pressure separately . This is believed to be true for all gases and gas mixtures (Figure 4.10) . In many other gases the electron

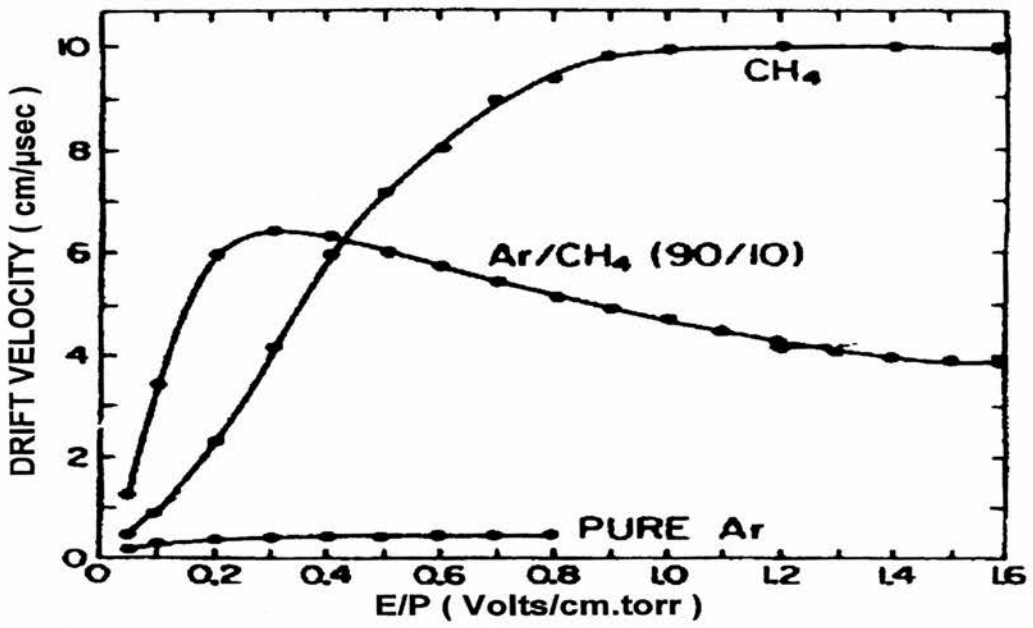

Figure 4.8: Electron drift velocities in three ifferent gases (Fulbright, 1979) .

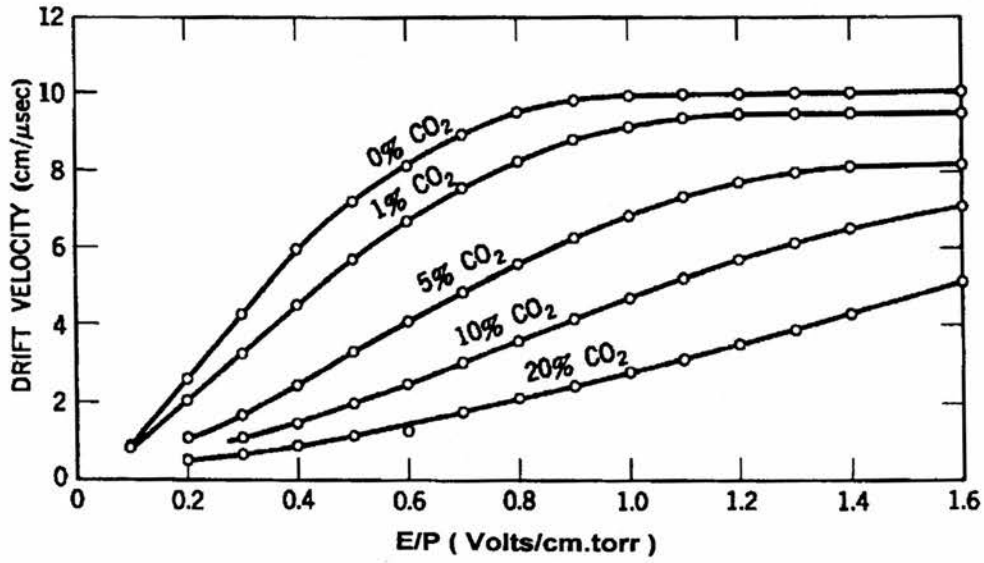

Figure 4.9: Electron drift velocity in methane-carbon dioxide mixtures (0% to 20% CO_2) ; (Morgan and Turner, 1973) .

drift velocity continues to increase for the largest, E/P, values which may be used in gas-filled detectors (Figure 4.11) . The choice of shorter electron drift times which are associated with higher drift velocities is helpful to minimise the uncertainties in detection timing . This objective can be achieved by keeping the electric field as high as possible in the drift region of the counter and by choosing a gas with high electron drift velocities . Figure (4.11) shows some examples of low and high drift velocity filling gases.

4.5.3 The behaviour of ion-pairs in gas counters

As has been shown above, there are various differences in the behaviour of ions and electrons produced in a gas-filled ionization chamber in regard to their drift and diffusion in gases . The electrons usually have much higher drift velocities (approximately 10^6 m/s) and diffusion coefficients than ions, under given conditions in a given gas . Electrons are accelerated readily by an electric field and, due to their small masses, they loose only little energy in elastic collisions with molecules . This lost energy is a fraction of the order of m_e /M , where m_e, and M, are the electronic and the molecular masses, respectively . Therefore, electrons can acquire kinetic energy from an electric field faster than ions and they can store this energy between collisions to a much greater degree until they reach energies at which inelastic collisions become important .

Another difference between electron and ion experiments relating to the effect of impurities in the gas can be noticed from the following . Molecular impurities in an atomic gas can hold the average electronic energy well below the level that would

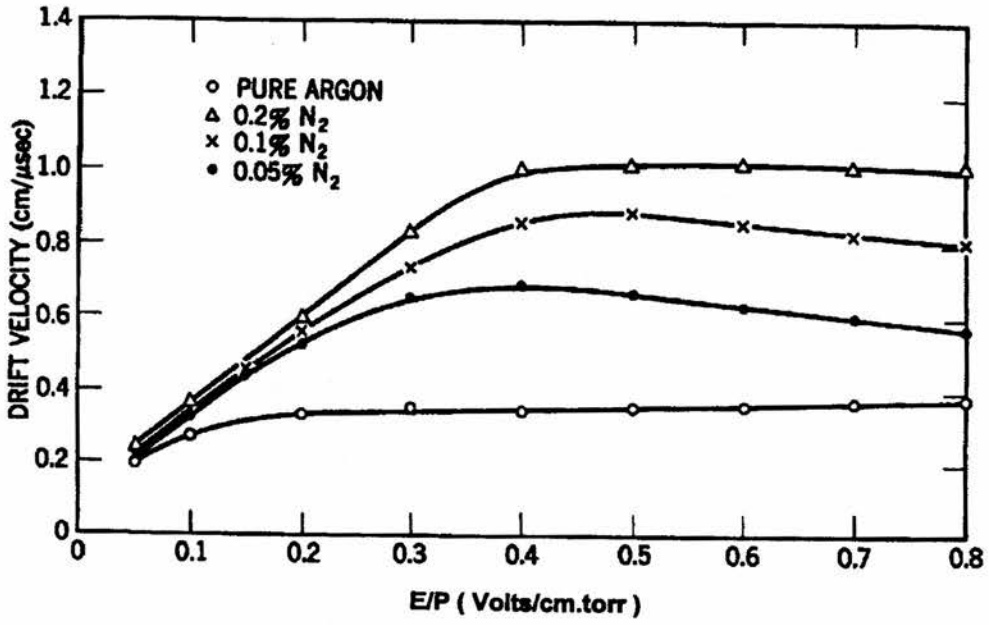

Figure 4.10: Electron drift velocity in argon-nitrogen (Morgan and Turner, 1973) .

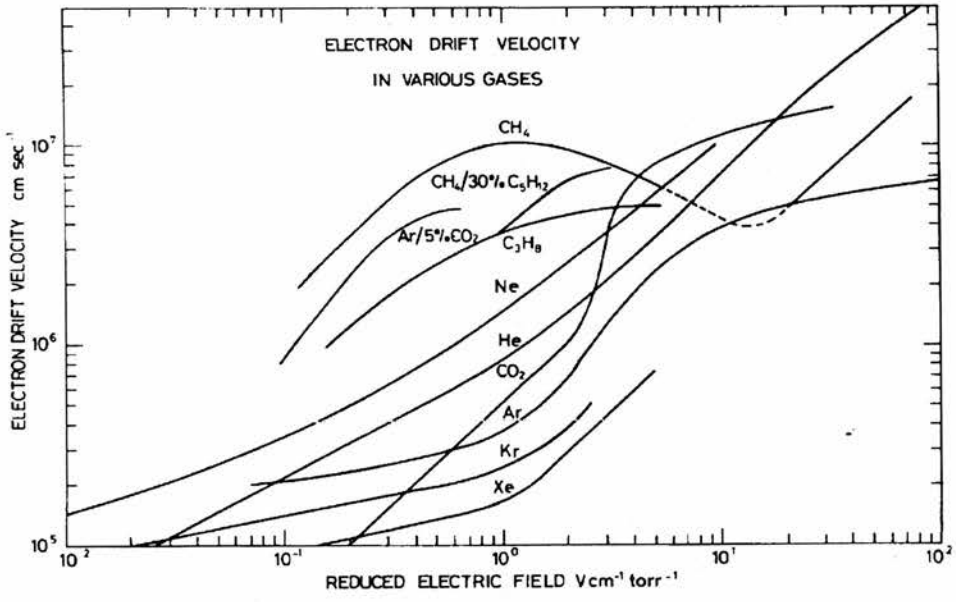

Figure 4.11: Electron drift velocity in various gases (Knoll, 1989) .

be attained in the pure gas because electrons can loose large fractions of their energy by exciting the rotational and vibrational levels of the molecules . The electronic velocity distribution can be seriously altered in this process . Impurities, however, have little effect on the average ionic energy and velocity distribution in ionic experiments, e.g when ion collection mode is utilized in a gas-filled ionization chamber . But the matter of serious concern is the production of impurity ions by the reaction of the ions of the main gas with the impurity molecules .

However, the differences in the behaviour of electrons and ions showed above can govern the mode of operation that can be chosen for a particular gas-filled ionization detector . For example, this can determine whether to operate it in the mode of electronic collection so that the output signal is due to electron collection or to be operated in an ionic mode to collect the ions for the signal output .

4.6 The role of some phenomena in operation of ion chambers

In addition to the mobilities of charges and the different behaviours of the ion-pairs produced in the gas-filled ionization counters, there are many more physical factors and phenomena that govern the operational behaviour of ionization chambers and proportional counters when ionisation is released within them . The advantageous ones are utilised for implementation to the desired functional features . Unfortunately, several of these phenomena are undesirable from functional considerations . Of these the most important are; diffusion of charges; recombination of ions; electron attachment and charge transfer; and polarity effect. A brief description is given below for each with some more details for the most significant phenomena .

4.6.1 Diffusion of charge carriers in gases

The ions created in an ionization chamber filled with gas will be in contact with the gas molecules and they partake of the random chaotic thermal motion of the molecules (Moseley et al, 1968) . Consequently, any concentration or accumulation of such charge carriers of one type in a gas will move in such a way that they will be spreading in space with decrement in the initial concentration . This process is the ion diffusion . This diffusive motion is ever present and superposed on the directed motion of the ions such as motion due to electric fields.

Diffusion of charges within the gas-filled ionisation chambers and proportional counters is a physical phenomenon of great importance in the operation of the instrument . This is mainly significant in certain regions in the chamber such as at the edge of a dense ion layer, where the concentration of ions is not uniform .

In all ionization chambers which have containing walls, at relatively low pressures and at especially high electron energies, the radial (ambipolar) diffusion of the electrons and ions to the walls causes a serious loss of charges thus affecting the number of charges to be collected (Loeb, 1955) . This means that diffusion of ions in gases causes many losses and the severity of the loss depends on the job the gaseous instrument is required to do . Therefore, the fundamental principles and characteristics of this important phenomenon must be understood early in the study of gaseous behaviour in any radiation measuring system which utilizes ionization of gases .

However, the practical complications in the use of ionization chambers and proportional counters are few in number . Probably the most important is the failure to collect all the ions formed, that is failure in saturation collection (Böhm, 1976) . This may be due to three aspects (Greening, 1985) . Losses of ions could be due to diffusion of charges, initial (geminate) or volume (general) recombination . The percentage diffusion of charges in parallel-plate ionization chambers is approximately 5 per number of volts applied if the charge carriers are ions and not free electrons . Then, a very small amount of applied voltage (about 50 volts) to the chamber can limit diffusion losses to less than 0.1 % .

4.6.2 Recombination of charges in gas-filled counters

The phenomenon of recombination of charges is of great importance for the operation of gas-filled ionisation and proportional counters . It is the collision of ions of opposite signs followed by neutralization of their electric charges . The ions become either atoms or molecules which are electrically neutral .

When equal densities n, of ions having opposite signs are uniformly produced in an ionization chamber, recombination causes the decay of ions in the absence of an electric field applied between electrodes . The decay occurs in a period of time, t, in accordance with the following equation which gives the rate of recombination per unit volume;

$$\frac{dn}{dt} = -\alpha n_+ n_- \qquad (4.26)$$

where α, is the recombination coefficient in ($cm^3.sec^{-1}.ion^{-1}$) n_+ and, n_- are the densities of the positive and negative ions respectively . The ion density n, can be calculated by solving equation (4.26); thus;

$$\frac{1}{n} = \frac{1}{n_0} + \alpha t \qquad (4.28)$$

or;

$$n = \frac{n_0}{1 + \alpha n_0 t} \qquad (4.27)$$

where n_0, is the initial ion density (for t = 0) . The second form of the above two equations (equation 4.28) is very useful, since it represents a straight line intersecting the ordinate at the point ($1/n_0$) and the slope of the line determines the coefficient of ion recombination (α) .

4.6.2.1 Types of recombination of ions

Different types of recombination of charges occurring during the formation of ion-pairs in a gas-filled counters can be distinguished such as electron, ion, volume, initial (geminate), preferential, columnar and wall recombination (Boag, 1950) . Each type of recombination is defined on the basis of the geometry of its occurrence .

4.6.2.1.1 Electron recombination

Electron recombination results from the collision between a free electron and a positive ion . In gases it mainly occurs when ions have very high densities . Schiller, (1993) showed that this type of recombination occurs when ion-pairs are

formed with electron energy below the lowest vibrational level of the medium . The coefficient of recombination, α, oscillates within wide limits (10^{-14} - 10^{-6} $cm^3.sec^{-1}.ion^{-1}$) depending on the conditions of operation of the system . Warman et al (1979) have studied this type of recombination as a function of the pressure of some molecular gases . The recombination coefficient for all the cases are found to increase with increasing gas density .

4.6.2.1.2 Ion and volume recombination

This type of recombination is sometimes known, also, as general recombination (Boag, 1966) . It occurs when the positive ions and the electrons or negative ions are uniformly produced and randomly distributed through the gas in the detector. It follows the simplest law of recombination and the rate of recombination per unit volume is given by equation (4.26) . The coefficient of volume recombination is of the order of 10^{-6} $cm^3.sec^{-1}.ion^{-1}$ in gases and about 10^{-9} in liquids .

4.6.2.1.3 Initial (geminate) recombination

The initial (or geminate) recombination occurs when, immediately after ionization has taken place, ions of opposite signs are closer to each other than could be expected on the basis of uniform distribution of ions . This type occurs in gases at low pressures and follows, mostly, irradiation with x-rays or γ-rays (Jaffe, 1940). When ion-pairs are created in a gas detector, electrons, initially speeding away from the parent ions, lose energy in collision with the surrounding molecules of the gas . Eventually, these electrons lose enough energy to be thermalised then initial or geminate recombination occurs if the electrons recombine with their parent ions

and homogeneous recombination if they recombine with different ions than their parents (Morgan, 1985) .

4.6.2.1.4 Preferential recombination

Preferential recombination occurs most frequently when electrons or negative ions are produced at the vicinity of the positive ions and instead of being uniformly distributed, they are formed into groups in certain specified regions . The ions are found to be so close to each other that their electrostatic attraction energy is greater than their relative Brownian motion . They may then recombine before diffusion or electric field has moved them further away . It occurs in gases under high pressure and in liquids especially when low-energy δ-electrons are produced forming small compact groups of ions (Adamczewski, 1969) . Unlike the other types of recombination, preferential recombination is independent of the density of ionization in the chamber (Wilkinson, 1950) .

4.6.2.1.5 Columnar recombination

Columnar recombination is a special type of preferential recombination . It is related also, to the initial recombination because both processes depend on the initial distances of separation of ions of opposite signs (Onsager, 1938) . It occurs during the first moments of formation of ion-pairs in a column along the track of the ionizing particle before the pairs can drift or defuse apart . It is most severe for densely ionizing radiation such as protons, α-particles and nuclear fragments; particularly in gases under high pressure and in liquids . It is more difficult to eliminate this type of recombination completely and may lead to small

losses of ions even at the highest applied voltages .

4.6.2.1.6 Wall recombination;

Wall recombination occurs when the charge carriers are close to and diffuse towards the walls of the gas container or vessel and subject to intensified recombination with walls .

4.6.3 Charge transfer and electron attachment

Different factors may contribute to the loss in saturation collection in gas-filled radiation detectors . In addition to recombination and diffusion losses, there are other factors and phenomena that can impair the operation of such radiation devices . Of these are the charge transfer and electron attachment processes .

4.6.3.1 Charge transfer

Many types of collision occur in gas-filled radiation detectors . Charge transfer collisions can occur when a positive ion encounters a neutral gas molecule . Then an electron may be transferred from the neutral molecule to the ion . This phenomenon is particularly significant when a gas mixture is used as the detection gas, such as argon-methane mixture . The problem with this process is that the role for which each gas is used in the detector is reversed (Wilkinson, 1950).

4.6.3.2 Electron attachment

Electron attachment is a process in which free electrons are captured by neutral atoms or molecules of the gas in the detector to form negative ions or molecular

anions . Electron attachment process can be classified into either dissociative or non-dissociative (Illenberger, 1994) .

In dissociative type of electron attachment, the interaction of low energy electrons with neutral molecules produce unstable transient negative ions (anions) which in turn may dissociate into two neutral fragments or into further combination of stable fragments, cations or anions . In non-dissociative type of electron attachment, the formed negative ion is collisionally stabilized to form stable molecular anion .

The electron attachment process is valid for any phase of matter (Sanche, 1995) . The possibility that an electron attachment to a neutral molecule can occur is expressed in terms of the electron attachment coefficient, h . It is defined as the probability of attachment per collision of an electron with neutral molecules or atoms . The values of h, vary widely with the type of gas and depend also strongly, on the electron energy and therefore on the electric field strength and the gas pressure (Price, 1958) . To prevent formation of negative ions, 1/ h, which is the number of collisions required per attachment, must be large compared to the number of collisions undergone by electrons in passing to the collector electrode (Llewellyn, 1957) .

The processes of charge transfer and electron attachment described briefly above, shows that the free electron of the original ion-pairs may undergo many collisions during their diffusive drifts . Thus heavy negative ions may be created during the collisions and the lighter electrons may be lost by the reactions that involve

attachment of free electrons to neutral gas molecules . This means that, the electrons with the preferable higher mobility may form massive ions of undesirable lower mobility . That is in addition to the general loss which will contribute greatly in the reduction in saturation collection in gas-filled radiation detectors.

4.6.4 Electrical breakdown and corona discharge

Ionization chambers and proportional counters may give rise to spurious results either as signals or currents. The main causes of these spurious results may be due to electrical breakdown or corona discharge in the chamber .

4.6.4.1 Electrical breakdown

If a potential difference is applied across ionization chamber electrodes separated by a distance d, and using a counting gas of number density n, it is well known that at some critical potential difference V_s, electrical breakdown of the gas occurs. This breakdown is characterized by the rapid transition of the counting gas from a poor electrical conductor with a resistivity of about 10^{14} ohm.m to a relatively good conductor with resistivity in orders of about 10^3 ohm.m depending on the particular condition of the experiment, such as the pressure and the type of the counting gas used . This critical potential difference at which the breakdown occurs is known as the breakdown or sparking potential, V_s (Dutton, 1978) . It depends on the nature and number density of the counting gas, the material and state of the electrodes and the degree of pre-existing ionization . For uniform electric field breakdown, the breakdown potential V_s, is a function of both the number density n, of the gas, which depends on the pressure of the gas, and the separation

distance between the electrodes involved in the breakdown process . Hence;

$$V_s = f(nd)_s \qquad (4.29)$$

where $(nd)_s$, is the value of nd, at which a spark occurs .

4.6.4.2 Corona discharge

Corona discharge is an electrical discharge at any sharp points which may produce high local electric fields within an ionization chamber . Corona discharge may also be due to electrostatic breakdown elsewhere in the chamber peripherals (Sigmond, 1978) or across various insulators inside the system . In general, the complete breakdown in a non-uniform applied electric field is often preceded by a corona discharge (Blair, 1978) .

Because corona discharge depends also on the critical potential between the involved parts, for example in an ionization chamber, impurities in counting gases have a marked effect on corona breakdown potential, specially in monatomic gases (Llewellyn, 1957) . The most important sites for corona discharge events in an ionization chamber would be associated with the connection points where the electrodes are connected to cables and where soldering could be necessary . So as to reduce the possibility of corona, such points of connection should be smooth and free of sharp irregular edges . Corona discharge may occur at sites outside the system, yet related to it, such as in capacitors in the filter box; and in the high tension cables .

Corona discharge is of considerable technical importance in the design and construction of radiation detectors . More often it acts as a nuisance than as a benefit . Method of minimizing corona discharge should be considered when designing and constructing radiation detectors such as ionization chambers and proportional counters .

4.6.5 Polarity effect in gas-filled ionization counters

The polarity effect is one of the most important factors needed to be expressed for characteristics of gas-filled ionization detectors . It is a charge balance effect caused by a difference in net electron deposition . The phenomenon is usually caused by the presence of extra cavities around the collecting lead of the chamber and may be caused also, by flow in or out of Compton scattered electrons from the irradiated chamber body, stem and the collecting cable materials which will eventually contribute to the measured charge . The effect is most pronounced when the chamber is used in areas where electron equilibrium is not reached (Wickman et al, 1992) . The effect can be eliminated by making two sets of measurements, the second with the voltages on the electrodes reversed in polarity with respect to the first . The true ionization is then given by;

$$Q = \frac{Q_1 + Q_2}{2} \qquad (4.30)$$

where Q_1, is the quantity measured in the first case; and Q_2, is the quantity the

quantity measured in the second case .

The fact that the polarity effect has been shown to be less serious in parallel plate ionization chambers rather than cylindrical ones is another reason for the preferring them for the present investigations .

CHAPTER FIVE

EXPERIMENTAL WORK

5.1 Introduction

The attempt to measure and detect radiation spectra with detectors that simulate nanometre dimensions; and then to relate these physical measurements to the bio-effectiveness of the radiation, is one of the most demanding tasks in experimental dosimetry . In the preceding Chapters, it has been concluded that, this goal can be achieved by different approaches (Chapter three) . Many diverse attempts have been made, first to specify the physical and biologically related parameters, in terms of single values capable of better unifying data for different radiation types (Watt, 1988; 1997) .

It has been concluded, also that, the matching of the mean free path for charged particle track interaction λ, with the double stranded DNA segment (i.e 2 nm) is the dominant mechanism of radiation action in mammalian cells (Simmons and watt, 1999) . Consequently, it has been suggested that, if a physical detector can be designed with a response which can simulate that of the DNA to radiation, then absolute dosimetry of ionizing radiation in a unified system becomes feasible .

In the sight of the outcome of the previous chapters, the approach of this work is concerned, initially, with the production of a high-gain gas-filled multi-gridded

ionization chamber (section 4.4) that can simulate a sensitive volume with dimensions of the order a nanometre .

5.2 The detection system

The choice of the detection system, viz, the gas-filled gridded system is according to the various possible approaches for the absolute detection system discussed in Chapter three (section 3.4; section 3.4.3.2) and the critical review of the gas-filled detectors made in Chapter four . This choice is guided by the favoured characteristics and properties of the gas-based system of detectors which have been tested as the desired features for the absolute dosimetry .

On the basis of the above, a prototype nanodosimeter has been designed with a sensitive volume with mean chord dimension as close as practically possible to 2 nm at unit density .

5.2.1 Design configuration and construction of the detector

The design and construction of the gas-filled nanodosimeter is based on the earlier experiences on the gridded-ionization chambers (Frisch, 1944; Bunemann et al, 1949; Ogawa and Doke, 1961; Watt et al, 1964) . The general idea of the design and construction of the device relies on the features that can ensure a means of creating a nominal sensitive volume that simulates the nanometre sensitive sites of interest; a means of amplification for the charge produced in the volume to enable the detection of single electron and multiples, and an effective method of

extracting the output signal out of the processes so that a proper interpretation can be achieved .

Therefore, the basic design features of the detector consists of the cathode-extractor assembly where in a nominal cylindrical sensitive volume of 1 mm diameter and 1.5 mm height is defined for the preliminary investigation of the basic functional tests . It consists also of the grid and a collector electrodes .

The nanodosimeter is designed and constructed in two stages each passed through several modifications . Consequently, two versions of prototype nanodosimeters were designed and constructed, viz, the initial and final versions .

5.2.1.1 The design of the initial prototype nano-detector

The basic design features of the initial version of the prototype nanodosimeter are shown in the schematic outline of Figure 5.1a, whereas the schematic block diagram of its experimental set-up is shown in figure 5.1b . The external features of the device are shown in the photograph of figure 5.1c .

In the initial design of the detector, two identical parallel plate gridded electrodes were situated between the cathode-extractor assembly and a solid plate collector (anode) of the detector . Each of the mesh electrodes is made up of two parts . The outer copper guard ring part surrounds a central part of wire

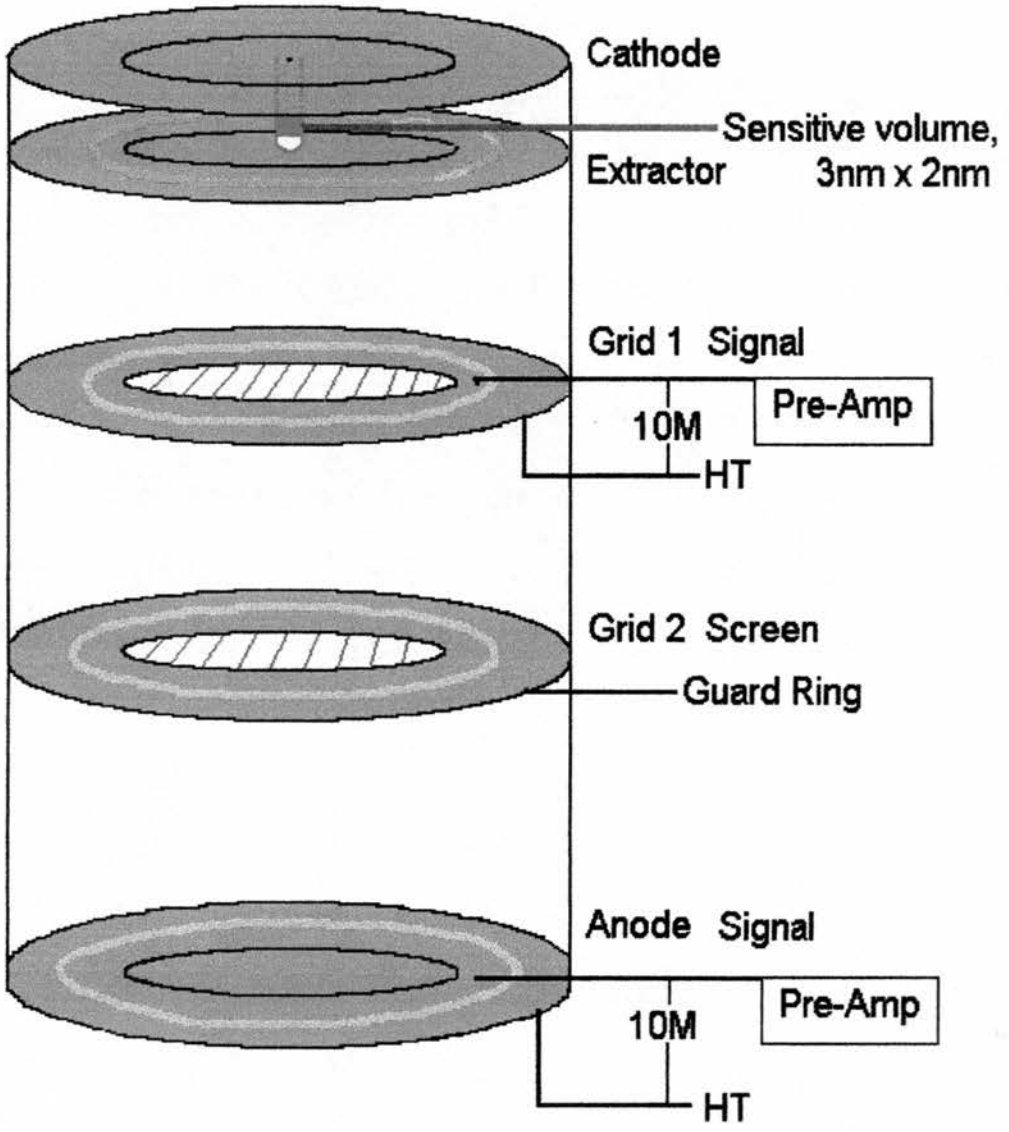

Figure 5.1a: Schematic diagram of the electrode system of the initial version of the prototype nanodosimeter .

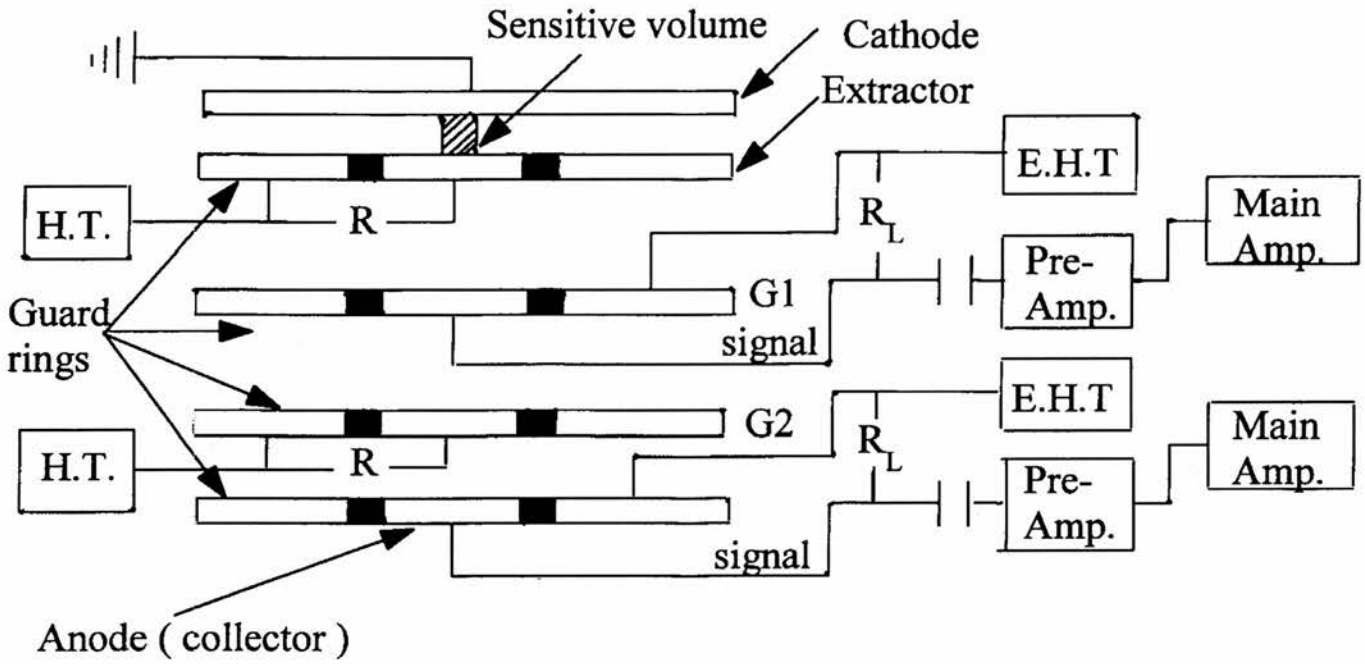

Figure 5.1b: A schematic block diagram of the experimental set-up of the initial version of the prototype nanodosimeter .

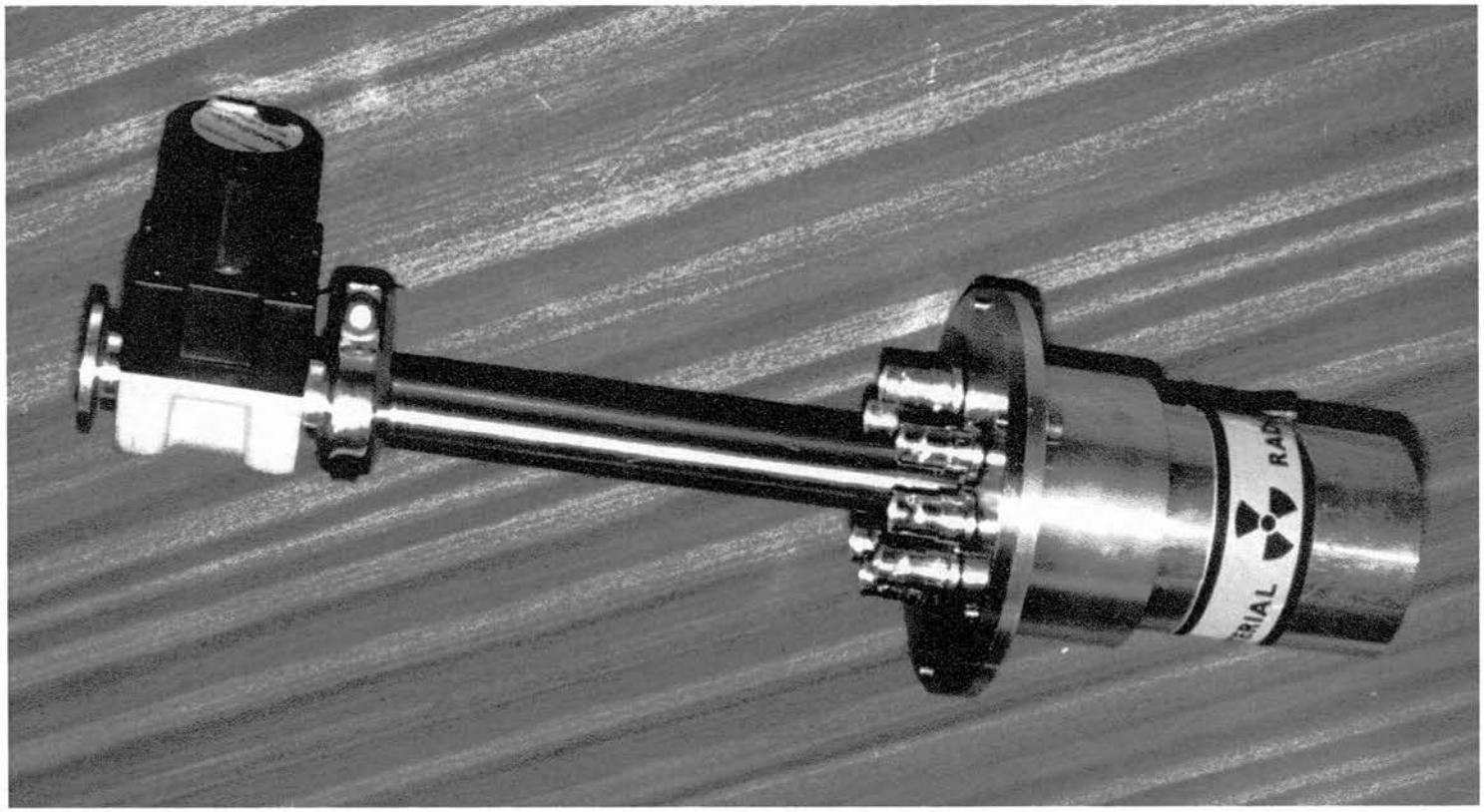

Figure5.1c: A photograph featuring the initial version of the prototype nanodosimeter .

mesh fitted into the centre to form a central active disc of the grid plate which is insulated from the outer guard ring by PTFE annular ring . The thickness and the dimensions of the electrodes are carefully chosen to suit the requirements for their particular functions . The grid mesh is made up of fine electroformed nickel wires of 18.54 μm diameter and spaced 344 μm from each other (pitched at 362 microns) . The physical transparency of the grid mesh is 95 % . These dimensions, togethe r with suitably applied and adjusted electric fields between the electrodes can improve the grid efficiency in transmitting electrons through to the collector region (with transparency increased to 98 %) and yet giving effective shielding to the collector from the positive charge effect (Bunemann et al, 1949) . Figure 5.2a shows the inefficiency of the grid used in this work as a function of the ratios of the spaces between the electrodes of the system .

In the initial prototype nano-device, the whole system is assembled in a cylindrical metallic container with well defined spacings between the electrodes . The electrodes are mounted on an insulating support . These spacings govern the values of the applied electric fields between the electrodes of the detector and control the behaviour of the charges produced in the device . In figure 5.2b, the ratios of the voltages V_{ag}, between the anode (collector) and the grid; and the voltage V_{gc}, between the grid and the cathode of the system is shown as a function of the ratios of the anode-grid spacing and the anode-cathode spacing for the dimensions of the grid and the wires used in the system (section 4.4.1) . The

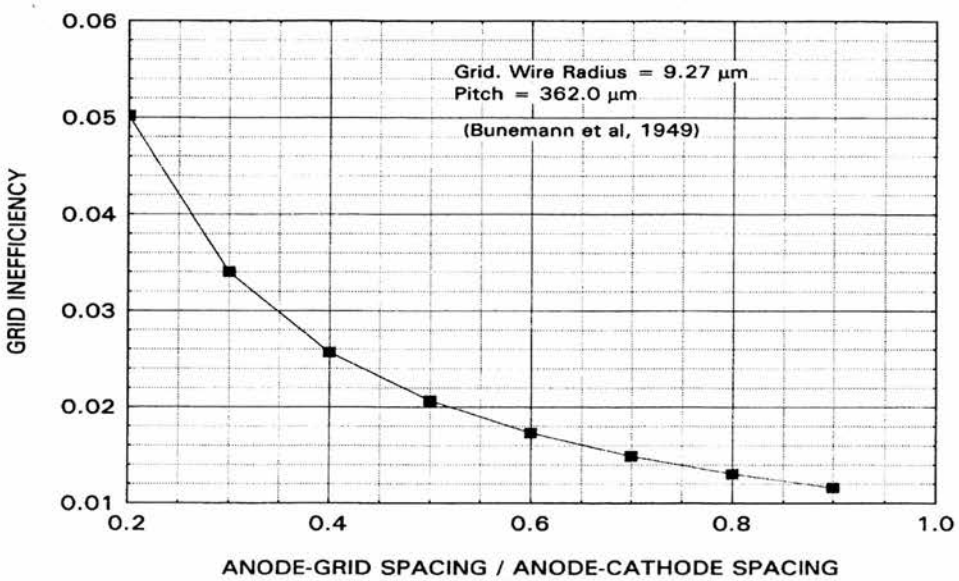

Figure 5.2a: Inefficiency of the grid used in the present nanodosimeter versus the ratios of the spaces between the electrodes.

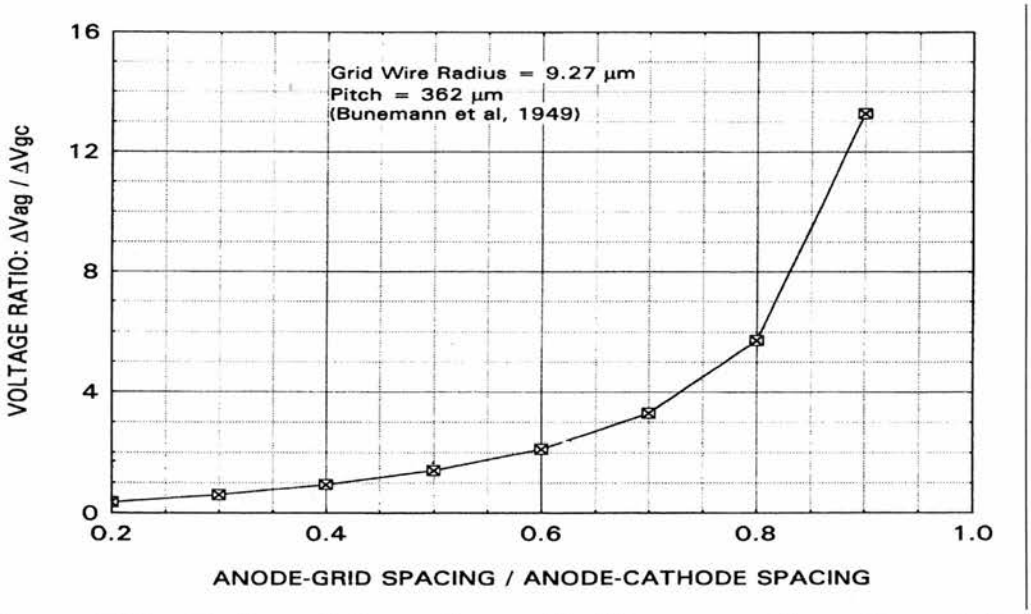

Figure 5.2b: Ratios of the voltages V_{ag}/V_{gc} versus the ratios of the distances between the electrodes (d_{ag}/d_{ac}) . Where, a = Anode, g = grid, c = cathode .

multi-step amplification method (Breskin and Chechik,1986) is used in the initial version to investigate the gain characteristics as a function of the reduced electric fields . In figure 5.1a, the region between the extractor and the grid G_1, (3 mm across); and the one between the grid G_1 , and grid G_2 (5 mm spacing) were used as the first and the second amplification regions respectively. Grid G1, functions as one of the elements of the first amplification region as well as the electrode from which a simultaneous signal extraction is possible, as a useful information carrying signal . This signal can be utilized usefully, for example, in the special cases of coincidence and anti-coincidence applications . Grid G_2, acts in this arrangement as a screening electrode to the collector against the effect of the induced charges (Ogawa and Doke, 1961) .

The region between the grid G_2, and the collector (5 mm across) is the region of electron drift towards the collector . This drifting process provides enough time for the positive ions produced in the region between the extractor and the first grid G_1, to be efficiently collected by the cathode and removed thus ensuring improved resolution of the signal obtained at the collector . This drifting process (Breskin et al 1995) can be maintained between, either, the extractor and G_1, region; or between G_1, and G_2, region . With this arrangement, the drifting charges can arrive at the amplification points each individual charge at a time and can be amplified and the resulting avalanche collected at the collector represents single charge counting which is the basis of the unified, nanodosimetry adopted in this work (Watt, 1988; 1989b) . Individual voltage supplies were provided for each

electrode (Figure 5.1b) to ensure adequate versatility for analysis of the main characteristics required to optimize the design of the detector . The choice of counting gas (section 5.2.2.1) to operate the device at maximum gain was one of the main requirements, as well as the factors governing the dependence of the intrinsic gain on reduced electric field (section 5.3.4) . The role of the electron and UV modulation of the internal gas multiplication, the consequence of the resolution of individual charge signals and unusual problems that arose because of the tiny size of sensitive volume (nanometre dimension at unit density) were all subjects of analysis .

5.2.1.2 The design of the final prototype nano-detector

In section 5.2.1.1, it has been shown that the initial version of the prototype nano-device is designed in a general form for the preliminary investigation of a wide range of the desired characteristics of a device for absolute measurement of radiation bio-effectiveness . Depending on the outcome of these preliminary investigations, it was necessary to design the final version of the prototype nano-device as an up-to-date version of the detector .

The general design configuration of the latest version of the gas-filled nano-device is shown in Figure 5.3a, whereas its electrode configuration is shown in figure 5.3b. V, is a cylindrical radiosensitive volume defined by the diameter of the aperture (1 mm) in the extractor electrode and the spacing (1.5 mm) between the latter and the cathode . The two electrodes are made from conducting tissue-

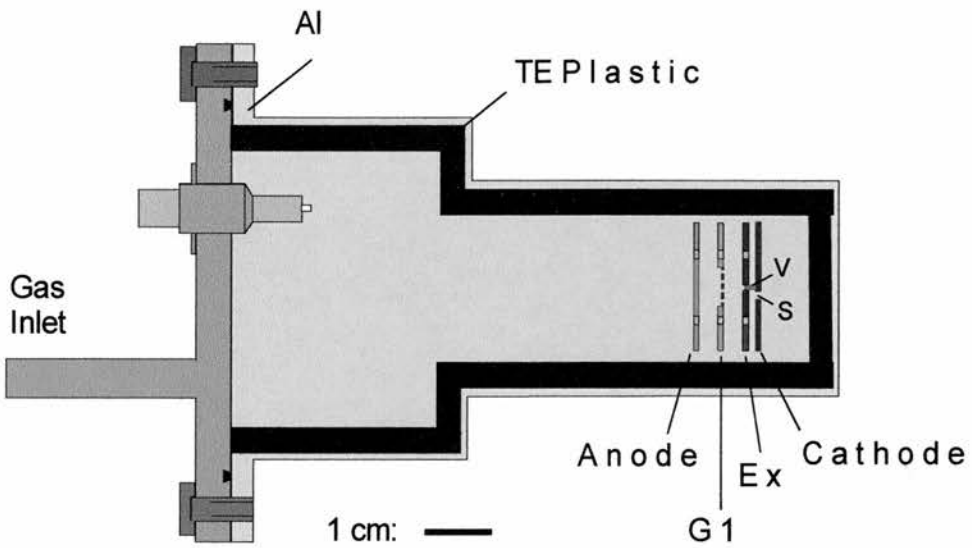

Figure 5.3a: A schematic drawing of the final, single grid, version of the nanodetector, with electrode assembly .

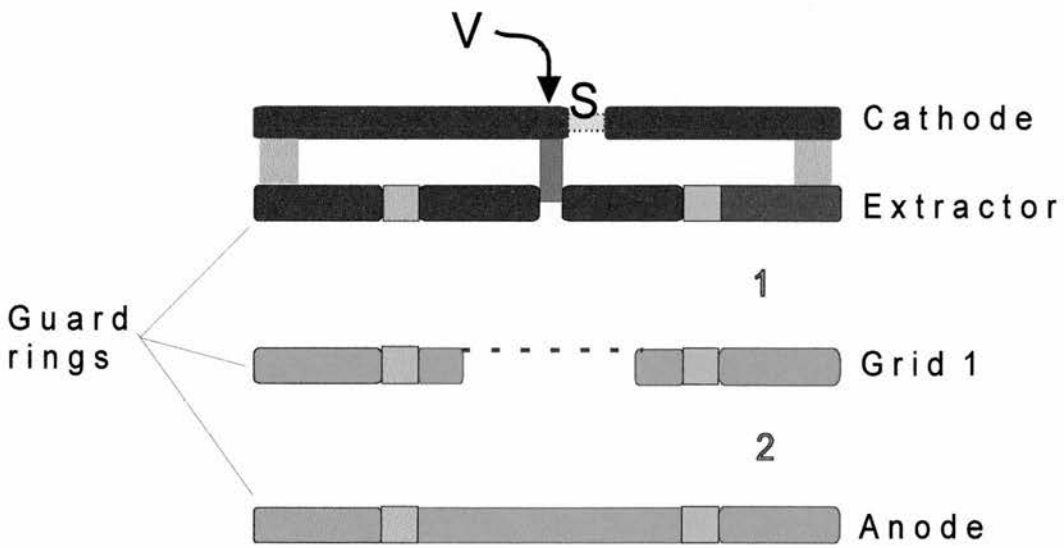

Figure5.3b: An enlargement of the electrode assemblyof the final version of the nanodetector .

equivalent (TE) plastic, type A150 . The electrode assembly is mounted in a nylon cradle which slips into the cylindrical TE container .

In Figure 5.3b electrons extracted from the volume V, are accelerated in region 1 with a gain of about 10^3 and pass through the grid G_1 , mesh into the second amplification region 2 and collected at the collector with over all counter gain of $>10^6$. The bias voltages applied depend on the type of the gas used and the pressure .

Although the general principles for the operation of the two versions of the nano-detector remained unchanged, major differences arose between them as the result of the modifications made in the design and construction of the final version of the prototype nano-detector . The main feature of these modifications is that, in the final version, the number of intermediate grids is reduced to a single grid instead of the multi-grid configuration used in the construction of the initial version of the prototype nano-detector . This modification was necessary because, the results of the preliminary investigations showed that the level of amplification needed for the desired operation of the detector can be reached ($>10^6$) by using a single grid system and thus, only two stages of amplification (figure 5.3b) . Furthermore it has been concluded that the maximum intrinsic gain of the detector (section 5.3.4) is limited by the density of the charge in the final stage of the amplification process regardless of the number of amplification stages included in the system.

An other major difference in the design and construction between the initial and the final prototypes of the nano-device is that the sensitive volume in the latter is situated in a region of complete tissue equivalent conditions provided by the combination of the TE electrodes of cathode and extractor . The construction of this region in tissue equivalent material ensures that the device will operate under TE conditions that in turn will provide the state of charged particle equilibrium that recommended for proper simulation of the radiation action in targets present in mammalian cells as well as for proper interpretation of the instrumental signal output .

To reduce effectively the large background signal observed associated with the signal output of the initial version of the nanodosimeter, the modification feature in the final version of the prototype detector includes also the reduced dead volumes of the detector, mainly at the regions 1 and 2 (figure 5.3b) . This is done basically, by reducing some of the dimensions in the operational regions of the detector, such as the radii of the effective disc areas of the electrodes involved in the amplification processes, and possibly by the reduction in the inter-electrode spacings .

5.2.2 The counting gas, evacuation and the gas filling system

The choice of a suitable gas is a vital aspect of the proper operation of the gas-based radiation detectors . The use of a standard and efficient evacuation and gas-filling system is also an important factor for the successful manoeuvre of the

device between the evacuation and gas-filling system, and the measuring electronic system and yet maintaining the effective control of the counting gas conditions, such as the durability of its purity, variation of its pressure etc .

5.2.2.1 The counting gas

When choosing a counting gas for a gas-based radiation detector, various factors should be borne in mind, such as the charge transport properties of that particular gas (section 4.5) . Different types of pure gases and mixtures were experimented using the initial version of the prototype detector to optimise the desired detection properties of the device .

The gas mixture used initially was Ar (90 %) + CH_4 which allowed for stable operation at lower gains . However, for the higher gain needed, it is necessary to use high applied voltages . Electrical breakdown was then noticed at much lower operating voltages, thus requiring higher electronic amplifier gain which, in turn, decreases the signal-to-noise ratio . Therefore different gases and gas mixtures were tried for much stable operation of the device and yet giving higher gain (Jean-Marie et al, 1979) . With tetramethylsilane (TMS) vapour, a wider range of E/P can be used to produce signals with better resolution and higher gain before reaching saturation and electrical breakdown in the counter operation but instability is observed in the output signal that may be due to instability in the purity of TMS vapour . Propane and propane based TE gases led to stable operation condition of the device under most of the conditions required for the test of the

counter (Grosswendt and Baek, 2000) . When filled with propane gas at pressure of 1 torr, the mean chord through the sensitive volume, V, of figure 5.3b, is equivalent to about 1.8 nm at unit density .

5.2.2.2 The evacuation and gas-filling system

As it was necessary to investigate the desired properties of the detector under various pressures, a high vacuum system capable of a minimum pressure of 10^{-5} torr, constructed from the facilities available in the laboratory of the Radiation Biophysics Unit in University of St. Andrews, is used in evacuation and gas-filling of the detector . The evacuation and gas-filling system consists of Edwards oil diffusion pump type backed by Edwards two stage rotary pump system . The detector is coupled to the high vacuum and gas-filling system via stainless steel and copper high vacuum pipelines .

The pressures at the diffusion and the rotary pumps are monitored by Penning and Pirani gauges, respectively . The gas pressure in the detector is accurately monitored and controlled using a Chell capacitance manometer.

5.3 The operation of the nano-detector

To operate the device in the desired mode, it was experimentally set-up in a way that can enable the production of the desired and controlled output for the proper interpretation .

5.3.1 Experimental set-up of the nanodosimeter

In general, the experimental set-up for both the initial and the final versions of the prototype nanodosimeter was identical except for the number of grids used in each as stated in section (5.2.1.2) . The detector set-up is shown in figure 5.1b for the initial version of the device as a general example .

The detector electrode system which is contained in a vacuum securing casing, with a suitable means of vacuum access, is carefully wired to the points of connection to various electronic systems and high voltage power supplies associated with it . The detector electronic system consists of a low-noise standard EG and G Ortec preamplifier type PC142 used for signal extraction from the anode of the detector . For the purpose of the preliminary investigation, both of the preamplifiers were used, one to extract a signal from one of the grids, appropriately from the first grid, G_1, of figure 5.1a, and the other to extract the anode (collector) signal simultaneously . The signals are then fed to the main amplifier, Ortec model 472A . Polarizing voltage up to 5 kV can be delivered to the guard rings and electrodes by different makes and types of high voltage power supplies available in the laboratory of the unit .

Output pulse analysis is performed using a variety of multi-channel analysers such as NORLAND, model IT5300 and the computerized, Ortec multi-channel analyser, type Analyst 100T . An Oscilloscope, model TEKTRONIX 2225 is used for the preliminary evaluation of the signals to be analysed .

5.3.2 The test charges, intrinsic sensitivity and calibration

To test the operation of the detector, test charges were introduced into the sensitive volume, V, in Fig. 5.3b, by mounting a plane disk of a 1.5 MBq source of Am-241 alpha emitter (S), 5.5 mm in diameter and in a position off-centred 5.5 mm from the axis of the sensitive volume (figure 5.3b and 5.8a) such that alpha tracks gave a good distribution of chord traversals whilst avoiding any unwanted penetration into the first amplification region . At 2 torr pressure of pure propane gas (C_3H_8), the mean number of statistically fluctuating charges produced was 14, estimated from the solid angle and the LET (ICRU, 1993) . The out put signal of the device depends on the collector applied voltage and the gas pressure . Figures 5.4a and 5.4b show the exponential relationship between the centroids of the spectra and the collector applied voltages for alpha particles at a pressure of 1 torr propane gas .

A beta source of Sr/Y-90 was also tried by mounting the source internally, but the charge generation rate at low pressures of C_3H_8, along the 2 nm chord of the sensitive volume was so low that somewhat higher pressures were used to get a suitably useful signal . Soft X-rays from Fe-55 (Mn K_α X-rays = 5.9 keV) were also tried . Although the signals from the latter source were detectable, there was difficulty in resolving the low intensity signals from the background noise levels . The weakness of the signal from X-rays produced from Fe-55 may be attributed to the loss of charges by diffusion . However, lower noise electronics and the use of an array of sensitive volumes would help to enhance the intrinsic sensitivity of

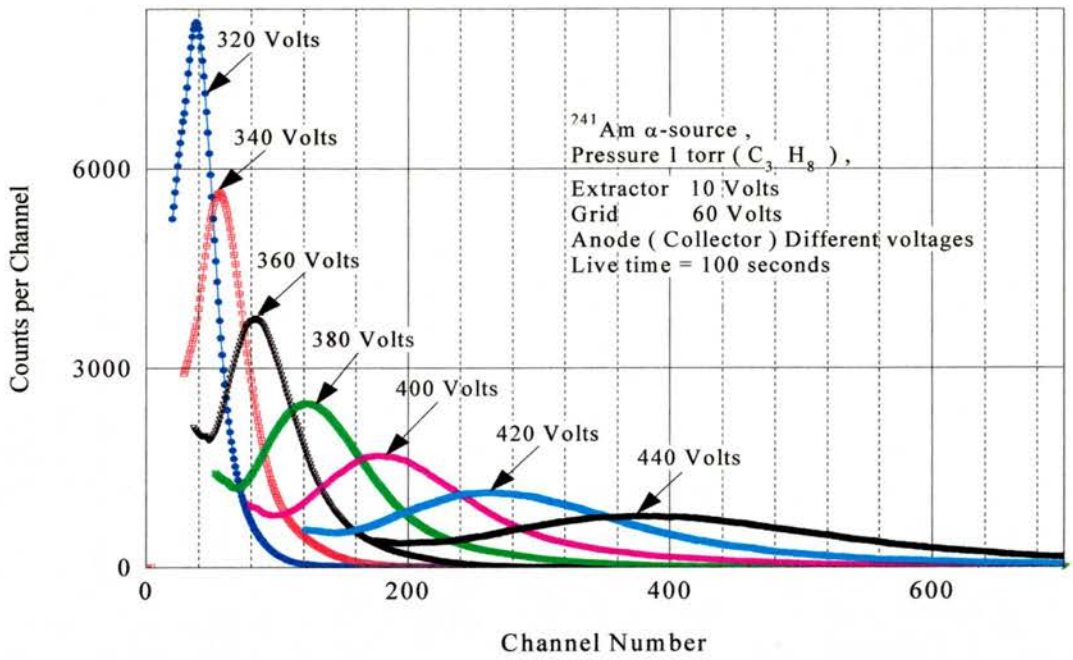

Figure 5.4a: ADC spectra for alpha particles of Am-241, at pressure of 1 torr of propane gas for different collector voltages. Centroids of the spectra depend on the voltages .

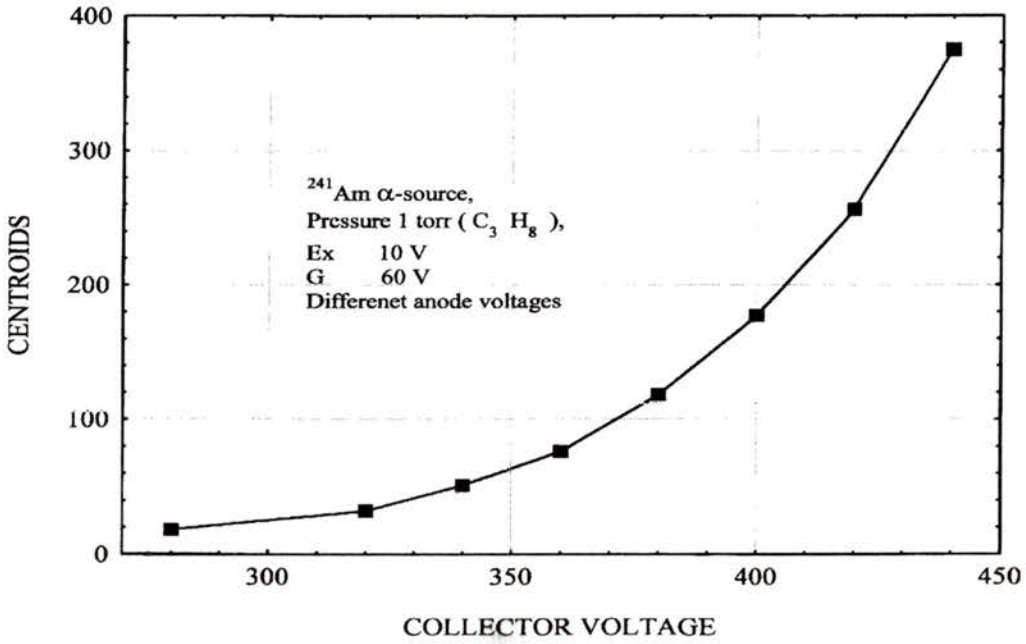

Figure 5.4b: Centroids of the spectra in fig. 5.4a plotted as a function of the collector applied voltages . Exponential relationship can be noticed.

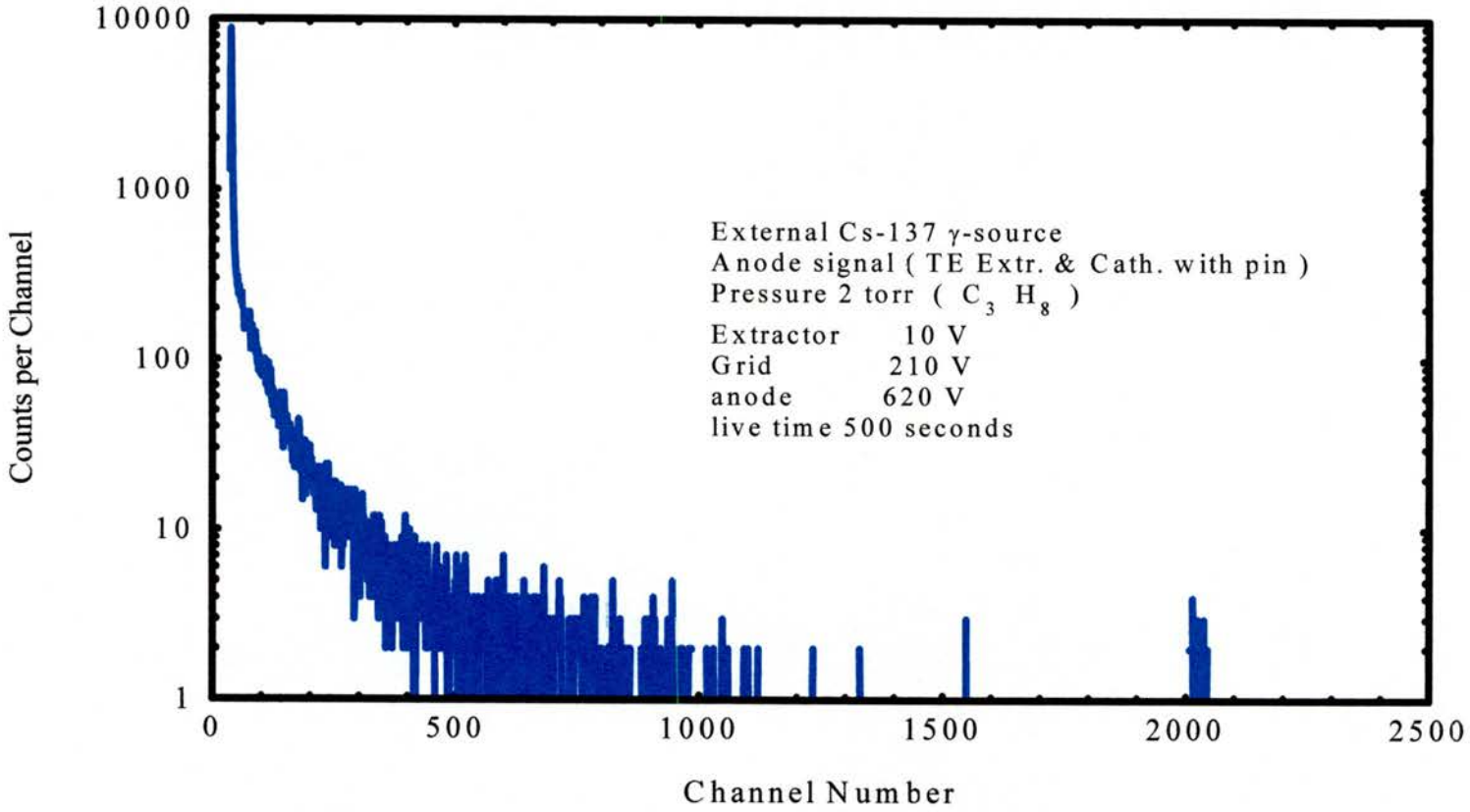

Figure 5.4c: ADC raw spectrum obtained for the gamma-rays from Cs-137 source.

the counter, needed specially for sparsely ionizing radiation .

To test the performance of the final version of the prototype operational nano-device for external neutron and gamma irradiation, first it was exposed to an operational beam of gamma rays from Cs-137 γ-emitter (3.14 MBq, 661 keV) . The device was sensitive to gamma rays but resolution of the signal from the background level was difficult also . That is due to the large number of interaction events in the larger dead volume in regions 1 and 2 of Figure 5.3b compared to the size of the sensitive volume . Figure 5.4c shows the ADC spectrum obtained for gamma rays from a Cs-137 source . However, better results were obtained for sparsely ionizing X-rays and gamma-rays using Co-57 source (section 5.5) . The counter is also exposed to Cf-252 spontaneous fission neutron source, 1.0 GBq, 50 μg, mounted in an X1 capsule . Good sensitivity was achieved, although the background, recoil events originate predominantly from the relatively large volumes, regions 1 and 2 (Figure 5.3b) of the device and seriously obscure the wanted events from the sensitive volume . To surmount this problem, signal gating techniques are being investigated and applied effectively (Tamboul and Watt, 2001) . Figure 5.5a shows an ADC spectrum obtained for Cf-252 neutrons by rejecting the background signals by the subtraction of spectra obtained without and with suppression of the charge extraction from the sensitive volume by reversing the extractor voltage to -20 volts. The results of the processed data of figure 5.5a are shown in figure 5.5b and discussed in section 5.5 .

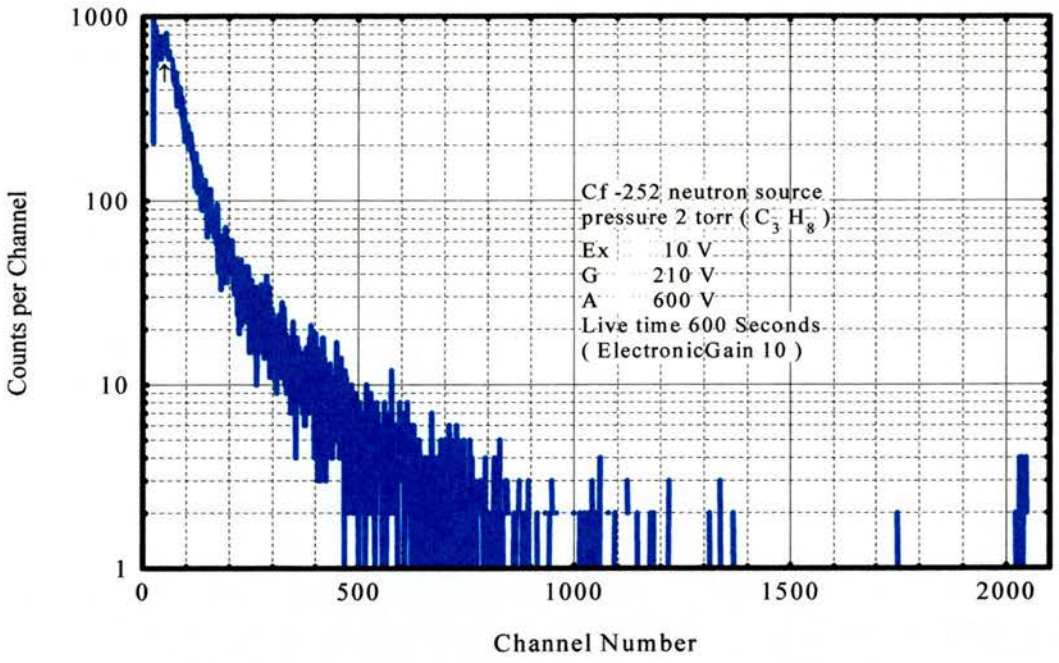

Figure 5.5a: Background corrected raw ADC spectrum for external Cf-252 spontaneous fission neutron source.

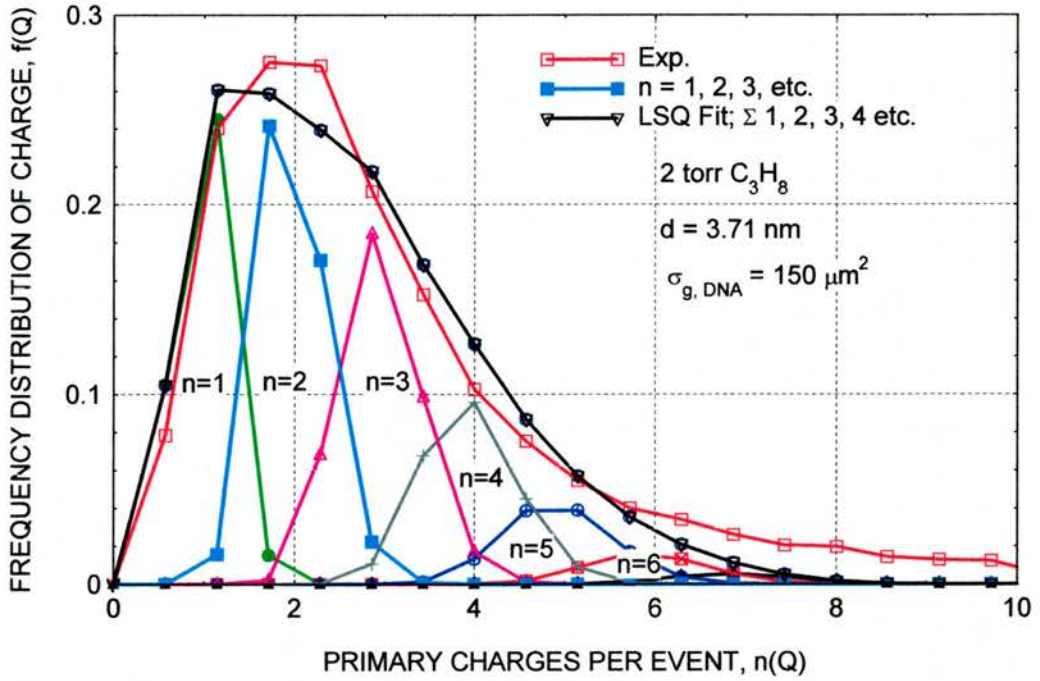

Figure 5.5b: Deconvoluted spectrum of fig. 5.5a to give the calculated frequence distributions of the LSQ Fit compared with the experimental data.

Plateau experiments were done for the detector with the α-particle source as well as with Cf-252 neutron source at different extractor voltages ranging between +20 to -20 volts while keeping the reduced electric fields in regions 1 and 2 (Figure 5.3b) constant . The results of these experiments (Figure 5.6) showed that the optimum operation voltage for the extractor is +10 volts whereas about -20 volts reversal of polarity was needed to reduce the number of charges extracted to a negligibly low level .

As the observed spectra are expressed as probability density distribution of the primary charges, the distributions are dependent on pressure because of the variation in the mean number of charges produced . Therefore, for comparison of the spectra, obtained at different intrinsic gain with alpha particles, calibration is performed by relating the centroid of each observed spectrum to the known average number of charges (Figure 5.7) .

Some difficulties were encountered with the large noise background, mainly of the microphonic noise associated with small amplitude mechanical vibrations around the detector . The source of these vibrations may be the mechanical roughing pumps . Some of the background signal problems was also from electrical interference loops across the other electrical and electronic devices such as the various types of MCAs used in the experiments . Some of the problems of the background were reduced by suitable electrostatic shielding and the use of convenient and efficient connection cables combined with the use of efficient

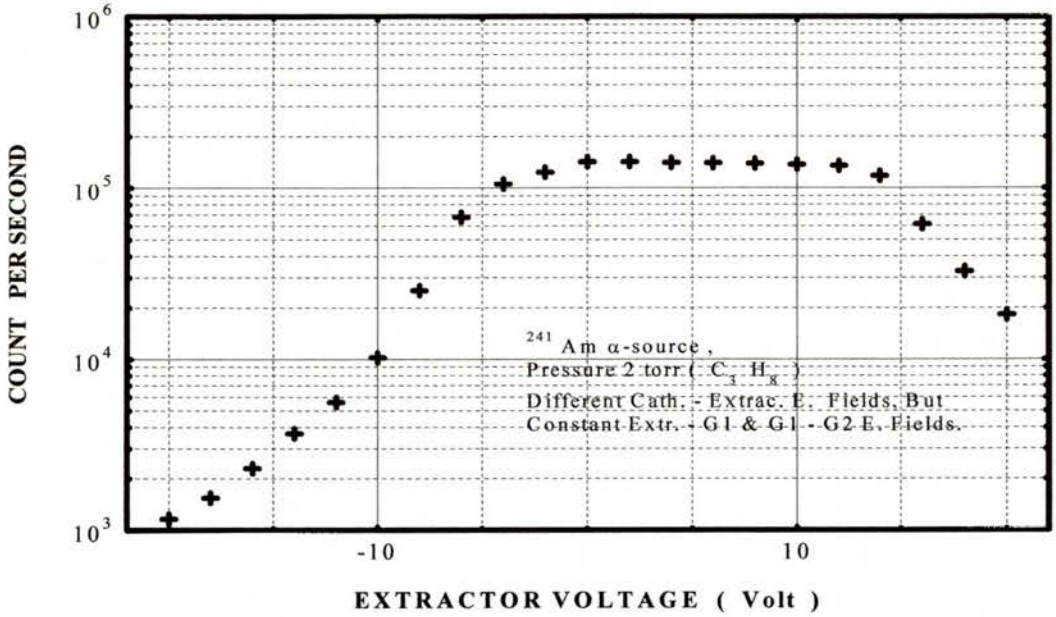

Figure 5.6: Count rates of primary electron clusters for α-particles extracted from the sensitive volume of the nano-device plotted as a function of the extractor voltages .The optimum extraction voltage is +10 volt, and -20 volt is required to significantly suppress the extraction.

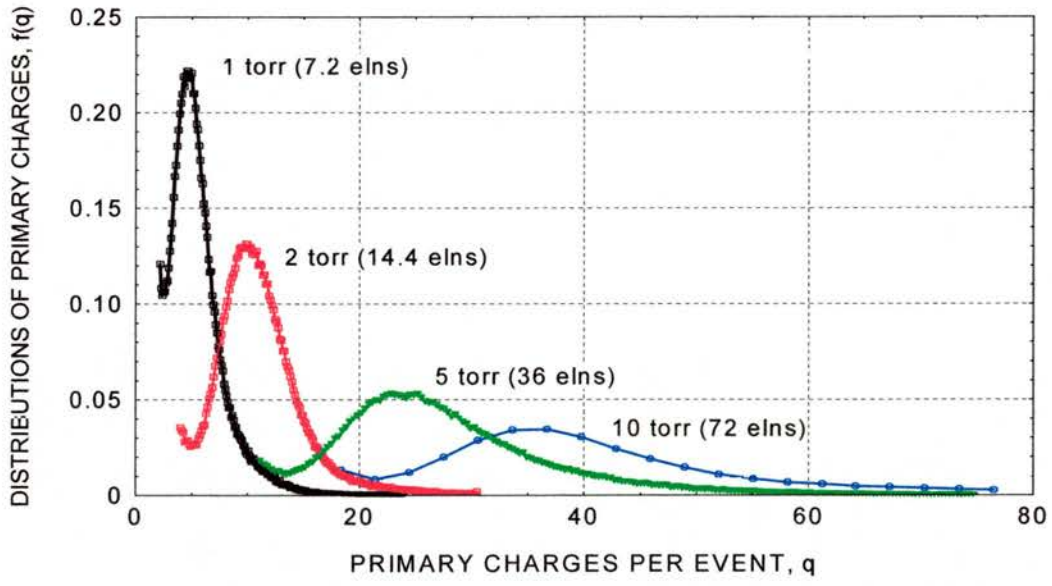

Figure 5.7: Experimental probability density distributions of primary electron charge for 1, 2, 5 and 10 torr pressure of propane gas as a function of the primary charges .

power stabilisers and filters.

In addition to minimizing the leakage currents, the guard rings (section 4.3.5.2) serve to reject the contribution to signal from UV modulated avalanches . This results in improvement of resolution of the collected charges . Typical optimized applied voltages to various electrodes are as follows : Cathode (earthed); extractor (+10 Volts), which is the optimum voltage needed to extract the primary charges produced in the sensitive volume V , into the first amplification region 1 (Figure 5.3b) without multiplication within the sensitive volume during extraction; the grid (+210 volts); the collector or the anode (+580 volts) optimized to the pressure and propane gas and for inter-electrode spacing of 5 mm . This latter voltage can vary depending on the type of counting gas used and the pressure .

5.3.2.1 Consistency check for the device measurements

As the present project is partially supported by the European community contract, it was to be checked, independently for the consistency of the measurements performed using the nano-device, which is expected to be an operational nanodosimeter for radiation protection and radiotherapy . Thus, the comparison among the first experimental nanodosimetric data and calculations was made (Grosswendt et al, 2000) . The geometry of figure 5.8a is used to simulate the nano-device for the purpose of the consistency test . To simulate the measurements of the device, a homogeneous α-particle source was assumed

which, isotropically emitted monoenergetic particles at the 5.4 MeV into the interaction chamber . The calculations were performed for gas pressures between 1 torr (1.35 mbar) and 10 torr (13.5 mbar) . The mean chord length of the α-particle track within the sensitive volume is between 1.9 nm and 18.8 nm at unit density .

Figure 5.8b shows the calculated frequency distribution f(N_c) as a function of cluster size N_c, produced in the sensitive volume by the α-particle in propane ($C_3 H_8$) and at pressure, P . Comparison of the calculated cluster size distribution of figure 5.8b with the experimental pulse height spectra measured using the nanodosimeter (figure 5.7), shows an obvious similarity between calculated and measured values, at least for the pressure dependence .

A more quantitative consistency test of the detector measurement is shown in figure 5.8c . The measured cluster size distribution at 2 torr is shown compared with the corresponding calculated distribution f(N_c) versus N_c, for measured detection efficiency of 20%, 30% and 100% . The detection efficiency of the nano-device is 20% (Tamboul et al, 2000) and a rather satisfactory agreement can be seen between the experimental and calculated data for detection efficiency between 20% and 30% . However, the detection efficiency is even better in the latest modification of the device (Tamboul and Watt, 2001) . Indeed, the efficiency of the device could be made more better in the future prospect (Chapter six) .

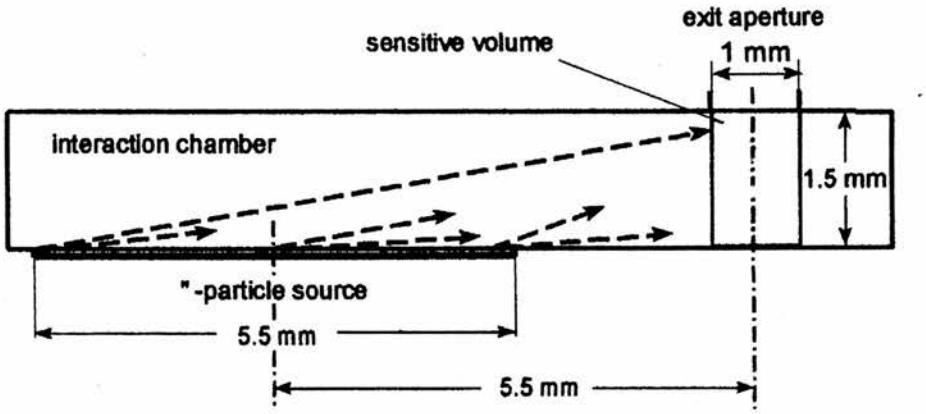

Figure 5.8a: Simulated geometry of the nanodosimeter for Monte-Carlo calculations to which the experimental data of the device were compared for the consistency check (Grosswendt et al, 2000) .

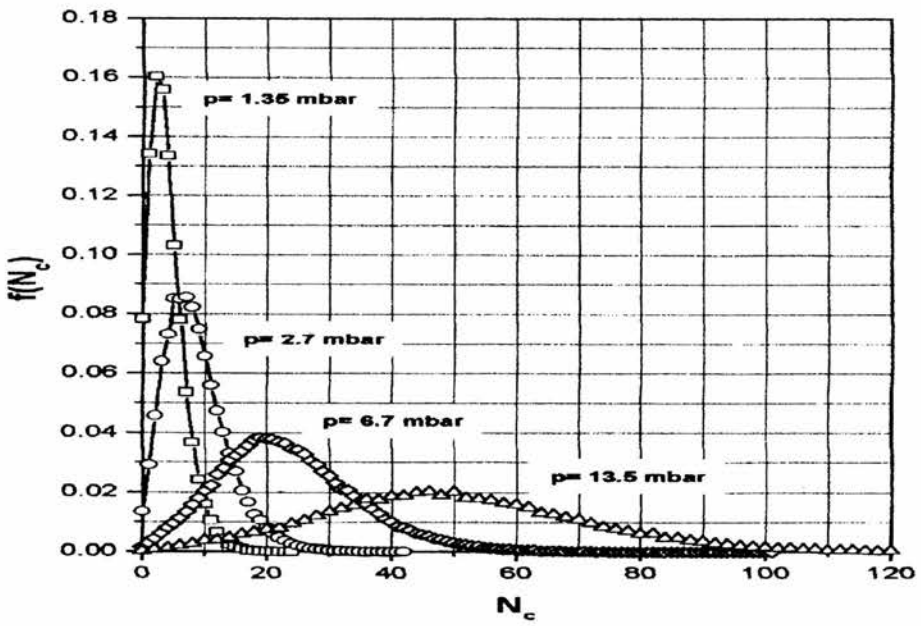

Figure 5.8b: Calculated frequency distribution $f(N_c)$ as a function of cluster size N_c, produced by α-particles of energy 5.4 MeV in a pressure P, of pure propane gas for the simulated geometry of fig. 5.8a.

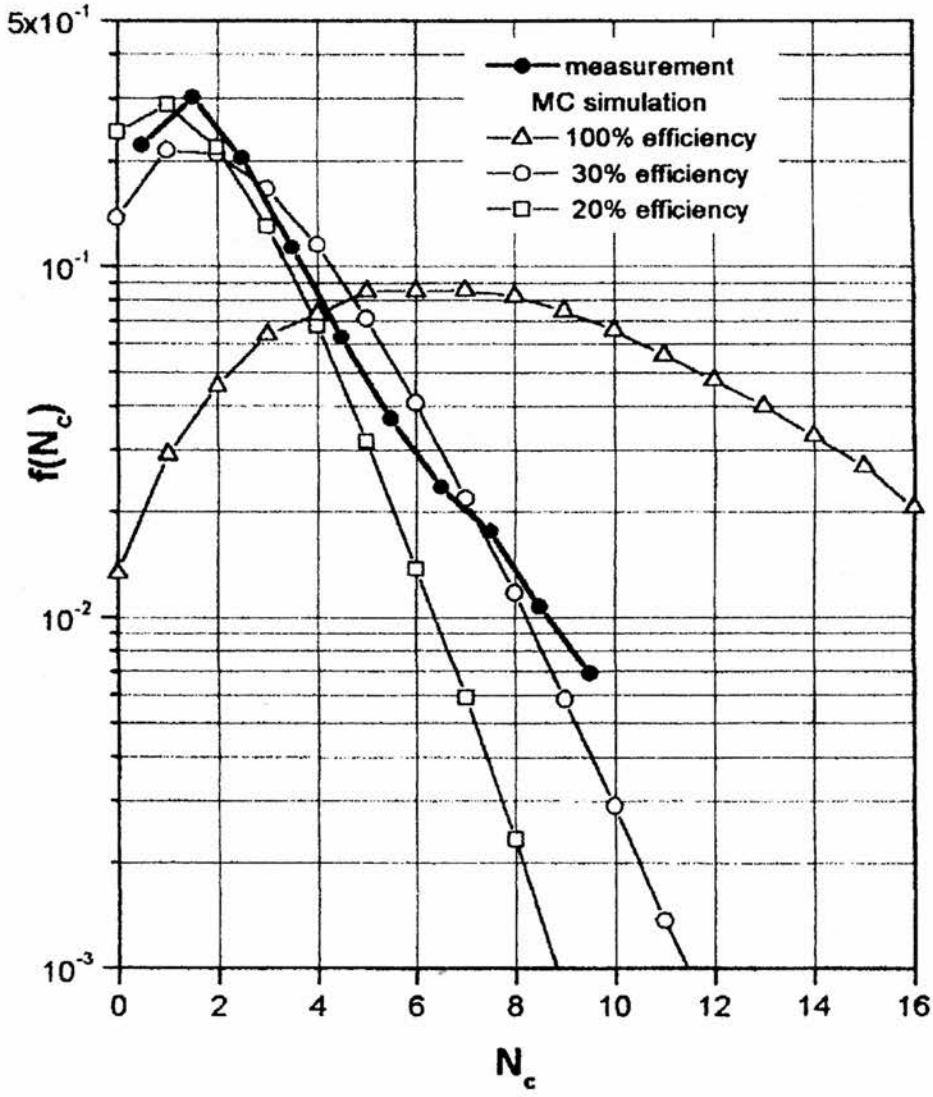

Figure 5.8c: The measured and calculated frequency distribution $f(N_c)$ are compared as a function of cluster size, N_c, produced by the α-particles in fig. 5.8a . It can be noticed that, the experimental data agree with the calculated data at the detector efficiency between 20% and 30% .

5.3.3 Size of the sensitive volume

The sensitive volume of this nanometric gas counter is a right circular cylinder 1 mm in diameter and 1.5 mm in height . It is a wall-less volume (Gross, 1970; willson, 1972) defined by the electric field lines between the parallel cathode and extractor electrodes separated by an insulating annular disk of PTFE 1.5 mm thick to form the height of the cylindrical volume (figure 5.3b) . Extraction of charge from the cylindrical volume was achieved through an aperture 1 mm in diameter, countersunk into the extractor to ensure better configuration of the electric field lines for a regular geometrical shape of the sensitive volume . There were problems concerning the efficiency of charge extraction which was attributed to diffusion losses (Takata and Yin, 1997; Takata et al, 1999) of electrons at low pressure and to the relatively large kinetic energies of the ionization electrons (Grosswendt and Baek, 2000) . To some extent, this loss is reduced because of the compensation in the charge equilibrium obtained from the TE electrodes and the wall of the container . But due to the fact that the compensation is not time coincident, the problem of determining the actual integral number of electron charges produced on each specific cluster remained unsolved directly . Several diameters of aperture ranging from 2 mm down to 0.2 mm were tried . A 1 mm diameter was found to give optimum results and was adopted in the design of the final version of the detector .

Field extraction of electrons was enhanced by using a tip/plane configuration of the field (Denat et al, 1987) . The tip of radius, r_t = 200 microns was mounted in the

cathode and the resulting reduced field, E/P, is given by;

$$E/P = \frac{2.V}{x.P.\ln\frac{4d}{r_t}} \qquad (5.1)$$

where V, is the voltage between extractor and cathode; d, is the inter-electrode spacing; x, is the distance from the tip and E, and P, are electric field and pressure respectively . At the tip, the reduced electric field was 147 $V.cm^{-1}.torr^{-1}$ decreasing to 29.5 $V.cm^{-1}.torr^{-1}$ at the aperture of the extractor .

Test of the initial charges extracted under high fields were made by observing the detector plateau of integral count rate versus reduced field in the sensitive volume whilst keeping the fields in regions 1 and 2 (Figure 5.3b) constant . The results in figure 5.9 shows no indication of unwanted internal multiplication within the sensitive volume at low pressure . Note that, although the plateau of figure 5.9 is made using alpha particles, in the initial version of the prototype nano-device, it completely agrees with the general and wider out look of the plateau of figure 5.6 (section 5.3.2) which is obtained using the final version of the device and in different experimental conditions .

The mean chord through the sensitive volume was calculated to be 1.85 X 10^{-7} g/cm^2 at pressure of 1 torr of pure propane gas, corresponding to 1.85 nm at unit density . This is nominally equivalent to the mean double-strand spacing in the DNA molecule .

For the tissue-equivalent version of the prototype nanodosimeter, the cathode and extractor electrodes were each 2 mm thick to provide a moderate degree of charged particle equilibrium conditions for application in prospective operational radiation fields . The enclosure of the electrode system of the final version of the prototype nanodosimeter is made of tissue equivalent (TE) material for further charged particle equilibrium conditions .

5.3.4 Maximum intrinsic gain of the detector

The gain of the detector is the key factor for its functional operation . Therefore, the basic design configuration of the system was to achieve the goal of attaining the highest possible gain in the detector . The operation of the detector at near maximum intrinsic gain was expected to have the desirable properties of optimization of the signal-to-noise ratio and attainment of sufficiently high statistical precision to resolve individual primary charges . The intrinsic gain G, of the detector was determined empirically from;

$$V_i = \frac{nq}{C} \tag{5.2}$$

and,

$$V_s = V_i . A . G \tag{5.3}$$

where V_i is the voltage generated by n initial electrons each of charge q in a primary cluster produced by the initial ionization electrons, and C is the capacitance measured for the detector in its operating condition . The magnitude

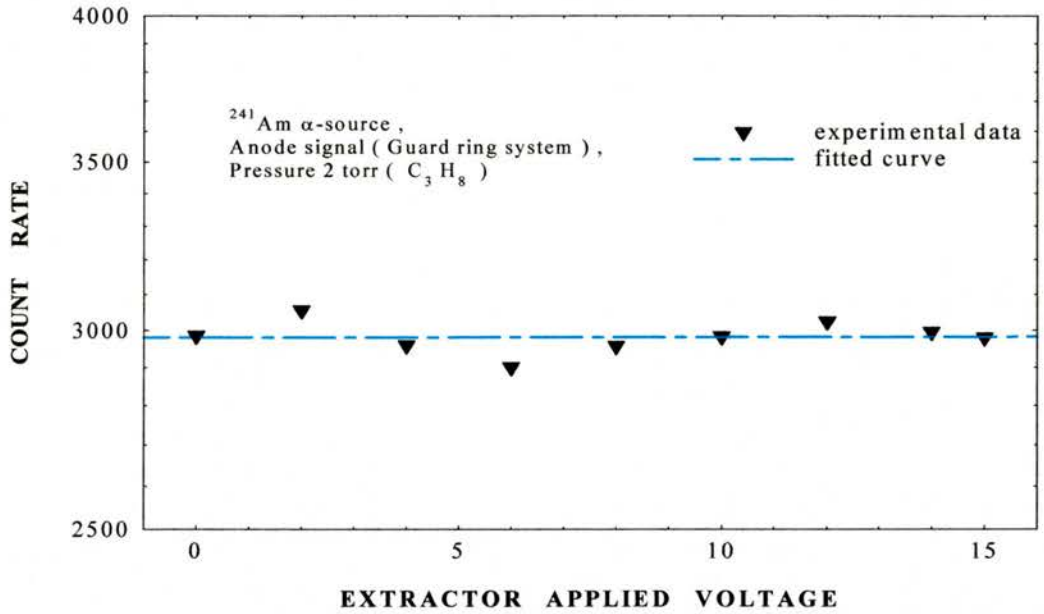

Figure 5.9: The plateau of integral count rates of α-particle in the initial version of the prototype nano-detector as a function of the extractor voltages whilst keeping the fields, in regions other than between the cathode and the extractor, constant .

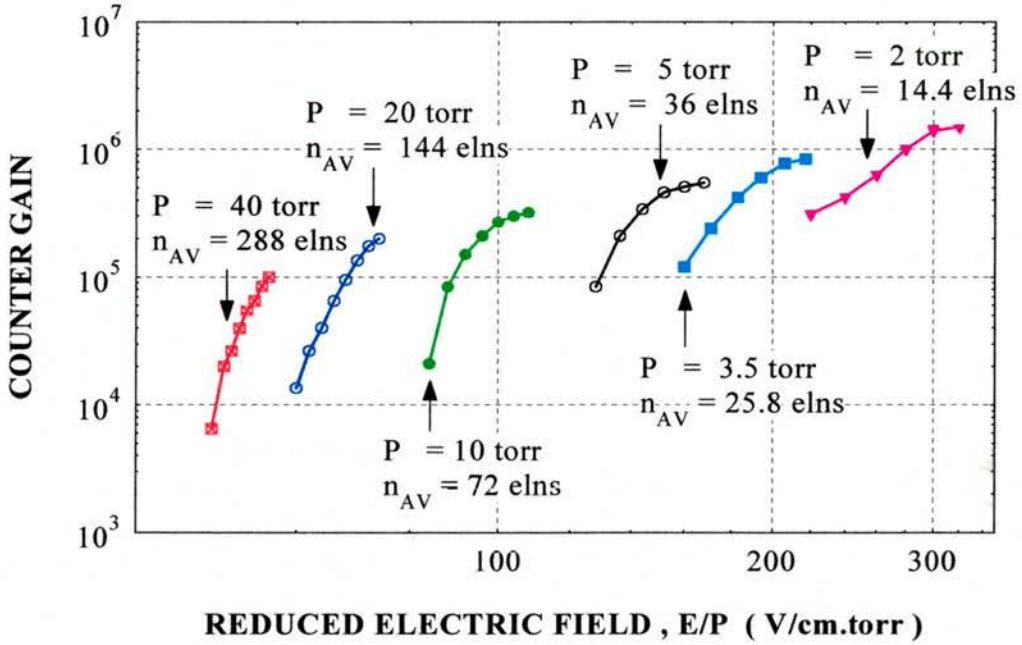

Figure 5.10: The intrinsic gain of the nanodosimeter as a function of gas pressure and the reduced electric field . The maximum gain is limited by the average number of the primary charges, n_{AV}, released in the sensitive volume.

of C is mainly due to stray capacitance (Watt et al, 1964) and is taken to be 5 X 10^{-11} Farad . V_i is typically calculated to be 3.2n nanovolts, (n = number of the initial electrons or charges) . V_s is the amplified output signal of a few volts, measured with an oscilloscope . The amplifier gain A includes gain at the preamplifier plus the gain at the main amplifier. Since;

$$G_{max} = \frac{V_s}{V_i . A} \tag{5.4}$$

with V_s, limited empirically, and the preamplifier gain is also limited to 5, it is important to minimize the electronic amplification A, to as near unity as possible in the main amplifier whilst taking steps to avoid saturation of electronics by the input signal . This had to be reduced at some stages of the experiments, by a measured factor of 100 times, using a screened potential divider to reduce the electronic saturation effects that were sometimes observed .

Results of the counter intrinsic gain G, are shown in Figure 5.10, plotted against the reduced applied electric fields in region 2 of the detector (Figure 5.3b) . The intrinsic gain is determined per electron cluster as a function of E/P (Ségur, et al, 1989) for various gas pressures of pure propane gas and n_{AV} is the calculated mean number of electrons per cluster . The results are obtained for 1 mm diameter extraction aperture . Guard rings were fitted to improve resolution .

From these results as well as from others obtained using the multi-gridded nano-device, compared to those obtained using the single grid system under the same

conditions, it is concluded that the maximum intrinsic gain in the detector is determined by the limitation to the charge density in the final stage regardless of the number of gain stages included . It seems that the same maximum gain is attainable whether the electron avalanches are electron or UV propagated . It is noted also that the maximum achievable gain reduced as the number of primary electrons in the initial cluster increases . For example, in figure 5.10, for the calculated number of the primary charges of 14.4 at the pressure of 2 torr, the maximum gain is $>10^{6,}$ where as for the number of the primary charges of 288 calculated for the pressure of 40 torr, the maximum gain is reduced to $<10^5$. This leads to the conclusion that formation of a charge plasma in the vicinity of the collector electrode (anode) is the probable mechanism limiting the intrinsic gain in low-pressure parallel plate devices .

On the basis of the fact that UV photons have much longer mean free paths for ionization than do charged particles, the action of UV is believed to be a major cause for the inferior resolution in gas-filled parallel plate detectors . As a test, the active electrodes were reduced in diameter and surrounded by guard rings . Although a proper evaluation of the effect is still needed to be performed, the action taken improved the resolution by a significant factor .

5.4 Detection and resolution of single charges

The detection and resolution of single electrons is a crucial need in the analysis of the results obtained from the measurements, using the nanodosimeter . This is

true especially when simulation of radiation action at the level of the DNA is involved . Although the nanodosimeter has adequate sensitivity to detect single electrons, and despite the high intrinsic gain that could be achieved, it was found difficult to resolve directly single and small integral numbers of electron charges in clusters. Collated spectra for experimental probability density distribution of primary charges for various pressures of pure propane gas are shown in figure 5.7. The number of primary charges per cluster is determined by the calculation of the expected primary charge yield . The increased events at the lower values of the primary charges is electronic background noise which leads to the increase in count rate . The limitation to resolution was attributed to the mechanism of formation of the charge avalanches in parallel plate devices whereby the statistical spread of the sub-avalanches dominates the resolution (williams, 1962) rather than the initial number of charges .

A solution to the problem was obtained by modifying convolution/deconvolution method reported by Srdoč et al, 1987; and Obileć et al, 1998, who analysed soft x-ray resolution in cylindrical proportional counters . In this, the gamma function, $Y = a\ x^{b}.\exp(-cx)$ is fitted to known single-electron distribution observed in a cylindrical PC . The convolution spectra for larger integral values n, of charges are then calculated using a generalised gamma function of the form; $Y = a\ x^{nb+n-1}$ .exp (- c x) where b, and c, are fitted coefficients and a, is a normalisation factor.

In the present work, the single-electron spectrum from the parallel plate gas-

filled nanodosimeter could not be uniquely resolved as it occurs among other stochastically varying cluster sizes . Thus the experimental distribution produced, such as by traversal of charged alpha tracks across the sensitive volume of the detector (Figure 5.3b), is assumed to comprise a Poisson-weighted distribution of plural (n = 2, 3, .. etc) electron primary charges in clusters with a mean number of charges per cluster . The number of primary electrons per cluster can be obtained either by calibration of the experimentally observed spectrum or by treating it as an unknown variable to be fitted along with parameters, b, and c . The results can then be convoluted to yield the single and higher order of charges per cluster . Shown in figure 5.11a, is an ADC spectrum generated by alpha particles in the sensitive volume of the nanodosimeter (figure 5.3b) with TE electrodes and guard rings, at a pressure of 1 torr of pure propane gas . The spectrum is obtained after the background rejection using the subtraction technique (section 5.3.2) . Figure 5.11b shows the frequency distribution of the charges of the spectrum in figure 5.11a deconvoluted into the individual components, n = 1,2,3,4 electron spectra .

5.5 Measurement and results

As it has been stated in earlier sections of this chapter, the prototype multi-wire nanodosimeter is used for the preliminary investigations and different measurements and experiments have been made . Various experimental results have been obtained for internally mounted sources such as alpha particles from Am-241; beta particles from Sr/Y-90 and soft X-rays from Fe-55 (Mn K_{α}

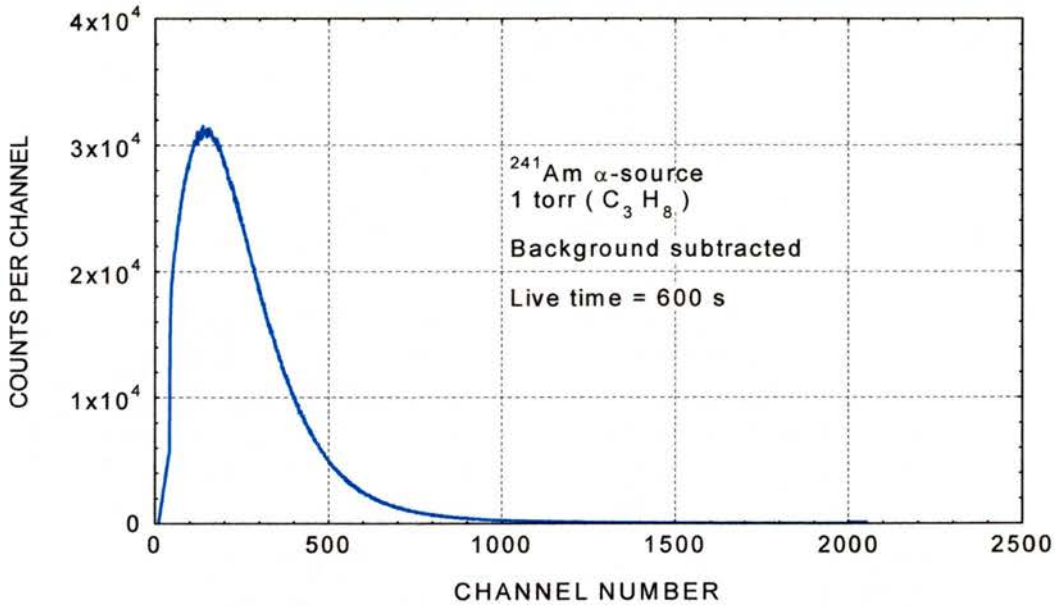

Figure 5.11a: An ADC spectrum for α-particles of an internally mounted emitted Am-241 source, measured by the nanodosimeter . Extractor = +10 V; Grid = 210 V; Anode = 500 V; pressure = 1 torr propane gas . the spectrum is corrected for the background .

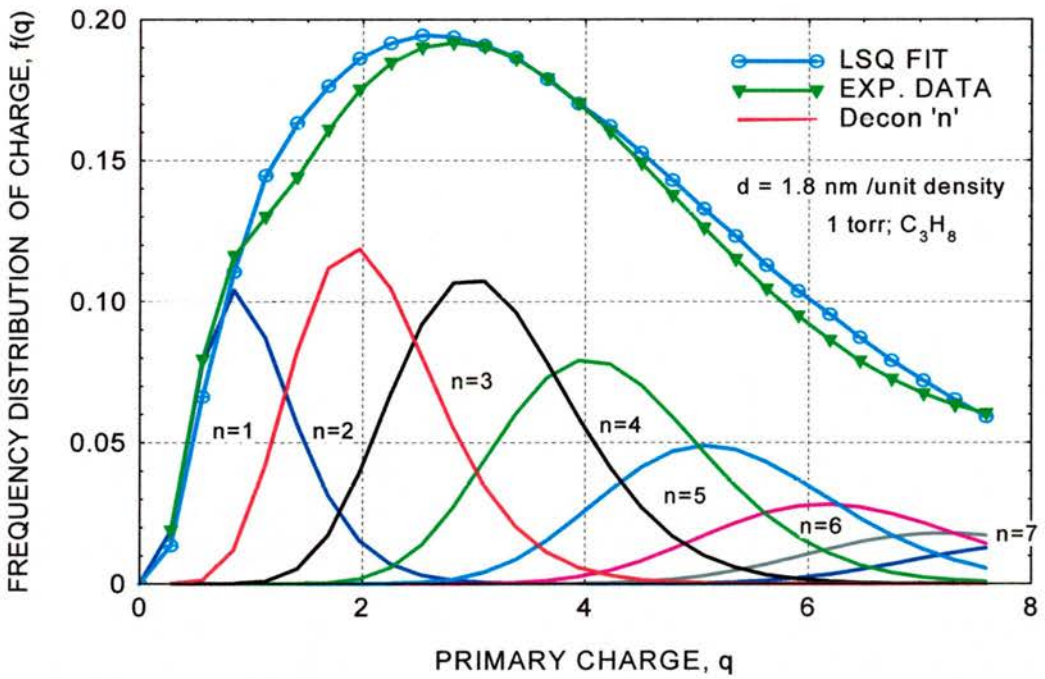

Figure 5.11b: The data in fig. 5.11a is processed and deconvoluted to give the integer of the experimental frequency distribution.

X-rays = 5.9 keV) . Different experimental conditions were used initially to explore the desired features of the device . Some of the fundamental conditions of these, such as the gas pressure, type of counting gas (section 5.2.2.1) and the applied voltages, are optimised during the measurements . However, of these optimised conditions, the pressure of 2 torr of pure propane gas and the tissue equivalent combination were the best conditions that provided the most stable operation for the device .

Laboratory tests were conducted using the final version of the prototype nanodosimeter on the following;

1 - 5.4 MeV α-particle Am-241 source internally mounted mainly for calibration purposes . Figure 5.11a shows an ADC spectrum for alpha particles at the pressure of 1 torr, pure propane gas . The spectrum is obtained after the rejection of unwanted background using the subtraction technique . The deconvoluted results of the spectrum in figure 5.11a are shown in figure 5.11b . This spectral result forms an example of the optimum experimental results obtained using the nanodosimeter, and they form the basis of the calibration of the measuring unit, in addition to testing the inherent method of calibration, analysis and interpretation of the operation of the nano-detector .

The efficiency of radiation damage is found to be 86.4% for alpha particle track traversals . Only 3% of the events did not interact in the passage through the sensitive volume due to stochastical process of interaction .

This is determined by subtraction of the deconvoluted spectra, n = 0 and n = 1 from the experimental spectrum, given by equation (6.1) . The corresponding bio-effect cross-section for inactivation, scaled by a factor n_0 = 15 to permit comparison with the multiplicity of targets (section 3.2.2.3) in mammalian cell, is 40.6 μm^2, marked "A" in figure 3.3 .

2 - As it has been stated in section (5.3.2), figure 5.5a shows the background discriminated ADC spectrum for the external irradiation of a mixed neutron, gamma source of Cf-252 spontaneous fission neutrons . The gas pressure of 2 torr, pure propane, was used as the optimised conditions . Figure 5.5b shows the results of the deconvolution of the spectrum in figure 5.5a, which data are processed to give the experimental and calculated frequency distributions and the deconvoluted integer charge spectra .

As it may be expected for the tiny sensitive volume involved in the process, 20% of events passed through the volume without any interaction . Therefore, the efficiency of damage was 47.5% and the associated effect cross-section is 22.3 μm^2 . Since the prototype nanodosimeter operates, in this stage, at the single volume mode, these results were scaled by a target multiplicity factor of 15 times to enable comparison with the effect cross-sections for mammalian cells . This is marked "N" in figure 3.3 .

3 - A Mossbauer source of Co-57 of low-energy X-rays and gamma rays was

used also, to irradiate the nano-detector externally to generate an equilibrium electron field in the sensitive volume region . For these sparsely ionizing radiations in equilibrium; 49% passed through the target without interaction . Therefore, the damage efficiency in this interaction was just 15.9% . Comparisons were made directly with the other photon sources as indicated by "G" in figure 3.3 .

Figure 5.12a shows the ADC, background rejected spectrum of low-energy X-rays and γ-rays from Co-57, measured using the prototype nanodosimeter, at the pressure of 2 torr pure propane gas . It can be noticed that the more significantly important lowest channels of the spectrum are not quite fully resolved for these sparsely ionizing radiations.

In figure 5.12b, the data of the spectrum in figure 5.12a are processed to compare the experimental frequency distribution with the deconvoluted spectra . A very low number of electrons per cluster is obtained .

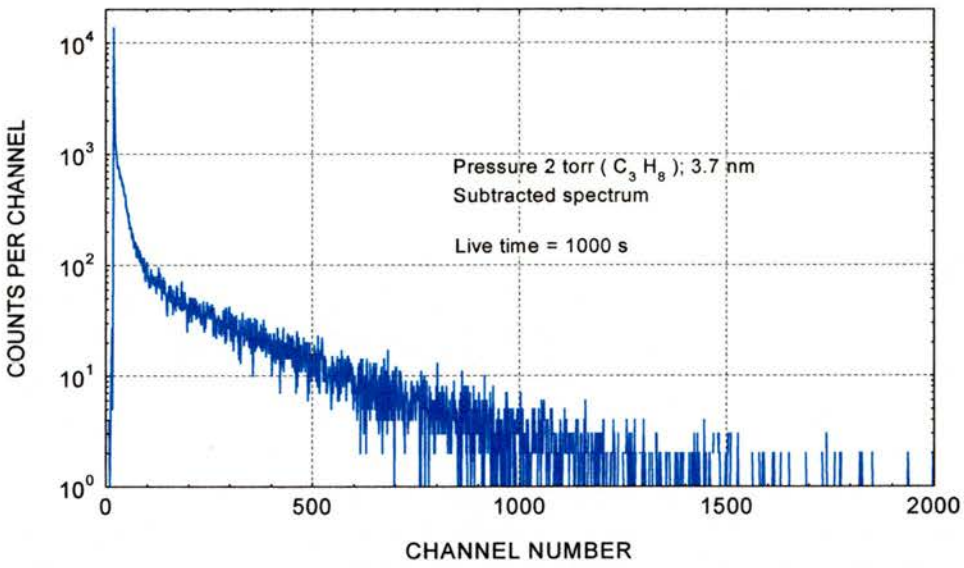

Figure 5.12a: A raw ADC spectrum produced in the nano-detector by a Mossbauer source of Co-57 emitting low energy x-rays and γ-rays .The source is externally mounted to generate an equilibrium electron field in the sensitive volume of the device .

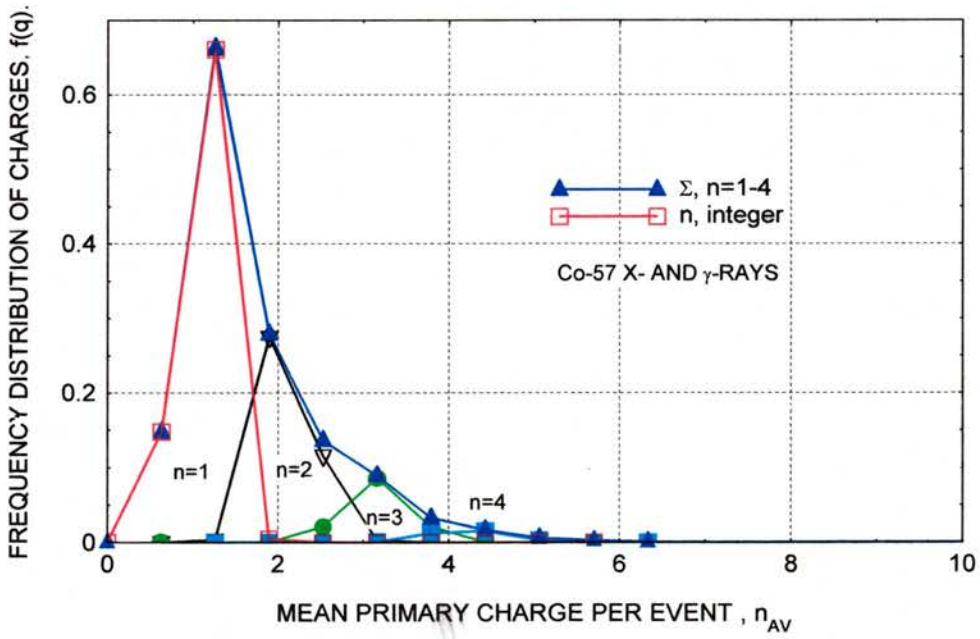

Figure 5.12b: The data in figure 5.12a is deconvoluted to give the experimental frequency distributions.

CHAPTER SIX
INTERPRETATION OF THE RESULTS; CONCLUSIONS AND FUTURE PROSPECTS

6.1 Interpretation of the results

The design and construction of the prototype, gas-filled nano-device aims to provide a means of implementing the transition from conventional microdosimetry to nanodosimetry at the molecular level, having dimensions corresponding to known bio-sensitive target sizes within mammalian cell nuclei (Pszona et al, 2000) . The output signals give a measure of damage efficiency, ε . Interpretation of these signals which arise from the radiation events offers the possibility of investigating the validity of various weighted quality parameters . These may be categorised, by their moments of energy transfer, into three;

a) Zeroth moment of charge

The efficiency of damage ε_0 , which represents the quality factor, is determined by the number of events each comprising $\geq$ 2 charges along a 1.85 nm chord such as the mean free path for linear primary charge λ . The notation ε, used here for the efficiency of damage should not be confused, with the macrodosimetry related quantity " Energy deposited " or with the microdosimetry related quantity "energy imparted" which are both also denoted by, ε . Experimentally, an approximation can be made by permitting the two charges to be at anywhere along the 1.85 nanometre chord rather than the desired value of two charges separated by 1.85 nm . Measurement of the quality for damage

efficiency ε_0, does not require knowledge of the type of radiation (Tamboul and Watt, 2000; Tamboul and Watt, 2001) . Hence; using Poisson's statistics,

$$\varepsilon_0 = \int_2^{\infty} f(q).dq \qquad (6.1a)$$

$$= 1-(1+n_{AV}).\exp(-n_{AV}) \qquad (6.1b)$$

where n_{AV}, is the average number of the primary charges .

b) First moment of charge

The efficiency of damage ε_1, is determined by the probability that charge ≥ 1 will be produced anywhere in the radiosensitive target, hence;

$$\varepsilon_1(\geq 1) = 1-\exp\left(-\frac{\bar{q}_F}{q_0}\right) \qquad (6.2)$$

where,

$$\bar{q}_F = \int_1^{\infty} f(q).q.dq \qquad (6.3)$$

q_0, is a reference charge evaluated at the onset of saturation damage and it is dependent on radiation type . Relevant quality parameters in the first moment of charges category are the restricted track LETs such as $L_{r,T}$; $L_{<100,T}$; and the microdosimetric parameters, average lineal energy $\bar{y}_F$, and the average specific energy $\bar{z}_F$, each can be obtained by replacing charge by the appropriate quantity.

c) Second moment of charge;

The efficiency of damage ε_2 , is given by the normalised weighted charge;

$$\varepsilon_2(\geq 1) = 1 - \exp\left(- \frac{\bar{q}_D}{\bar{q}_F \cdot q_0} \right) \qquad (6.4)$$

where the normalized weighted charge is given by;

$$\frac{\bar{q}_D}{\bar{q}_F} = \frac{\int_1^\infty f(q) \cdot q^2 \cdot dq}{\int^\infty f(q) \cdot q \cdot dq} \qquad (6.5)$$

q_0, is also a reference charge evaluated at the onset of saturation damage and it is dependent on radiation type as in the first moment of charge category . The relevant parameters are the dose restricted LETs, such as $L_{r,D}$; $L_{<100,D}$; and the microdosimetric quantities, average y_D, and average z_D .

The cut-off in LET is taken as the radius of the chord r, determined by the simulated target size of the detector, rather than the more usual 100 eV cut-off used for larger target sizes such as mass of tissue or cells (Bartels and Harder, 1990) . For these various quantities, the charge q, can be replaced as required; by the lineal primary charge (q/d) for the quantity related to the zeroth moment, the lineal energy (y = w.q/d) for the first moment; or the energy imparted, (w.q) for the second moment related quantity . d, is the mean chord for the radiosensitive volume of interest and w, is the differential mean energy expended to produce an ion pair .

In figure 6.1, values of the lineal charges (q/d) are shown for the experimental spectrum obtained by firing α-particles from Am-241 source into the sensitive

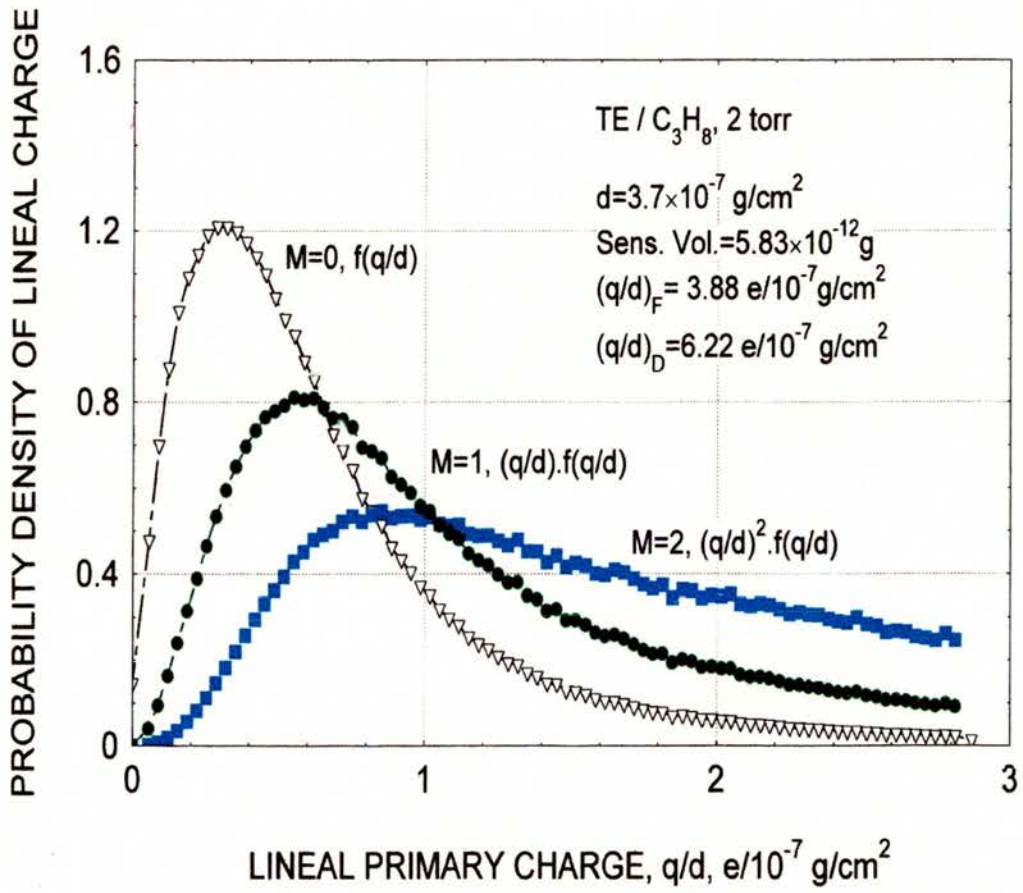

Figure 6.1: Zeroth, first and second moments of the observed experimental distributions for lineal primary charges (q/d) generated by α-particles in the nanodosimeter at the pressure of 2 torr pure propane gas .

volume of the nanodosimeter (figure 5.3b) at the pressure of 2 torr of pure propane gas . The values are shown for the zeroth, first and second moments and comparative probability densities of the lineal charges are plotted as a function of the lineal primary charges .

On the basis of the foregoing, the instrumental measurement of the bio-effect cross-section σ_B , is given either by equation 3.18, or by;

$$\sigma_B = \sigma_g . n_0 . \varepsilon_M \tag{6.6}$$

where ϵ_M, is the probability of initial damage in the sensitive volume for single charged particle tracks of moment M, which is zero for zeroth moment; $\sigma_g.n_0$ is the product of the projected geometrical cross-sectional area of a single biological radiosensitive site and n_0, which is the multiplicity of targets at risk for a single track . The rate of damage during exposure to the radiation field is equal to $\sigma_B.\varphi_{eq}$, where φ_{eq}, is the equilibrium charged particle fluence rate which is given by;

$$\varphi_{eq} = \frac{\dot{N}_C}{\sigma_V} \tag{6.7}$$

where $\dot{N}_C$, is the observed count rate in a detector having a sensitive volume of projected geometrical cross-sectional area σ_V . Thus the rate of damaging events recorded by the instrument is;

$$\dot{N}_B = \dot{N}_C \frac{\sigma_g}{\sigma_V} . n_0 . \varepsilon_M \tag{6.8}$$

Typically for mammalian cells σ_g , is about 3 μm^2 . In the present state of the development of the nano-device, only a single sensitive volume, that is n = 1, is

almost fully investigated . Nevertheless, the observed rate of simulated critical lesions, is directly related to the ICRP risk coefficient (Watt, 1997; Pszona et al, 2000; Alkharam and Watt, 1997) .

For the prototype multi-wire proportional counter with nanometre sensitive volume, the factors required for radiation damage are taken to be;

a) The energy imparted with an energy cut-off of 100 eV, that is about 1.5 nm radius in the sensitive volume which is probably a reasonable representation of dose-limited LET, L_D ; and,

b) Two or more charges released by single track action in the sensitive volume, which approximates the quality factor lambda, λ, but with a random spacing up to 1.8 nm between the ionizations within the sensitive volume . This is a single track action represented by the frequency of events given by the zeroth moment of energy transfer . On the other hand, the dose restricted LET, is a volume quantity which is weighted by the second moment of energy transfer . To investigate these aspects, it is necessary to be able to resolve single primary charges (Breskin et al, 1995) from two or more charges produced in clusters by using track traversals of the sensitive volume.

6.2 Conclusions

As the objective of this work is to design, produce and test a gas-filled prototype nanodosimeter for operational radiation protection and radiotherapy (section

1.3.1), a tissue equivalent (TE) gridded parallel plate proportional counter has been constructed having a minimum mean chord of 1.8 nm through the sensitive volume . Since the ultimate objective of the work is to simulate the response of known radiosensitive bio-molecular sites in mammalian cells, the detector is designed to have a response to the radiation similar to that of these targets in mammalian cell nuclei, such as a segment of the DNA . Therefore, the designed and produced detector records the stochastical frequency distributions of the initial primary charges produced in its sensitive volume . Single electron charges as well as plural charges can be resolved using a least square fitting routine combined with a deconvolution technique to determine the unknown parameters in the gamma function (section 5.4) used by Srdoč et al (1987) and Obelić et al (1998) . This makes the inherent calibration of the system possible .

The real success towards the objective is that, the nano-device can measure simultaneously the key parameters for the absolute system of radiation measurement . These parameters are the charged particle fluence and the bio-effect cross-section (Watt, 1997) . A method for interpreting the output signals of the device is described . The output signal is directly related to the bio-effect cross-section for the cell inactivation (Alkharam and Watt, 1997) which in turn, can be converted into radiation risk using the ICRP risk coefficients (section 3.2.3) .

The application of the zeroth, first and the second moments of the energy transfer

and density distributions permits the evaluation of the main parameters proposed historically for quality specification . This in turn, enables us to recognize and choose the most reliable parameter for a unified system of radiation measurement.

The nanodosimeter has been successfully tested with internally mounted α-particle, β-particle and X-ray sources . When exposed to laboratory external sources of operational means of spontaneous fission neutrons or γ-rays, the experimental results prove that the device can be used as an operational device, but further improvement of the signal-to-background ratio is to be enforced specially for the sparsely ionizing radiations . However, the unit is believed to be an absolute radiation measuring unit, applicable in any radiation field of mixed radiation without requiring foreknowledge of the radiation type (section 3.3.1) .

6.3 The future prospects and recommendations

Analysis of the results obtained in the present experimental work, using the gridded parallel plate nanodosimeter, shows that the basic working conditions of the detector are satisfactory, at least at this pioneering stage of the device . The results obtained here, are promising for the ultimate aim of devising an absolute radiation detector that can be applicable in operational radiation protection and radiotherapy.

It is obvious that, for a pioneering project such as the present work, its final success needs stages of investigations, modifications and planning for the future

prospects . Therefore, the present stage of success reached in designing, constructing and experimenting the prototype nanodosimeter, needs to be further supported by proper planning of the future prospect of the device to solve the problems and difficulties that hinder it from achieving its maximum efficiency of operation . There exists a number of limiting factors which must be overcome before the nano-device can be declared as a practical monitor for risk assessment .

One of the main problems associated with the operation of the gridded parallel plate nano-detector, is the difficulty in extracting and removing the signal from the vicinity of the background (noise) levels at the important lowest channels of the spectrum . Therefore, in the future planning of the device, it is important and vital that;

1 - More efficient, low noise background electronics should be utilized to operate the unit so that the overall level of the background signal remains reasonably low to permit the lowest channels of the spectrum of interest remain free of the background signal .

2 - The mechanical contribution to the background signal of the device should be reduced effectively in the future by using more adequate shielding and proper material associated with the detector and its experimental works .

3 - The "dead volume" of the detector should remain reduced to the minimum possible level without impairment to the other important functional factors, such as the charge amplification needed and the associated electric fields

applied to the different sites in the device .

These measures, together with more effective electronic vetoing of unwanted background signals should improve the signal-to-noise ratio of the detector .

Another chronically known problem with the operation of the gridded parallel plate nanodosimeter is the difficulty in resolving readily, single and plural ionizations produced in the sensitive volume . In the following sections, are some of the recommendations that may help in improving the applicability of the device . The recommendations are mainly concerned with the use of the gridded parallel plate counter combined with other appropriate systems such as the hybrid photomultiplier .

6.3.1 The hybrid chambers

The hybrid photo-diodes are simply gas discharge detectors that have the detection characteristics of maximum efficiency (Böhmer, 1973) . Unlike the conventional photomultipliers, the hybrid photodiode combines the fast resolution time of a conventional proportional counter (about 75 ns); the excellent event selectivity with spacial resolution (about 0.33 mm) and inexpensive operation and readout of the spark chamber (Fischer and Shibata, 1972) . Comparison is given in table 6.1, of the characteristics of a hybrid photo-diode with those of two conventional ionization chambers (a spark chamber and proportional counter).

However, the idea is to combine the nanodosimeter with this efficient hybrid photomultiplier that would be triggered by the light signal rather than the electronic charge emitted from the final avalanche in the region 2 of the figure 5.3b of the nano-device .

The idea of this combination has already been suggested and supplementary test experiments have been completed successfully at the University of St. Andrews using a hybrid photodiode (McDougall et al, 1997) . The advantage would be taken here, by combining the electrode assembly of the successfully tested nanodosimeter that gives a single electron spectrum, with the hybrid photo-diode system that would be able to resolve efficiently the single and plural charges (D'Ambrosio, et al 1993) . consequently, the convolution/deconvolution routine may no longer be needed for the extraction of the single electron spectra .

Table 6.1 : Characteristics of a hybrid photodiode compared to that of two conventional ionization chambers .

Characteristics	Spark chamber	Hybrid photodiode	counter Proportional
experimental resolving time	400 ns - 800 ns	≈75 ns	30 ns - 100 ns
recovery time for recorded events	≈ 1 ms	≈ 80 μs	≤ 1 μs
Spatial resolution	≈ 0.3 mm	≈ 0.3 mm	1 mm

A detector has already been designed and constructed to accommodate such a combination . Figure 6.2 shows the schematic diagram of the expected

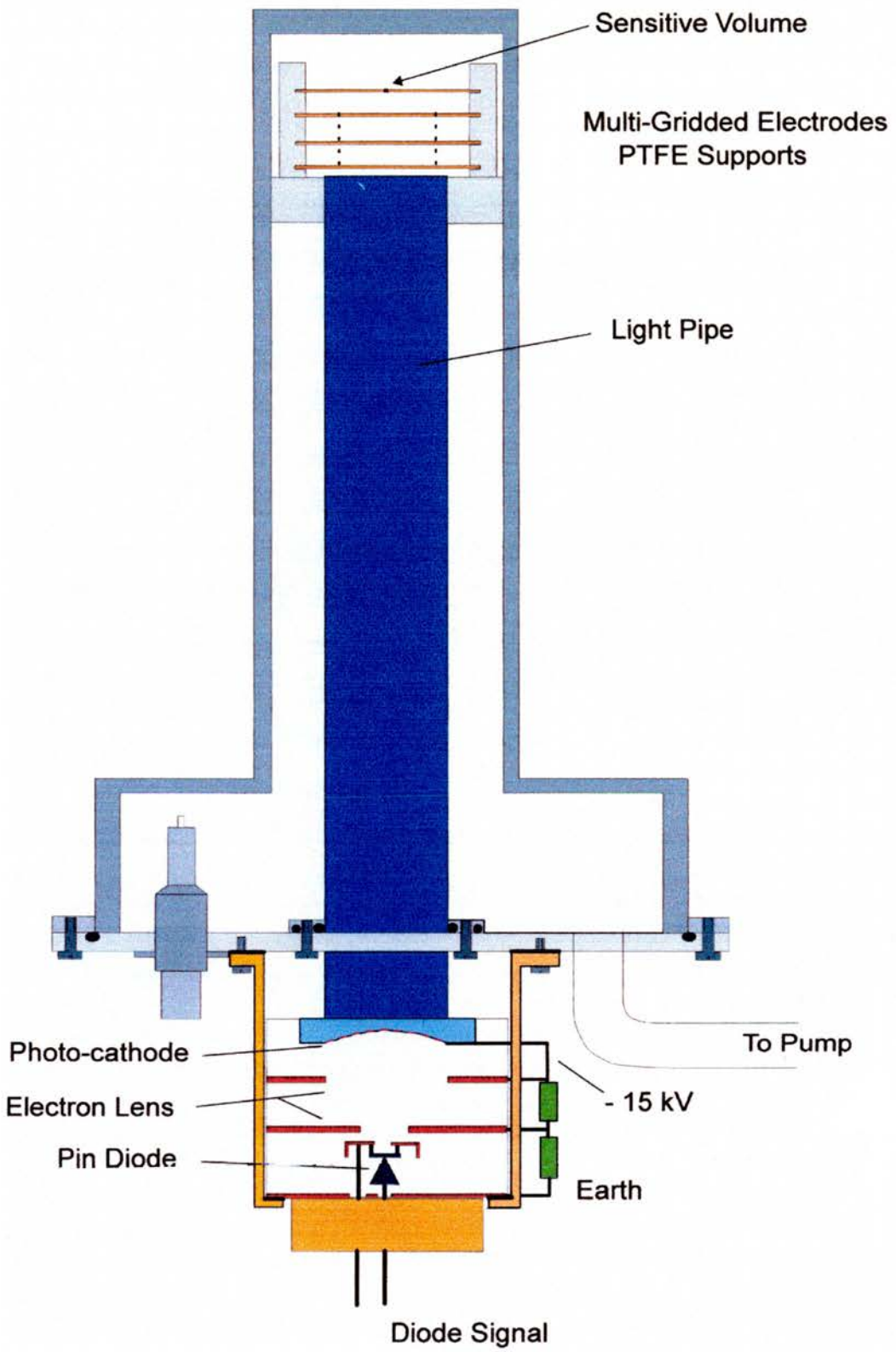

Figure 6.2: Schematic diagram of the expected combination of the gridded parallel plate nanodosimeter and the hybrid photo-diode .

combination of the nano-device with the hybrid photo-diode .The electrode assembly of the initial multi-grid version is used here, but the electrode system of the final version (figure 5.3b) would be the most suitable since the multi-stage multiplication would no longer be needed with the hybrid photomultiplier .

In figure 6.2 the collection electrode (anode) of the nano-device would be replaced with the hybrid photo-diode . The light pipe is meant to concentrate and prevent the scattering of the light emitted by drifting avalanche electrons, e.g in region 2 of figure 5.3b . The latter region can be adjusted so that a suitable drifting distance can be maintained for the avalanche electrons to give effective emission of light . Application of such a combination is expected to yield much better resolution by recording the UV photons emitted in the nano-detector by the electron avalanche of the primary charges originating from the sensitive volume, V, of figure 5.3b . However, due to the time factor, this supplementary part of the work could not proceed beyond the design and construction stage . Therefore, the experimental and investigative part of this part-work would be a recommendation for an interesting future prospect of the project .

6.3.2 Multi-volume system

The present nano-device operates with a single sensitive volume that is formed by a single extraction aperture in the centre of the extractor electrode . Consequently, it was necessary to scale the obtained results by the target multiplicity factor, 15 (section 5.5) to enable comparison with the effect cross-section for mammalian cells .

However, it was recommended that the detector could be operated at the multiple sensitive volumes mode by making the extractor electrode with multiple apertures evenly distributed into the central active part of the electrode . This is believed to increase the resolution of the output signal and the efficiency of the device . This makes also better simulation of the distribution of the DNA segments in the nuclei of the mammalian cells .

Although this arrangement has been tried, yet more investigation is need before a useful conclusion can be derived concerning the arrangement . Therefore, it is a strong recommendation that the multi-sensitive volume should be carefully investigated and implemented in the operation of the nanodosimeter in the future. The combination of such arrangement with the hybrid photo-diode would be a significant step forwards in the future evolution of the detector as an absolute operational measuring device in the fields of radiation protection and radiation therapy .

REFERENCES

Adamczewski, I. (1969) Ionization, conductivity and breakdown in dielectric liquids; Taylor and Francis Ltd, London .

Alkharam, A. S. and Watt, D. E. (1997) . Risk scaling factor from inactivation to chromosome aberrations, mutations and oncogenic transformations in mammalian cells, Radiat. Prot. Dosim. Vol. 70, Nos 1-4, pp 537 - 540 .

Alkhazov, G. D. (1970) . Statics of electron avalanches and ultimate resolution of proportional counters, Nucl. Instr. and Meth. 89, pp 155 - 165 .

Attix, F. H. (1986) . Quantities for describing the interaction of ionizing radiation with matter, in (Introduction to radiological physics and radiation dosimetry), John Wiley and Sons, pp 20 - 37 .

Bartels, E. R. and Harder, D. (1990) . The microdosimetric regularities of nanometre regions; Radiat. Prot. Dosim. Vol. 31, No. 1/4 PP 211 - 215 .

Baum, J. W; Varma, M. N; Wingate, C. L; Paretzke, H. G and Kuchner, A. (1974) . Nanometre dosimetry of heavy ion tracks; In Proceedings of Fourth Symp. on Microdosim., Vol. 1, pp 93 - 109 .

Blair, D. T. (1978) . Breakdown voltage characteristics; In Electrical Breakdown of gases, pp 533 -654; Ed. J. M. Meek and J. D. Craggs; John Wiley and Sons .

Boag, J. W. (1950) . Ionization measurement at very high intensities, Br. J. Radiol. 23, pp 601 - 6611 .

Boag, J.W. (1964) . Distortion of the electric field in an ionization chamber due to a difference in potential between guard rings and collector, Phys. Med. Biol. vol.

9, No. 1, pp 25 - 32 .

Bochagov, B. A.; Vorob'ev, A. A. and Komar, A. P. (1957) . A pulse ionization chamber as an instrument for the simultaneous study of energy and angular distribution of charged particles; In Soviet Physics (Technical Phys.), pp 1458 -1460 .

Böhm, J. (1976) . Charge collection defect in small ionization chambers due to initial recombination and diffusion loss; In Proceedings of Fifth symp. on Microdosim. pp 1055 - 1065 .

Böhmer, V. (1973) . New investigations into the detection properties of hybrid chambers; Nucl. Instr. and Meth. 107, pp 157 - 163 .

Breskin, A; Charpak, G; Majewski, S. and Melchart, G. (1979) . The multistep avalanche chamber : A new family of fast, High -rate particle detectors; Nucl. Instr. and Meth. 16, pp 19 - 34 .

Breskin, A; Chechik, R; Levin, I. and Zwang, N. (1983) . Heavy particle timing and imaging with low-pressure multi-wire proportional counters; Nucl. Instr. and Meth. 217, pp 107 -111 .

Breskin, A. and Chechik, R. (1986) . Low-pressure multi-step detectors, Application to high energy particle identification; Nucl. instr. and Meth. Phys. Res. A 252, pp 488 - 497 .

Breskin, A. Chechik, R; Colautti, P; Conte, V; DeNardo, L. and Pansky, A. (1995) . A single-electron counter for nanodosimetry, Radiat. Prot. Dosim. Vol. 61, No. 1 - 3, pp 199 - 204 .

Bryant, P. E; (1985) . Enzymatic restriction of mammalian cell DNA : evidence for

double-strand breaks as potentially lethal lesions; International J. Radiat. Biol. 48, pp 55 - 60 .

Bunemann, O.; Cranshaw, T. E. and Harvey, J. A. (1949) . Design of grid ionization chambers, Canadian J. Res. Vol 27, pp 191 - 206 .

Campion, P. J. (1968) . A study of proportional counter mechanism; Int. J. Appl. Radiat. Isotopes, Vol. 19, pp 219 -234 .

Campion, P. J. and Kingham, M. W (1971) . The measurement of gas amplification in tissue equivalent gas; Int. J. Appl. Radiat. Isotope, 22, pp 703 - 706.

Cannell, R. J. and Watt, D. E (1984) . Biophysical mechanisms of damage by fast ions to mammalian cells in vitro, Phys. Med. Biol. 30 (3) pp 255 - 258 .

Chaar, M. (1998) . Charge transport in liquid hydrocarbons for microdosimetry, PhD Thesis, University of St. Andrews, Scotland, U. K .

Chadwick, K. and Leenhouts, H. P. (1973) . Chromosome aberration and cell death; In 4th symp. on Microdosimetry; EUR 5122, pp 585 - 599 .

Chadwick, K. H and Leenhouts, H. P (1981) . The molecular model for cell survival following radiation, In the Molecular Theory of Radiation Biology, Springer-Verlag, pp 25, New York .

Charpak, G. and Sauli, L. (1978) . The multistep avalanche chamber, a new high-rate, high accuracy gaseous detector; Phys. letters, 78B, pp 523 - 528 .

Chase, R. L. (1961) . Nuclear pulse spectrometry; McGraw-Hill, New York .

Chen, C.Z. and Watt, D. E (1986) . Biophysical mechanism of radiation damage to mammalian cells by X-rays and γ-rays; International J. Radiat. Biol., Vol. 49, No. 1, pp 131 - 142 .

Colautti, P. et al, (1994) . Measurements of ionization distribution around a particle track at the nanometre level, Rad. Prot. Dosimetry, Vol. 52, Nos 1 - 4, pp 329 - 334.

Coon, J. H. and Barschall, H. H. (1946) . Angular distribution of 2.5 MeV neutrons scattered by deuterium; Phys. rev. Vol. 70, No. 9-10, pp 592 - 596 .

Cunningham, J. W. (1982) . Quantitative analysis of enzymes, viruses, bacteria and higher cells by ionizing radiation; PhD Thesis, University of Dundee, Scotland, UK .

Cunningham, J. W; Al-Kazwini, A. T. and Watt, D. E. (1982) . Quality parameters description of radiation damage to enzymes, viruses and bacteria; in Eighth Sympo. on Microdosimetry, Scientific programme and abstract, pp 7 - 8, Germany.

Curran, S. C and Craggs, J.D (1949) . Counting tubes , Academic Press, London.

D'Ambrosio, C.; Gys, T.; Leutz, D.; Piedigrossi, C.; Purtolas, D. and Tailhardat, S. (1993) . Photon counting with the hybrid photomultiplier tube (HPMT); Nucl. Instr. and Meth. 338, pp 389 - 397 .

Dertinger, H; Jung, H. and Zimmer, K. G (1969) . Molecular Radiation Biology , Heidelberg Science Library, Vol. 12, Springer-Verlag, pp 1 - 23, Berlin .

Dutton, J. (1978) . Spark breakdown in uniform fields, In Electrical Breakdown of gases, pp 209 -318; Ed. J. M. Meek and J. D. Craggs; John Wiley and Sons .

Emery, E. W. (1966) . Geiger-Mueller and proportional counters; In Radiaytion Dosimetry, second Edition, Vol. 2 , Instrumentation; pp 73 - 120; Editted by F. H. Attix and W. C. Roesch; Academic Press, New York .

Emery, E. W. (1970) . Wall-less counters and the lines of their future development; Proceedings of The Second Symp. on Microdosim. pp 219 - 229 .

Facchini, U; Gatti, E. and Pellegrini, F. (1959) . A new method for track angle measurement in a gridded ionization chamber; Nucl. Instr. and Meth. 4, pp 221 - 227 .

Fischer, J. and Shibata, S. (1972) . The hybrid chamber: A proportional chamber with gated spark readout; Nucl. Instr. and Meth.101, pp 401 - 404 .

Frankenberg, D. (1994) . Repair of DNA double-strand breaks and its effect on RBE; In Advances in Space Res. 14, pp 235 - 248m .

Frisch, O. R. (1944) . Isotope analysis of Uranium samples by means of their α-ray group; British Atomic Energy, Report Br. 49 .

Fulbright, H. W. (1979) . Ionization detectors (chambers); Nucl. instr. Meth. 162, pp 21 - 28 .

Göpfert, A.; Hambsch, F. -J and Bax, H. (2000) . A twin ionization chamber setup as detector for light charged particles with energies around 1 MeV applied to the $^{10}B(n, \alpha)^{7}Li$ reaction; Nucl. Instr. and Meth. in Phys. Res. A 44, pp 438 - 451 .

Greening, J. R; (1985) . Fundamentals of Radiation Dosimetry, Medical Physics

Handbook, Second Edition, Adam Hilger ltd, Bristol .

Gross, W. (1970) . Microdosimetry of directly ionizing particles with wall-less proportional counters, Second Symp. on Microdosim. pp 249 - 263 .

Grosswendt, B.; Baek, W. Y. (2000) . Basic physical data in organic gases; In Radiation Quality Assessment Based on Physical Radiation Interaction at Nanometre Level, pp 5 - 26, Editor : P. Colauti , Italy .

Grosswendt, B.; Baek, W. Y.; Alka, A.; Colauti, P.; Chechik, R.; Conte, V.; DeNardo, L.; Ségur, P.; Shchemelinin, S.; Tornielli, G.; Tamboul, J. Y.; McDougall, I. C.; Watt, D. E.; Pszona, S.; Kula, J.; and Marjanska, S. (2000) . Ionization-pattern investigation in nanometric gas volumes; In Radiation Quality Assessment Based on Physical Radiation Interaction at Nanometre Level, pp 61 - 70 , Editor : P. Colauti , Italy .

Harder, D ; blohm, R and Kessler, M. (1988) . Restricted LET remains a good parameter of radiation quality; In Sixth symposium on neutron dosimetry, CEC, 23, pp 79 - 82 .

Hiraoka, T; Fukumura, A; Omata, K. and Takeshita, M. (1998) . Polarity effect of parallel plate ionization chamber, Abstract of Joint Meeting of JARP-JAMP98 20aB11.

ICRP (1950) . International Recommendation on Radiological Protection; revised by the International Commission on Radiological Protection; Brit. J. Radiol. 24 (1951), pp 46 - 53 .

ICRP (1989) . RBE for deterministic effects; ICRP publication 58, Vol. 20 (4), Pergaman Press, Oxford .

ICRP (1990) . Recommendation of the International Commission on Radiological Protection, Annals of the ICRP, Publication 60, Pergamon Press, Oxford .

ICRU (1950) . International Recommendation on Radiological Units; revised by the International Commission on Radiological Units; Brit. J. Radiol. 24 (1951), pp 54 - 56 .

ICRU (1962b) report 10b . Physical aspects of irradiation; National Bureau of Standards, Hand book 85, Washington .

ICRU (1968) report 11 . Radiation quantities and units; International Commission on Radiation Units and Measurement; Washington .

ICRU (1970) report 16 . Linear energy transfer, International Commission for Radiation Units and Measurement; Washington .

ICRU (1977) report 26 . Neutron dosimetry for biology and medicine; International Commission on Radiation Units and Measurement; Washington .

ICRU (1978) report 28 . Basic aspects of high energy particle interactions and radiation dosimetry; International Commission on Radiation Units and Measurement; Washington .

ICRU (1979) report 31 . Average energy required to produce an ion pair; International Commission on Radiation Units and Measurement; Washington .

ICRU (1980) report 33 . Radiation quantities and units; International Commission on Radiation Units and Measurement; Washington .

ICRU (1983a) report 36 . Microdosimetry; International Commission on Radiation Units and Measurement; Washington .

ICRU (1986) report 40 . The quality factor in radiation protection; report for a joint task group of the ICRP and the ICRU, to the ICRP and the ICRU; Washington.

ICRU (1993) Report 49 . Stopping powers and ranges for protons and alpha particles; International commission on radiation units and measurements, 7910 Woodmount Avenue, Bethesda, Maryland 20814, USA .

ICRU (1993) report 51 . Quantities and units in radiation protection; International Commission on Radiation Units and Measurement; Washington .

ICRU News (2), (1992) . Radiation quantities and units; Germany .

ICRU News (3), (1993) . Physical quantities and units (interaction coefficients, dosimetry), Germany .

ICRU News (1), (1995) . 1895 W. C. Roentgen discovers X-rays, International Commission on Radiation Units and Measurement; Germany .

Illenberger, E. (1994) . Electron attachment to molecules; In Linking the Gaseous and Condensed Phases of Matter, Vol. 326, pp 355 - 376; Ed. L. G. Christophorou; E. Illenberger; and W.F. Schmidt , Plenum Press, New York .

IX-RRPC (1934) . International Recommendation for X-Ray and Radium Protection, revised by the International X-ray and Radium Protection commission; British J. Radiol. 7 (1934), pp 695 - 699 .

Jaffe, G. (1940) . On the theory of recombination; Phys. Rev. Vol. 58, pp 968 - 976.

Jawad, H. H and Watt, D. E. (1987) . Physical mechanism for inactivation to metalloenzymes by characteristic X-rays; Int . J. Radiat. Biol. Vol. 50 (4)

pp 665 - 674 .

Jean-Marie, B. ; Lepeltier, V. and L'hote, D. (1979) . Systematic measurement of electrons drift velocity and study of some properties of four gas mixtures : A-CH_4, A-C_2H_4 , A-C_2H_6 , A-C_3H_8 ; Nucl. Instr. and Meth. 159, pp 213 - 219 .

Jennings, W. A (1994) . Quantities and units in radiation protection dosimetry; Nucl. Instr. and Meth. in Phys. Res. A346, pp 548 - 549 .

Jin, T; Watt, D. E; and Kobayashi, K. (1994) . Damage induced by monochromatic synchrotron X-rays at resonance absorption energy of intracellular phosphorus in yeast cells; In Applied Radiat. Isotope, Vol. 45, No. 7, pp 767 -772, UK

Kadiri, L.. A., (1990) . Dosimetry for absolute biological effectiveness of ionizing radiation, PhD thesis, University of St. Andrews Scotland .

Kadiri, L.A. and Watt, D. E (1988) . Determination of total probabilities for cellular mutagenesis in vitro, Internal report, University of St. Andrews, Scotland, UK .

Katz, R ; Sharma, S. C and Homayoonfar, M ; (1972) . The structure of charged particle tracks; Topics in Radiation Dosimetry; Radiation Dosimetry supplm. 1, pp 317 - 383; Ed. F.H. Attix et al .

Kellerer, A. M. and Rossi, H. H. (1978) . Generalised formulation of dual radiation action ; Radiat. Res. 75, pp 471 - 488 .

Kellerer, A. M and Rossi, H.H. (1992) . Intermediate Dosimetric Quantities; Radiat. Res 130, pp 15 - 25 .

Kliauga, P. (1990) . Microdosimetry at middle age : Some old experimental problems and new aspiration; Radiat. Res. 124, pp S - S15 .

Knoll, G. F. (1989) . Ionization chambers, in (Radiation Detection and Measurement), John Wiley and Sons, pp 131 - 159 .

Korolev, G. A. and Kocharov, G. E. (1960) . Investigation of pulses arising on the grid of an ionization chamber, Acad. sci. Bull. Phys. Sci, Vol. 24 (3), pp 342 - 349.

Llewellyn, J. F. (1957) . Ionization and breakdown in Gases; Methuen, London.

Loeb, L. B. (1955) . Basic processes of gaseous electronics; University of California Press, Brekeley and Los Angeles .

Malamud, G; Breskin, A. and chechik, R. (1991) . A systematic study of primary ionization cluster counting at low gas pressures; Nucl. Instr. and Meth. in Phys. Res. A307, pp 83 - 96 .

McDaniel, E. W. and Mason E. A. (1973) . The mobility and diffusion of ions in gases, Wiley, New York .

McDougall, I. C.; Alkharam, A. S.; Thomas, G. E. and Watt, D. E. (1997) . A scintillation method for measurement of the bio-effectiveness of ionizing radiation by simulation of the cellular response, The IRPA Regional Symposium on Radiation Protection in Neighbouring Countries of Central Europe, Prague . Proceedings, pp 548 - 551 .

McWhirter, R. W; Palit, P. and Bellamy, E. H. (1958) . Distinguishing between He^3 and He^4 particles by 'dE/dx' and "E" measurement; Nucl. Instr. and Meth. 3, pp 80 - 84.

Morgan, K. Z. and Turner, J. E. (191973) . Principles of radiation protection; Robert E. Krieger Publishing Company, New York .

Morgan, Wm. L. (1985) . Molecular dynamics simulation of geminate recombination by electrons in liquid methane; J. Chem. Phys. 84 No. 4, pp 2298 - 2303 .

Moseley, J. T.; Gatland, I. R.; Martin, D. W. and McDaniel, E. W. (1968) . Measurement of transport properties of ions in gases; Results for K^+ ions in N_2; Physical Review, Vol. 178, No. 1, pp 234 - 239 .

Neary, G. J. (1965) . Chromosome aberration and the theory of RBE: general considerations; Int. J. Radiat. Biol. 9, (5), pp 477 - 502 .

Obileć ,B. ; Srdoč, D. D. and Marino, S.A. (1998) . The frequency distribution of the number of ion-pairs in irradiated tissue , Radiat. Prot. Dosim. 149; pp 411-415.

Ogawa, I. (1961) . Waveform and pulse-height distribution of the grid pulses from gridded ionization chambers, Supplemento al volume XXI, Serie X Del Nuovo Cimento, N. 1, 3^0 trimestre.

Ogawa, I. and Doke, T. (1961) . The double-grid ionization chamber, J. Phys. Soc. Japan 16, pp 1025 .

Onsager, I. (1938) . Initial recombination of ions; Phys. Rev. Vol. 54, pp 554 - 557.

Pansky, A; Breskin, A; Chechik, R. and Malamud, G. (1993) . Detection of X-ray fluorescence of light elements by electron counting in a low-pressure gaseous electron multiplier; Nucl. Instr. and Meth. in Phys. Res. A 330, pp 150 - 157 .

Pelticcioni, M. and Silari, M. (1993) . A critical view of radiation protection quantities for monitoring external irradiation; J. Radiol. Prot. Vol. 13 No. 1, pp 65 - 70 .

Policarpo, A. J. (1977) . The gas proportional counters; In Space Science Instrumentation 3, pp 77 - 107 .

Price, W. J. (1958) . Nuclear radiation detection, McGraw-Hill, New york (London) .

Pszona, S; Kula, J and Marjanska, S; (2000) . A new method for measuring ion clusters produced by charged particles in nanometre track sections of DNA size; Nucl. Instr. and Meth. in Phys. Res. A, 447, pp 601 - 607 .

Rossi, H. H. (1959) . Specification of radiation quality; Radiat. Res. 10, pp 522 - 531.

Rose M. E and Korff, S. A. (1941) . Investigation of the properties of the proportional counters ; Phys. Rev., 59, pp 850 - 859 .

Rossi, H. H and Kellerer, A. M (1994) . Why Cema, In ICRU News (2), International Commission on Radiation Units and Measurements .

Salikin, M. S. (1995) . An improved system of damage limitation for better risk control in radiological protection near environmental level, PhD Thesis, University of St. Andrews, Scotland .

Sanche, L. (1995) . Knowledge of particle interaction with gaseous and dense material : the behaviour of secondary electrons; Radiat. Prot. Dosim. Vol. 61, No. 1-3, pp 231 - 236 .

Schiller, R. (1993) . Ion-electron recombination in pairs : Critical appraisal of a theory; Nucl. Instr. and Meth. in Phys. Res. A 327, pp 37 - 40 .

Ségur, P.; Pérès, I.; Bœf, J. P. and Bordage, M. C. (1989) . metric calculation of the gas gain in cylindrical proportional counters; Radiat. Prot. Dosim., Vol. 29, No. 1/2, pp 23 - 30 .

Shapira, D; Devries, R. M; Fulbright, H. W; Töke, J. and Clover, M.R. (1975) . The rochester heavy ion detector; Nucl. Instr. and Meth. 129, pp 123 - 130 .

Sherr, R. (1946) . Electron collection in ionization chamber; Phys. Rev. 70 A, pp 450.

Sherr, R. and Peterson, R. (1947) . A study of pulse shapes in a parallel-plate ionization chamber; In The Review of Scientific Instruments, Vol. 18, No. 8, pp 567-575.

Shonka, J. J. (1998) . The use of plane parallel ionization chambers in high energy electron and photon beam . An International Code of Practice for Dosimetry, Technical Report Series No. 381, pp 125 .

Sigmond, R. S. (1978) . Corona discharge, In Electrical Breakdown of Gases, pp 319 -384; Ed. J. M. Meek and J. D. Craggs; John Wiley and Sons .

Sikkema, C. P. (1970) . A parallel-plate ionization chamber with gas multiplication; Nucl. Instr. and Meth. 81, pp 189 - 194 .

Sikkema, C. P. (1974) . A study of proportional chamber as a polarimeter for fast neutrons, Nucl. Instr. and Meth. 122, pp 415 - 431 .

Simmons, J. A. (1992) . Absorbed dose - an irrelevant concept for irradiation with

heavy charged particles ? J. Radiat Prot. 12, pp 173 - 179 .

Simmons, J. A. and Watt, D. E. (1999) . Radiation Protection Dosimetry: A Radical Reappraisal .Medical Physics Publishing, 4513 Vernon Blvd, Madison Wisconsin . W. I. 53705-4964, USA .

Sinclair, W. (1972) . Cell cycle dependence of the lethal radiation response in mammalian cells; In Current Topics in radiation Res. 7, pp 264 -285 .

Snell, H. (1962) . Nuclear instruments and their uses, Vol. 1, John Wiley and Sons, New York; London .

Srdoč, D.; Obileć, B. and Bronić, K. (1987) . Statistical fluctuations in the ionization yield for low-energy photons absorbed in polyatomic gases; J. Phys. B: At. Mol. Phys. 20, pp 4473 - 4484, UK .

Tait, W. H. (1980) . Radiation detection; Butterworths, London .

Takata, N.; and Yin, Z. (1997) . Decrease in output current due to back diffusion of ions in ionisation chambers, Radiat. Prot. Dosim. 71 (4) pp 309 .

Takata, N.; Takeda, N. and Yin, Z. (1999) . Diffusion loss of ions and charge collection volumes for thimble type ionization chambers, Radiat. Prot. Dosim., 81 (3) pp 229 .

Tamboul, J. Y.; .McDougall I. C. and Watt, D.E. (2000) . Nanometric gas counters, in Radiation quality assessment based on physical radiation interaction at the nanometre level. Ed. P. Colautti. LNL-I.N.F.N. (REP) 161/2000. I.N.F.N. Laboratori Nazionali di Legnaro, Via Romea, 4-I-35020, Padova, Italy.

Tamboul, J. Y. and Watt, D. E. (2001) . A proportional counter for measurement

of the bio-effectiveness of ionizing radiation at DNA level; Nucl. Instr. and Meth. in Phys. Res. B, Vol.184(4), pp 597 - 608 .

Tsoulfanidis, N. (1983) . Measurement and detection of radiation; McGraw-Hill, New York - London .

Turner, J. E (1986) . Atom, radiation and radiation protection, Pergamon Press, New York .

Virsik, R. P; Blohm, R; Hermann, K. P; Modler, H. and Harder, D (1983) . Chromosome aberrations and the mechanism of primary lesion interaction; in Proceedings of the eighth Symp. on Microdosimetry; Ed. by J. Booz and H. G. Ebert (Luxemburg , Commission of the European Communities) 8395; pp 409 - 422 .

Volkle, H; Robert, L; Halter, J. Huger, O. and Winger P. (1974) . Alpha-spektroskopie mit gitter ionistionkammer, Helvetica Physica Acta, Vol. 47 , pp 97 - 105 .

Wang, L.L; Tung, C. J. (1989) . Lineal distribution and effective quality factor for ^{35}S β-particles; Health Phys., Vol. 57. No. 4, pp 659 - 663 .

Warman, J. M; Sennhauser, E. S. and Armstrong, D. A. (1979) . Three body electron - ion recombination in molecular gases; J. Chem. Phys. 70 (2), pp 995 - 999 .

Watt, D. E (1975) . Hit cross-section in single target theory, Phys. Med. Biol. Vol. 20 (6) pp 944 - 954 .

Watt, D. E. (1989a) . On absolute biological effectiveness and unified dosimetry; Int. J. Radiat. Prot. , Vol. 9, No. 1 pp 33 - 49 .

Watt, D. E. (1989b) . An approach towards a unified theory of damage to mammalian cells by ionizing radiation for absolute dosimetry, Radiat. Prot. Dosim. Vol. 27, No. 2, pp 73 - 84 .

Watt, D. E. (1994) . Heavy particle track structure parameters for biophysical modelling, Nucl. instr. and Meth. Phys. Res. B93, pp 215 - 221 .

Watt, D. E. (1997) . A unified system of radiation bio-effectiveness and its consequences in practical application . Radiat. Prot. osim. Vol. 70, No. 1 - 4, pp 529 - 536 .

Watt, D. E.; Williamsom , J.; Martin , J. H. (1964) . Range-energy relationship for heavy charged particles in gases using the double-gridded ionization chamber, Proceedings of the symp. on biological effects of neutron irradiations, IAEA, Vol. 2, pp 57 - 70 .

Watt, D. E and Sutcliffe, J. F (1975) . Cross-sections for the inactivation of ribonuclease by slow heavy ions, Phys. Med. Biol. Vol.20 (6), pp 926 - 943 .

Watt, D. E; Al Kazwini, A. T; Al-shaibani, H. M. and Twaij, D. A (1980) . Studies in enzyme inactivation as a prelude to damage modelling; In Proceedings of Seventh Sym. on Microdosimetry, Vol. II, pp 1475 -1488, Harwood Academic Publication ltd, Oxford .

Watt. D. E; Al-Affan, I. A; Chen, C. Z and Thomas, G. E (1985) . Identification of biophysical mechanisms of damage by ionizing radiation, Radiat. Prot. Dosim. Vol. 13, No. 1-4, pp 285 - 294 .

Watt. D. E and Younis, A-R S (1987) . Damage to metalloenzymes by characteristic X-rays , Letter to the Editor, Int. J. Radiat. Biol.

Watt, D. E; Chen, C. Z; Kadiri, L. and Younis, A, R-s; (1987) . Towards a unified system for expression of biological damage by ionizing radiation . In Conference on Health Effects of Low dose ionizing radiation, Recent Advances and their Implications; London , Paper 6, pp 36 - 42 (British Nucl. Energy Society) .

Watt, D. E. and Kadiri, L.-A (1990) . Physical quantification of the biological effectiveness of ionizing radiations; International J. of Quantum Chemistr, Vol. XXXVIII, pp 501 -520 .

Watt, D. E. and Alkharam, A. S; (1994) . Charged particle track structure parameters for application in radiation biology and radiation chemistry, International J. of quantum Chemistry, Quantum Biology symposium 21, pp 195 -207.

Watt, D. E; Alkharam, A. S; Child, M.B; and Salikin, M. S; (1994) . Dose as a Damage Specifier in Radiobiology for Radiation Protection, Rad. Res. 139 (2), pp 249 - 251 .

Watt, D. E. and Alkharam, A. S. (1995) . A feasibility study of scintillation microdosimeters for measurement of the biological effectiveness of ionizing radiation, Radiat. Prot. Dosim. Vol. 61, No. 1-3, pp 211 - 214 .

Watt, D. E. and Hill, S. J (1997) . An empirical model for the induction of double-strand breaks in DNA by the indirect action of ionizing radiation; Radiat. Prot. Dosim. 52, (1/4), pp 17 - 20 .

Wickman, G. and Holmström, T. (1992) . Polarity effect in plane-parallel ionization chambers using air or a dielectric liquid as ionization medium; Med. Phys. Vol. 19, No. 3, pp 637 - 640 .

Wilkinson, D. H. (1950) . Ionisation chambers and counters; Cambridge

University Press .

Williams, A. and Sara, R. I. (1962) . Parameters affecting the resolution of proportional counter, J. Appl. Radiat. Isotopes 13, pp 229 - 238 .

Willson, K. S. and Emery, E W. (1972) . Experience with wall-less counter; Third Symp. on Microdosim. pp 645 - 652 .

Younis, A-R. S and Watt, D. E (1990) . Interpretation of damage to mammalian cells, E.colli and bacteriophages by incorporated radionuclides for prolonged irradiation; In Radiat. Prot. Dosim., Vol. 31, No. 1/4, pp 339 -342 .

Younis, A-R. S and Watt, D. E. (1989) . The quality of ionizing radiations emitted by radionuclides incorporated into mammalian cells, Phys. Med. Biol.; Vol. 34, No. 7, pp 821 - 834, UK .

Zirkle, R. E.; Marchbank, D.F. and Kuck, K.D. (1952) . Exponential and Sigmoidal Survival Curves Resulting from Alpha and X-irradiation of Aspergillus Spores. J. Cell. Comp. Physiol. 39, Suppl. 1, pp 75 .